

**HYBRID PLASMA ENHANCED CHEMICAL VAPOUR  
DEPOSITION/SPUTTERING SYSTEM  
FOR PREPARATION OF LUMINESCENT  
SILICON CARBON FILMS**

**NUR MAISARAH BINTI ABDUL RASHID**

**DISSERTATION SUBMITTED IN FULFILMENT OF  
THE REQUIREMENT FOR THE DEGREE OF  
MASTER OF SCIENCE**

**DEPARTMENT OF PHYSICS  
FACULTY OF SCIENCE  
UNIVERSITY OF MALAYA  
KUALA LUMPUR**

**2013**

UNIVERSITI MALAYA

**ORIGINAL LITERARY WORK DECLARATION**

Name of Candidate: **NUR MAISARAH BINTI ABDUL RASHID** (I.C/Passport No: **861102-02-5124**)

Registration/Matric No: **SGR090108**

Name of Degree: **MASTER OF SCIENCE**

Title of Project ~~Paper/Research Report/Dissertation/Thesis~~ ("this Work"):

**HYBRID PLASMA ENHANCED CHEMICAL VAPOUR DEPOSITION/SPUTTERING  
SYSTEM FOR PREPARATION OF LUMINESCENT SILICON CARBON FILMS**

Field of Study: **THIN SOLID FILMS**

I do solemnly and sincerely declare that:

- (1) I am the sole author/writer of this Work;
- (2) This Work is original;
- (3) Any use of any work in which copyright exists was done by way of fair dealing and for permitted purposes and any excerpt or extract from, or reference to or reproduction of any copyright work has been disclosed expressly and sufficiently and the title of the Work and its authorship have been acknowledged in this Work;
- (4) I do not have any actual knowledge nor do I ought reasonably to know that the making of this work constitutes an infringement of any copyright work;
- (5) I hereby assign all and every rights in the copyright to this Work to the University of Malaya ("UM"), who henceforth shall be owner of the copyright in this Work and that any reproduction or use in any form or by any means whatsoever is prohibited without the written consent of UM having been first had and obtained;
- (6) I am fully aware that if in the course of making this Work I have infringed any copyright whether intentionally or otherwise, I may be subject to legal action or any other action as may be determined by UM.

Candidate's Signature:

Date: 1<sup>st</sup> August 2013

Subscribed and solemnly declared before,

Witness's Signature:

Date: 1<sup>st</sup> August 2013

Name:

Designation:

## ABSTRACT

Radio frequency plasma enhanced chemical vapour deposition (r.f. PECVD) process is a well-established technique for depositing amorphous silicon carbon (a-SiC) films. However, an environmental friendly deposition technique which does not involve the use of toxic gas, silane ( $\text{SiH}_4$ ) is a much preferred technique. In this work a hybrid r.f. PECVD/sputtering system was designed for this purpose. This system combines the use of radio frequency (r.f.) reactive sputtering with r.f. PECVD for the growth of amorphous a-SiC films. The use of amorphous silicon (a-Si) target as a sputtering source eliminates the use of  $\text{SiH}_4$  as Si source for the films. This work is divided into three parts consisting of studying (i) film deposited by r.f. PECVD through discharge of hydrogen ( $\text{H}_2$ ) diluted methane ( $\text{CH}_4$ ) with different total gas pressure; (ii) films deposited by sputtering of a-Si target at different Argon (Ar) flow rate; and (iii) films deposited by the hybrid r.f. PECVD/sputtering system from  $\text{CH}_4$  discharge and sputtering of a-Si target at different r.f. power with a fixed Ar to  $\text{CH}_4$  ratio of 7.5:1. In the first part, the effect of total gas pressure on the film properties were studied with  $\text{CH}_4$  to  $\text{H}_2$  flow rate ratio fixed at 1:5. The effects of Ar flow rate of 5.7, 7.5, 15.0 and 30.0 sccm on the properties of the films were studied in the second part of the work. The last part of the work involved the study of the effect of r.f. power of 60, 80, 100, 120 and 150 W on the film properties. Raman, Fourier transform infrared, Auger electron and photoluminescence emission spectroscopies were used to analyze the properties of the films. Film thickness was measured using mechanical profilometer to study the film growth rate. It is established from the results that the films deposited by hybrid r.f. PECVD/sputtering system are multiphase in structure which consist of a-Si, a-SiC, a-C:H and  $\text{SiO}_x$  phases. The origin of PL emission in the films is mainly through recombination processes in the  $\text{sp}^2$ -C clusters embedded within the a-C:H and  $\text{SiO}_x$  phases in the film structure.

## ABSTRAK

Proses pemendapan frekuensi radio secara peningkatan plasma wap kimia (r.f PECVD) merupakan suatu teknik yang telah diakui untuk pemendapan filem amorfus silikon karbon (a-SiC). Walau bagaimanapun, teknik pemendapan mesra alam yang tidak melibatkan penggunaan gas toksik, silana ( $\text{SiH}_4$ ) adalah teknik yang diinginkan. Dalam kajian ini, sistem hibrid r.f. PECVD/percikan telah direkabentuk untuk tujuan ini. Sistem ini menggabungkan penggunaan frekuensi radio (r.f.) percikan reaktif dan r.f. PECVD dalam menghasilkan filem a-SiC. Penggunaan sasaran silikon amorfus (a-Si) sebagai sumber percikan mengelakkan penggunaan  $\text{SiH}_4$  sebagai sumber Si. Kajian ini dibahagikan kepada tiga bahagian iaitu (i) filem yang dimendapkan menggunakan r.f. PECVD melalui nyahcas metana ( $\text{CH}_4$ ) yang dicairkan bersama hidrogen ( $\text{H}_2$ ) pada jumlah tekanan gas yang berbeza; (ii) filem yang dimendapkan dengan percikan sasaran a-Si pada kadar aliran gas Argon (Ar) yang berbeza; dan (iii) filem yang dimendapkan menggunakan system hibrid r.f. PECVD/percikan daripada nyahcas  $\text{CH}_4$  dan percikan sasaran a-Si dengan nisbah Ar kepada  $\text{CH}_4$  pada 7.5:1. Dalam bahagian pertama, kesan jumlah tekanan gas pada sifat filem dikaji dengan nisbah kadar aliran  $\text{CH}_4:\text{H}_2$  ditetapkan pada 1:5. Kesan kadar aliran Ar pada 5.7, 7.5, 15.0 dan 30.0 sccm kepada sifat filem telah dikaji dalam bahagian kedua. Bahagian terakhir melibatkan kajian terhadap kesan kuasa r.f. pada 60, 80, 100, 120 and 150 W ke atas sifat filem. Spektroskopi Raman, transformasi inframerah jelmaan Fourier, elektron Auger dan pemancaran fotoluminesen digunakan untuk menganalisa sifat-sifat filem tersebut. Ketebalan filem diukur menggunakan profilometer mekanikal untuk mengkaji kadar pertumbuhan filem. Keputusan kajian telah menunjukkan bahawa filem yang dihasilkan menggunakan sistem hibrid r.f. PECVD/percikan mengandungi struktur dalam pelbagai fasa yang terdiri daripada fasa a-Si, a-SiC, a-C:H dan  $\text{SiO}_x$ . Pemancaran PL dalam filem adalah melalui proses-proses penggabungan di dalam kelompok  $\text{sp}^2\text{-C}$  yang terbenam di antara fasa-fasa a-C:H dan a- $\text{SiO}_x$  di dalam struktur filem.

## ACKNOWLEDGEMENT

In the name of Allah, the most gracious, the most merciful. All praise and thanks to Allah, the Lord of existence, for the strength, patience, faith and bless to make the completion of this dissertation come true.

First and foremost, special thanks to my beloved parents, En. Abdul Rashid Abdul Rahman and Pn. Aliah Mat Ali, and my sisters, Nor Ezaty and Nurwashifa for their love, support, encouragement and endless prayers.

I wish to extend my sincere gratitude and appreciation to my supervisor, Associate Professor Dr. Siti Meriam Ab. Gani for her supervision and support. A note of thank to Professor Dato' Dr. Muhamad Rasat Muhamad for his kindness and advice.

I am indebted to Professor Datin Dr. Saadah Abdul Rahman for her priceless ideas, knowledge and guidance throughout my MSc work. My deepest thank to Dr. Richard Ritikos and Dr. Goh Boon Tong for their help and comments.

I would also like to thank my colleagues, Pn. Maisara Othman, Pn. Noor Hamizah Khanis, En. Mohd Ragib Badaruddin and Ms. Nor Khairiah Za'aba for their kindness, thought, help and friendship to make me strong in facing all the trials. To Chong Su Kong, Chan Kee Wah, Saipul, Siti Hajar, Dila, Rehana, Syahino, Syed and Linda, your support means so much to me.

Last but not least, I would like to thank Pn. Zurina Marzuki, En. Mohamad Aruf, Pn. Norlela Shahardin and all members of the Department of Physics for their assistance.

The financial support provided by the University of Malaya (UM) for SBUM scholarship scheme for this two year work and grants including University Research Grant RG064-09AFR, Fundamental Research Grant FP016/2008C and FP052/2010B and short term grant PS309/2009C are gratefully acknowledged.

# TABLE OF CONTENT

<b>ORIGINAL LITERARY WORK DECLARATION.....</b>	<b>i</b>
<b>ABSTRACT .....</b>	<b>ii</b>
<b>ABSTRAK .....</b>	<b>iii</b>
<b>ACKNOWLEDGEMENT.....</b>	<b>iv</b>
<b>TABLE OF CONTENT.....</b>	<b>v</b>
<b>LIST OF FIGURES .....</b>	<b>ix</b>
<b>LIST OF TABLES .....</b>	<b>xii</b>
<b>LIST OF ABBREVIATIONS .....</b>	<b>xiii</b>
<b>LIST OF PUBLICATIONS .....</b>	<b>xv</b>
<b>CHAPTER 1 .....</b>	<b>1</b>
INTRODUCTION.....	1
1.0 Chapter Outline.....	1
1.1 Research Background .....	1
1.1.1 Hydrogenated Amorphous Carbon and Amorphous Silicon Carbon Thin Films .....	1
1.1.2 Plasma Enhancement of Chemical Vapour Deposition and Sputtering Processes.....	4
1.2 Inspirations and Research Objectives .....	4
1.3 Thesis Outline .....	6
<b>CHAPTER 2 .....</b>	<b>7</b>
LITERATURE REVIEW .....	7
2.0 Chapter Outline.....	7
2.1 Review on Deposition Techniques for Silicon and Carbon Based Films..	7
2.1.1 Radio Frequency Plasma Enhanced Chemical Vapour Deposition System: Hydrogenated Amorphous Carbon Thin Films .....	8
2.1.2 Sputtering Mechanism and Techniques: Amorphous Silicon Carbon Thin Films .....	9

2.1.3	Hybrid System Involving Sputtering Technique .....	10
2.2	Review on Properties of Hydrogenated Amorphous Carbon Thin Films	12
2.2.1	Growth Rate of Hydrogenated Amorphous Carbon Thin Films.....	13
2.2.2	Structural Properties of Hydrogenated Amorphous Carbon Thin Films ..	15
2.2.3	Energy Gap and Photoluminescence Emission Properties of Hydrogenated Amorphous Carbon Thin Films .....	20
2.3	Review on Properties of Amorphous Silicon Carbon Thin Films .....	21
2.3.1	Growth Rate of Amorphous Silicon Carbon Thin Films .....	22
2.3.2	Structural Properties of Amorphous Silicon Carbon Thin Films .....	23
2.3.3	Photoluminescence Emission Properties of Amorphous Silicon Carbon Thin Films.....	26
<b>CHAPTER 3</b>	<b>.....</b>	<b>28</b>
	EXPERIMENTAL SETUP .....	28
3.0	Chapter Outline.....	28
3.1	Deposition System Setup .....	28
3.1.1	The Evacuation Subsystem.....	31
3.1.2	The Gas Distribution Subsystem .....	32
3.1.3	The Electrical Subsystem.....	33
3.1.4	The Reaction Chamber .....	33
3.2	Pre-deposition Preparation.....	36
3.2.1	Substrate Cleaning Procedure.....	36
3.2.1 (a)	Silicon Substrate Cleaning Process .....	37
3.2.1 (b)	Quartz and Glass Substrate Cleaning Process.....	37
3.2.2	Amorphous Silicon (a-Si) Target Cleaning Procedure .....	38
3.3	Operation of the Deposition System.....	38
3.3.1	Pre-deposition Procedure .....	38
3.3.2	Deposition Procedure.....	40

3.3.2 (a)	Deposition Parameters for Hydrogenated Amorphous Carbon Films Deposited by Radio Frequency Plasma Enhanced Chemical Vapour Deposition System .....	40
3.3.2 (b)	Deposition Parameters for Hydrogenated Amorphous Silicon Carbon Films Deposited by Hybrid Radio Frequency Plasma Enhanced Chemical Vapour Deposition/Sputtering System .....	42
3.3.3	Post-deposition Procedure .....	44
3.4	Characterization Techniques.....	44
3.4.1	Surface Profilometer .....	45
3.4.2	Fourier Transform Infrared Spectroscopy .....	46
3.4.3	Ultra Violet-Near Infrared Spectroscopy.....	50
3.4.4	Raman Spectroscopy.....	52
3.4.5	Photoluminescence Spectroscopy .....	55
3.4.6	Auger Electron Spectroscopy .....	56
<b>CHAPTER 4</b>	.....	<b>58</b>
RESULTS AND DISCUSSION	.....	58
4.0	Chapter Outline.....	58
4.1	Hydrogenated Amorphous Carbon Films Prepared by Plasma Enhanced Chemical Vapour Deposition .....	58
4.1.1	Growth Rate of Hydrogenated Amorphous Carbon Thin Films.....	59
4.1.2	Structural Properties of Hydrogenated Amorphous Carbon Thin Films ..	62
4.1.3	Optical Energy Gap of Hydrogenated Amorphous Carbon Thin Films ...	67
4.1.4	Photoluminescence Emission Properties of Hydrogenated Amorphous Carbon Films .....	70
4.1.5	Summary .....	72
4.2	Effect of Argon Flow Rate on the Properties of Films Produced by r.f. Sputtering Process .....	74
4.2.1	Effect of Argon Flow Rate on Growth Rate of the Deposited Thin Films .....	75



4.2.2	Effect of Argon Flow Rate on Structural Properties of the Deposited Thin Films .....	76
4.2.3	Effect of Argon Flow Rate on Photoluminescence Properties of the Deposited Thin Films .....	85
4.2.4	Summary .....	87
4.3	Effects of r.f. Power on Amorphous Silicon Carbon Films Prepared by Hybrid PECVD/Sputtering Deposition System.....	88
4.3.1	Growth Rate of Amorphous Silicon Carbon Thin Films .....	88
4.3.2	Structural Properties of Amorphous Silicon Carbon Thin Films .....	90
4.3.3	Photoluminescence Properties of Amorphous Silicon Carbon Thin Films .....	94
4.3.4	Summary .....	96
4.4	Overall PL Emission Analysis .....	97
<b>CHAPTER 5 .....</b>		<b>99</b>
<b>CONCLUSION AND FUTURE WORK.....</b>		<b>99</b>
5.1	Conclusion .....	99
<b>References .....</b>		<b>102</b>

## LIST OF FIGURES

<b>Figure 1.1:</b> Carbon hybridization comprised of $sp^1$ , $sp^2$ and $sp^3$ structure (Silva 2003)..	2
<b>Figure 2.1:</b> Schematic illustration for deposition setup of (a) Unbalance magnetron sputtering combined with inductively coupled r.f. plasma chemical vapour deposition (b) Magnetron sputtering and PECVD (c) Co-deposition process of r.f. sputtering and r.f. PECVD (d) Combined metal vapour vacuum arc (MEVVA) ion implantation with ion beam assisted deposition (IBAD)....	11
<b>Figure 2.2:</b> Schematic diagram of the deposition process in a-C:H film growth involving (1) ion subplantation, (2) creation of surface dangling bond by ion impact, (3) creation of surface dangling bond by H-abstraction, (4) radicals passivating the surface dangling bond, (5) H-abstraction from subsurface C-H bonds, (6) H repassivating subsurface dangling bonds (Neyts et al., 2007). ....	14
<b>Figure 2.3:</b> Ternary diagram illustrates four classes of a-C:H (Casiraghi et al. 2005). .	16
<b>Figure 2.4:</b> Typical Raman spectra for different types of a-C:H thin films (Casiraghi, Ferrari, et al., 2005) .....	17
<b>Figure 2.5:</b> Typical Raman spectra with significant PL background (Buijnsters et al. 2009).....	18
<b>Figure 2.6:</b> Typical FTIR spectra within the range of 2600 to 3200 $cm^{-1}$ which assigned to C-H stretching modes (Son et al. 2001). ....	19
<b>Figure 2.7:</b> Raman spectra of a-SiC films composed of various Si content (Shi et al., 1999).....	24
<b>Figure 2.8:</b> Typical deconvoluted peak of Si-Si network for a-SiC:H thin films (Swain and Dusane, 2007). ....	25
<b>Figure 2.9:</b> FTIR spectra of SiC thin films (Jung et al. 2003). ....	26
<b>Figure 3.1:</b> Summary of sample preparation variables. ....	29
<b>Figure 3.2:</b> Home-built r.f. PECVD/sputtering deposition system. ....	30
<b>Figure 3.3:</b> Schematic diagram of r.f. PECVD/sputtering deposition system. ....	31
<b>Figure 3.4:</b> The schematic diagram of reaction chamber of (a) custom-built r.f. PECVD and (b) custom-built hybrid r.f. PECVD/sputtering system. ....	35
<b>Figure 3.5:</b> Top view of stainless steel mask. ....	39
<b>Figure 3.6:</b> Mechanical surface profilometer (KKA Tencor P-6) and its stylus tip.....	45

<b>Figure 3.7:</b> The step edge of a deposited thin film displayed by profilometer, representing the thickness of the films. ....	46
<b>Figure 3.8:</b> FTIR spectrometer (Perkin Elmer 2000 system). ....	47
<b>Figure 3.9:</b> Typical FTIR spectra obtained from a-C:H and a-SiC thin films. ....	48
<b>Figure 3.10:</b> Final information gained from curve fitting by OriginPro 8.1. ....	49
<b>Figure 3.11:</b> Jasco V-570 Uv-Vis-NIR spectrometer. ....	50
<b>Figure 3.12:</b> Reflectance, transmittance and absorption of light by the deposited thin films. ....	51
<b>Figure 3.13:</b> Extrapolation of $\alpha E^{1/2}$ versus E to obtained $E_{Tauc}$ and optical absorption edge of $E_g$ . ....	52
<b>Figure 3.14:</b> Raman and Photoluminescence spectroscopy. ....	53
<b>Figure 3.15:</b> Energy level diagram of Rayleigh scattering and Stokes-Raman shift. ....	54
<b>Figure 3.16:</b> JAMP-9500F Field Emission Auger Microprobe. ....	56
<b>Figure 3.17:</b> Energy level diagram of Auger process. ....	57
<b>Figure 3.18:</b> Depth profile mechanism of AES. ....	57
<b>Figure 4.1:</b> Growth rate of a-C:H films deposited on c-Si and quartz substrate at different total gas pressure, $P_T$ . ....	59
<b>Figure 4.2:</b> Raman spectra of a-C:H films deposited at different total gas pressure, $P_T$ . Dashed line shows slanting background of Raman spectra which indicate the photoluminescence (PL) of films, where m is the slope of PL. ....	63
<b>Figure 4.3:</b> FTIR absorption spectra of C-H <sub>n</sub> vibrational bands of a-C:H films deposited at different total gas pressure, $P_T$ . ....	64
<b>Figure 4.4:</b> Hydrogen content, $C_H$ of films deposited at different total gas pressure, $P_T$ . .....	65
<b>Figure 4.5:</b> Transmission (a) and reflection (b) spectra of a-C:H thin films. ....	68
<b>Figure 4.6:</b> Energy gap, $E_g$ variation of a-C:H films deposited at different total gas pressure, $P_T$ . ....	69
<b>Figure 4.7:</b> Variation of photoluminescence (PL) spectra of a-C:H films prepared at various total gas pressure, $P_T$ . ....	71
<b>Figure 4.8:</b> Variation of the growth of deposited films as a function of Argon (Ar) flow rate. ....	75
<b>Figure 4.9:</b> Variation of the growth of deposited films as a function of Argon (Ar) flow rate. ....	77
<b>Figure 4.10:</b> Relative concentration at the surface of the films relative to Ar flow rate	79

<b>Figure 4.11:</b> The whole range of Raman spectra for a-SiC thin films deposited at various Ar flow rate and their corresponding slope, m. ....	81
<b>Figure 4.12:</b> Raman spectra in the range of 100 to 850 $\text{cm}^{-1}$ which consists of several overlapping peaks indicating the existence of Si-Si network in the films.	82
<b>Figure 4.13:</b> Raman spectra in the range of 1000 to 1800 $\text{cm}^{-1}$ which consists of D and G peak indicating the existence of C-C network in the films .....	83
<b>Figure 4.14:</b> FTIR spectra of silicon carbon films deposited at different Ar flow rate showing the absorption band within the spectral range. ....	84
<b>Figure 4.15:</b> PL spectra of silicon carbon film deposited at different Ar flow rate. ....	86
<b>Figure 4.16:</b> Growth rate of a-SiC thin films prepared by hybrid PECVD/sputtering deposition system.....	89
<b>Figure 4.17:</b> The whole range of Raman spectra for a-SiC thin films and their corresponding slope, m. ....	90
<b>Figure 4.18:</b> Silicon network of a-SiC thin films observed from Raman spectra in the range of 100 to 850 $\text{cm}^{-1}$ .....	91
<b>Figure 4.19:</b> Carbon network of a-SiC thin films observed from Raman spectra which was baseline corrected in the range from 850 to 1800 $\text{cm}^{-1}$ . ....	92
<b>Figure 4.20:</b> FTIR spectra of the silicon carbon films deposited at different r.f. power showing the absorption bands expected in silicon carbon films within the spectral range. ....	93
<b>Figure 4.21:</b> PL spectra of silicon carbon film deposited at different r.f. power. ....	95
<b>Figure 4.22:</b> Normalized PL intensity of the highest PL emitted from three sets of films.....	97

## LIST OF TABLES

<b>Table 3.1:</b> Parameters applied during Hydrogen treatment process.....	41
<b>Table 3.2:</b> Total gas pressure, $P_T$ relative to $CH_4:H_2$ flow rate ratio.....	41
<b>Table 3.3:</b> Deposition parameters used to deposit a-C:H thin films. ....	41
<b>Table 3.4:</b> Parameters applied for Argon treatment. ....	42
<b>Table 3.5:</b> Deposition pressure relative to Ar flow rate. ....	43
<b>Table 3.6:</b> Deposition parameters for deposition of a-SiC thin films: Effect of Ar flow rates. ....	43
<b>Table 3.7:</b> Deposition parameters for deposition of a-SiC thin films: Effect of r.f. power. ....	44
<b>Table 3.8:</b> Chemical bonding at specific range of wavenumbers (Deng et al. 2011; Higa et al. 2006; Liu et al. 1997; Yoon et al. 2000). ....	48
<b>Table 3.9:</b> Assignments of Raman shift of a-C:H a-SiC films taken from (Shi et al.1999; Swain and Dusane 2007; Wang et al. 2002).....	55

**LIST OF ABBREVIATIONS**

AES	Auger electron spectroscopy
a-C:H	Hydrogenated amorphous carbon
Ar	Argon
a-Si	Amorphous silicon
a-SiC	Amorphous silicon carbon
C	Carbon
C <sub>2</sub> H <sub>2</sub>	Acetylene
C <sub>H</sub>	Hydrogen content
CH <sub>4</sub>	Methane
Cu	Copper
c-Si	Crystal silicon
DLCH	Diamond-like hydrogenated carbon
E <sub>g</sub>	Energy gap
FTIR	Fourier transform infrared
GLCH	Graphite-like hydrogenated carbon
GLCHH	Highly hydrogenated GLCH
H <sub>2</sub>	Hydrogen
LA	Longitudinal acoustic
LO	Longitudinal optic
nc-Si:H	Hydrogenated nanocrystalline silicon
O	Oxygen
PECVD	Plasma enhanced chemical vapour deposition
PL	Photoluminescence
PLCH	Polymer-like hydrogenated carbon

PVD	Physical vapour deposition
r.f.	Radio frequency
Si	Silicon
SiH <sub>4</sub>	Silane
SiO <sub>x</sub>	Silicon oxide
TA	Transverse acoustic
ta-C:H	Tetrahedral hydrogenated amorphous carbon
TO	Transverse optic
UV-Vis-NIR	Ultraviolet-visible-near infrared

---

## LIST OF PUBLICATIONS

### Full-paper (ISI-cited)

1. **Nur Maisarah Abdul Rashid**, Richard Ritikos, Maisara Othman, Noor Hamizah Khanis, Siti Meriam Ab Gani, Muhamad Rasat Muhamad, Saadah Abdul Rahman, 'Amorphous silicon carbon films prepared by hybrid plasma enhanced chemical vapor/sputtering deposition system: Effects of r.f. power', *Thin Solid Films*, 2012.
2. Maisara Othman, Richard Ritikos, Noor Hamizah Khanis, **Nur Maisarah Abdul Rashid**, Saadah Abdul Rahman, Siti Meriam Ab Gani, Muhamad Rasat Muhamad, 'Effects of rf power on the structural properties of carbon nitride thin films prepared by plasma enhanced chemical vapour deposition', *Thin Solid Films*, 519 (15), 4981-86.
3. Maisara Othman, Richard Ritikos, Noor Hamizah Khanis, **Nur Maisarah Abdul Rashid**, Siti Meriam Ab Gani, Saadah Abdul Rahman, 'Effect of N<sub>2</sub> flow rate on the properties of CN<sub>x</sub> thin films prepared by radio frequency plasma enhanced chemical vapour deposition from ethane and nitrogen', *Thin Solid Films*, 2012.
4. Noor Hamizah Khanis, Richard Ritikos, Maisara Othman, **Nur Maisarah Abdul Rashid**, Siti Meriam Ab Gani, Muhamad Rasat Muhamad, Saadah Abdul Rahman, 'Effect of pre-deposited carbon layer on the formation of carbon nitride nanostructures prepared by radio-frequency plasma enhanced chemical vapour deposition', *Materials Chemistry and Physics*, 130 (1), 218-22.
5. Noor Hamizah Khanis, Richard Ritikos, Maisara Othman, **Nur Maisarah Abdul Rashid**, Siti Meriam Ab Gani, Saadah Abdul Rahman, 'Catalyst free carbon nitride nanostructures prepared by rf-PECVD technique on hydrogenated amorphous carbon template', *Materials Chemistry and Physics*, 2013.

### Conference papers (non-ISI cited)

6. **Nur Maisarah Abdul Rashid**, Richard Ritikos, Goh Boon Tong, Siti Meriam Ab Gani, Muhamad Rasat Muhamad, Saadah Abdul Rahman, 'Effect of thermal annealing on the properties of highly reflective nc-Si:H / a-CN<sub>x</sub>:H multilayer films prepared by r.f. PECVD technique'. Paper presented at the 25<sup>th</sup> Regional Conference on Solid State Science and Technology (RCSSST 2009), Penang.
7. **Nur Maisarah Abdul Rashid**, Richard Ritikos, Maisara Othman, Noor Hamizah Khanis, Siti Meriam Ab Gani, Muhamad Rasat Muhamad, Saadah Abdul Rahman, 'Physical characteristics of amorphous carbon films prepared by plasma enhanced chemical vapour deposition'. Paper presented at the 5<sup>th</sup> International Conference on Technological Advances of Thin Films and Surface Coating (Thin Films 2010), China.



## CHAPTER 1

### INTRODUCTION

#### 1.0 Chapter Outline

This chapter gives an introduction for this work which covers hydrogenated amorphous carbon (a-C:H) and amorphous silicon carbon (a-SiC) thin films. Plasma enhancement of chemical vapour deposition (CVD) and sputtering processes are also presented. This is followed by research objectives and thesis outline.

#### 1.1 Research Background

##### 1.1.1 Hydrogenated Amorphous Carbon and Amorphous Silicon Carbon Thin Films

Carbon (C) based materials such a-C:H and C-rich a-SiC are well known for having various kind of structures. This has captured a great deal of interest since decades ago, due to their interesting properties and potential candidate for application in various optoelectronic devices (Jun et al., 2002).

The ability of C atoms to form three hybridized states as shown in Figure 1.1 is very unique and this makes a-C:H film a very interesting material with many potential applications. These group of films also referred to as ‘diamond-like carbon’ (DLC) films consist of various forms of unhydrogenated and hydrogenated a-C films with a wide range of hydrogen content (Maréchal et al., 1998).

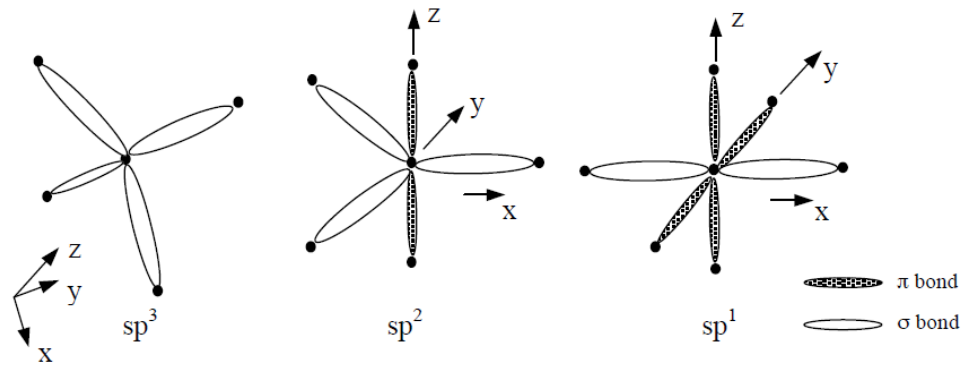


**Figure 1.1:** Carbon hybridization comprised of  $sp^1$ ,  $sp^2$  and  $sp^3$  structure (Silva 2003).

Doping a-C:H with other materials makes it even more interesting. In 1990s, doping elements such as phosphorus, lithium, fluorine, titanium, chromium, nitrogen, boron, and silicon (Si) have been widely used to release the internal stress and improve the adhesion strength of DLC films. The latter is to avoid the films from ‘peeling-off’ the substrate during the deposition process (Ji et al., 2008; Liu et al., 1997). Incorporation of Si into a-C:H also reduces film stress while maintaining the hardness, friction, and wear (Shi et al., 1999). In this sense, Si can either be incorporated into the film as dopant elements or be directly bonded into the C network to form Si-C bonds. The product of the incorporation will form a-SiC film. This Si based thin film has attracted even more interest since the discovery by Spear and Lecomber in 1975 that amorphous silicon (a-Si) can be doped by C (Bulot et al., 1987). The unique aspect of a-SiC is that its properties can be easily controlled by manipulating the composition of either C or Si in the films (Pascual et al., 1995).

Various deposition techniques have been employed to deposit a-SiC films. CVD technique such as radio frequency plasma enhanced chemical vapour deposition (r.f. PECVD), inductively coupled plasma CVD, helicon wave PECVD, electron cyclotron resonance CVD, catalytic CVD and hot wire CVD have been widely used. In most work, these technique uses gas sources for both Si and C elements, typically silane ( $\text{SiH}_4$ ) and methane ( $\text{CH}_4$ ), respectively. For these work, the film compositions have been widely studied in terms of the variation in  $\text{CH}_4$  to  $\text{SiH}_4$  gas ratio (Cheng et al., 2008; Chew, 2002; Kumbhar et al., 2001; Swain, 2006; Xu, 2005; Yu et al., 2004). By manipulating the ratio of  $\text{CH}_4$  and argon (Ar) or  $\text{CH}_4$  and  $\text{SiH}_4$  gas sources, the films can be tailored from C-rich a-SiC to Si-rich a-SiC.

One of the disadvantages of these systems is the use of highly flammable or toxic gasses, particularly when  $\text{SiH}_4$  is used. There are reports of alternative gasses used such as that reported by Rajagopalan et al. (2003) who proposed the use of organosilicon sources containing both Si and C as constituent. Examples of organosilicon sources are tetramethylsilane, diethylsilane and hexametyldisilane. These gas sources have the advantage of using a single source for both silicon and carbon. However these gases are also toxic in nature.

An even better alternative is the use of pure solid Si source. Such solid sources can be used together with physical sputtering technique. Moreover, sputtering methods are preferable due to their versatility and widespread use (Park et al., 2004). Sputtering technique has been well developed throughout the years after having gone through various modifications to enhance its performance and making it suitable for various materials including a-SiC (Bulot et al., 1987). However, there are still grounds for further improvement and versatility.

### **1.1.2 Plasma Enhancement of Chemical Vapour Deposition and Sputtering Processes**

The kinetics of r.f. discharge employing a two parallel electrodes setup is an important criteria in film deposition process (Mutsukura et al., 1995). Generally, plasma generation between the powered and grounded electrode are related to the movement of ions between them. The understanding of plasma kinetics, dissociation of the precursor and other sequential plasma chemical reactions are very important in the use of plasma process to grow C based thin films from CH<sub>4</sub> gas mixed with other gases like hydrogen (H<sub>2</sub>) and Ar.

Dissociation of CH<sub>4</sub> gives rise to multitude of neutral, free radicals and ionic species from collisions between molecule-molecule, neutral-molecule, ion-molecule and electron. Amongst these, the electron collision remains the main interaction which maintains the dissociation of the precursors.

In a sputtering process, heavy Ar ions effectively bombard a target surface and sputter atoms off the target resulting in film growth. Sputtering amorphous silicon (a-Si) target in CH<sub>4</sub> atmosphere can result in the growth of a-SiC or Si doped a-C:H films. Another advantage of this process is that CH<sub>4</sub> fragmentation can be enhanced by the Ar gas in the plasma (Raveh et al., 1992). Nasser et al. (1971) have noted that Ar can be an important additional source of active species which contributes to the gas phase process such as the charge transfer reaction.

## **1.2 Inspirations and Research Objectives**

The home-built r.f. PECVD in Low Dimensional Material Research Centre, Department of Physics, University of Malaya has been developed to produce Si based thin films such as hydrogenated a-Si (Goh et al., 2012), hydrogenated nanocrystalline

silicon (nc-Si:H) (Goh et al., 2011) and multilayered nc-Si:H/hydrogenated amorphous carbon nitride (Ritikos et al., 2009). However, this process uses  $\text{SiH}_4$  gas as the precursor gas source. There is a need for a new system in the laboratory which is capable of depositing Si based films without the use of this highly toxic and flammable gas. The idea is to combine the advantages of both r.f. PECVD and sputtering technique in this system to grow Si based thin films. This home-built hybrid r.f. PECVD/sputtering system can fulfill the need for a simple, affordable, flexible and environmental friendly deposition system for growth of Si based thin films.

The main objective of this work is to develop an environmental friendly deposition system for the growth of Si based thin films without the use of  $\text{SiH}_4$ . In this work, hybrid r.f. PECVD/sputtering system which combines the r.f. PECVD and r.f. sputtering deposition processes is tested and used for the growth of a-SiC films. In order to achieve this main objective, sub-components of this work are done with the following objectives:

1. To determine the structural and optical properties of a-C:H films grown by the r.f. PECVD component of the hybrid system at different total gas pressure.
2. To determine the structural and photoluminescence (PL) emission properties of a-SiC films grown by the r.f. sputtering component of the hybrid system at different Ar gas flow-rates.
3. To determine the structural and PL emission properties of a-SiC films grown by the newly developed hybrid r.f. PECVD/sputtering system at different r.f. power.

### 1.3 Thesis Outline

Chapter 1 presents a brief introduction to this research work. This is then followed by Chapter 2 which highlights literature reviews related to this study. This chapter covers two major aspects. The first aspect focuses on describing the deposition system used in this work, namely the r.f. PECVD and hybrid r.f. PECVD/sputtering system. The second aspect looks into various properties of hydrogenated a-C:H and a-SiC thin films. The properties are reviewed based on the growth rate, structural and optical characteristics of the films.

Chapter 3 describes in detail the experimental and analytical measurements used in this study. These include the brief description on the setup of the r.f. PECVD and hybrid r.f. PECVD/sputtering system. This is followed by the sample preparation, deposition procedures for both systems, and film characterization techniques.

Chapter 4 presents and discusses the results of the film characterization. This chapter emphasized on the effects of total gas pressure,  $P_T$  to a-C:H thin films prepared by r.f. PECVD techniques. Effects of Ar flow rate and r.f. power on a-SiC deposited by hybrid r.f. PECVD/sputtering system is also reported.

Finally, Chapter 5 presents the conclusions and also lists a few suggestions for future work.

## CHAPTER 2

### LITERATURE REVIEW

#### 2.0 Chapter Outline

This chapter explicates the literature review which covers two major aspects of this research work. The first aspect focuses on the two different types of deposition techniques which combine makes up the home-built hybrid radio frequency plasma enhanced chemical vapour deposition (r.f. PECVD)/sputtering used in this work. These techniques include stand-alone r.f. PECVD and sputtering deposition systems typically used in the fabrication of silicon (Si) and carbon (C) based materials. The second aspect of this chapter looks into various properties of hydrogenated amorphous carbon (a-C:H) and amorphous silicon carbon (a-SiC) thin films studied by other researchers.

#### 2.1 Review on Deposition Techniques for Silicon and Carbon Based Films

Numerous deposition techniques have been explored and employed for the development of Si and C based materials such as r.f. PECVD (Ritikos et al., 2009), r.f. magnetron sputtering (Higa et al., 2006; Xu et al., 2005), r.f. sputtering (Vovk et al., 2009), ion-beam deposition (Liao et al., 2002; Silinskas et al., 2008; von Keudell et al., 2002), middle frequency plasma chemical vapour deposition (Guo et al., 2011), and electron cyclotron resonance chemical vapour deposition (Yoon et al., 2000). Among these, r.f. PECVD and sputtering are of keen interest in this research work. The following section discusses these two techniques to show why these processes are favored.

### **2.1.1 Radio Frequency Plasma Enhanced Chemical Vapour Deposition System: Hydrogenated Amorphous Carbon Thin Films**

The r.f. PECVD system used in this research work is available in Low Dimensional Material Research Centre, University of Malaya. It has been well-developed and widely used in producing Si and C based thin films (Awang et al., 2006; Azis et al., 2007; Khanis et al., 2011; Othman et al., 2012; Othman et al., 2011; Ritikos et al., 2009). This home-built system not only reduces the cost of its setup and maintenance but also allows modification according to the need of the user.

r.f. PECVD is different from the physical vapour deposition (PVD) technique such as sputtering, reactive sputtering, and ion beam sputtering as it offers a low temperature deposition condition (Jutarosaga et al., 2006; Vakerlis et al., 1991) and gas pressure (Cavallotti et al., 2004; Jaskorzynska et al., 2008). It can deposit thin films at higher deposition rate due to the advantage of the plasma generated by the system (Cavallotti et al., 2004; Ritikos et al., 2009). Plasma activates the chemical reaction at the surface of the substrate by generating reactive species in gas phase (Cavallotti et al., 2004). r.f. PECVD is also a favorable technique since it is cost-effective, relatively easier to operate (Motta et al., 2004; Ritikos et al., 2009) and can produce large uniform area of deposited films (Jutarosaga et al., 2006; Motta et al., 2004). Furthermore, it possesses the benefits of the high-energetic electrons that can break the chemical bonds when colliding with neutral gas molecules (Zhi-hong et al., 2008).

In r.f. PECVD system, plasma is generated by an alternating current power supply. A conventional r.f. generator operating at frequency of 13.56 MHz is typically used to initiate the plasma. It accelerates the electrons and ions of reactant gases to generate reacting species (Jaskorzynska et al., 2008). Parallel electrodes configuration is used in most of the commercial system (Cavallotti et al., 2004). Typically, the r.f. is



applied on one electrode while another electrode is grounded. Plasma is generated between these parallel anode and cathode electrodes (Alexandrov, 1995; Viana et al., 2010). This is called capacitively coupled r.f. plasma (Alexandrov, 1995; Vakerlis et al., 1991). The plasma allows chemical reaction of precursor gases to take part inside the chamber. The use of capacitive coupling makes the production of plasma more efficient since the molecules, radicals and ions of gases gain higher energies as they follow oscillatory paths between the electrodes. Dissociation and ionization of the gas molecules inside the plasma result in collisions of the radicals with excess molecules and other radicals which contribute to the film formation.

According to Ritala et al. (2008) the interdependence between deposition parameters are minimal for r.f. PECVD system. Thus, by controlling the deposition parameters such as gas ratio and r.f. power, customization of the film properties can be obtained.

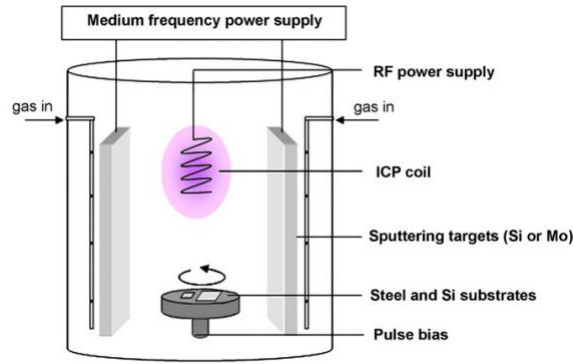
### **2.1.2 Sputtering Mechanism and Techniques: Amorphous Silicon Carbon Thin Films**

Sputtering is a PVD technique which does not involve any complicated chemical reaction. Physical sputtering becomes very popular several decades ago since it is versatile due to its low operational cost and employs solid sources, thus avoiding the use of toxic gases such as  $\text{SiH}_4$ . Normally, the sputtering process is carried out by using heavy ions such as helium and argon (Ar) (Bullot et al., 1987). The presence of reactive gases also contributes to the sputtering, in addition to the deposition conditions. Sputtering is also a very versatile method since a variety of material such as metals can be sputtered to form a metal-doped film (Bullot et al., 1987). However, the disadvantage of this technique is its low deposition rate (Bullot et al., 1987) with considerable amount of impurities from the target such as oxides (Kassiba et al., 2002).

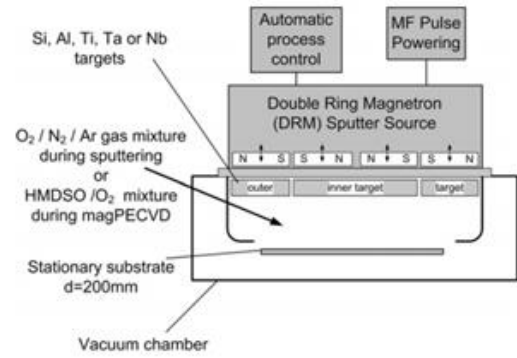
Sputtering is a process whereby the atoms are ejected from the surface of a solid target material due to bombardment by energetic particles. Ion bombardment is a critical parameter which strongly influences the structure and properties of the deposited films (Kelly et al., 2000; Wang et al., 1998). r.f plasma is used to split gas molecules into energetic ions and create high energy particles which bombard and sputter the target. Movements of the sputtered atoms are facilitated by charge difference between the target (powered) and substrate (grounded) electrodes. The sputtered atoms from the target material will move towards the grounded electrode and form thin films on the substrate. It is normal that the deposited films from sputtering process hold the compositions of the target. Generally, SiC thin films deposited by sputtering technique involve the process of bombarding a single SiC target or co-sputtering of two different targets made up of Si and graphite in Ar environment (Bulot et al., 1987; Li et al., 2007). Additionally, adding gas sources such as  $\text{SiH}_4$  and  $\text{CH}_4$  could provide the necessary Si and C elements for the films.  $\text{SiH}_4$  would bombard the graphite target while  $\text{CH}_4$  tends to bombard the Si target in order to produce SiC thin films (Ghodselahi et al., 2008; Le Contellec et al., 1979; Wang et al., 1998).

### **2.1.3 Hybrid System Involving Sputtering Technique**

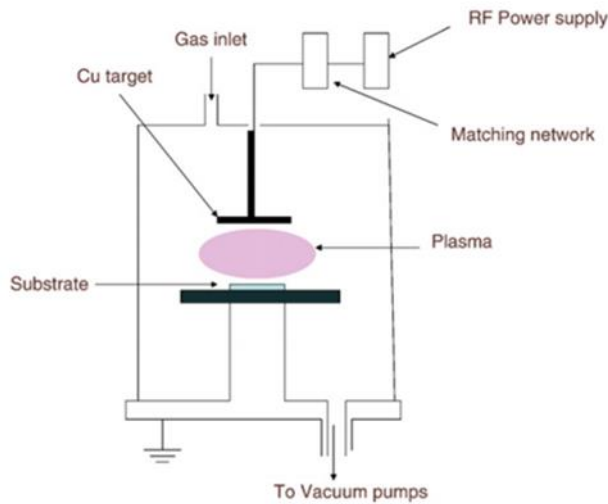
Hybrid or combined deposition system has been widely employed by researchers by combining typical sputtering technique with another deposition system. Examples of different hybrid setup are shown in Figure 2.1.



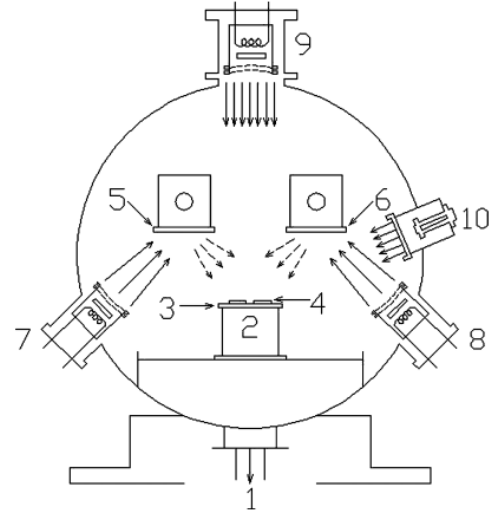
(a) (Ji et al., 2008)



(b) (Frach et al., 2010)



(c) (Ghodselahi et al., 2008)



(d) (G. Li et al., 2007)

**Figure 2.1:** Schematic illustration for deposition setup of (a) Unbalance magnetron sputtering combined with inductively coupled r.f. plasma chemical vapour deposition (b) Magnetron sputtering and PECVD (c) Co-deposition process of r.f. sputtering and r.f. PECVD (d) Combined metal vapour vacuum arc (MEVVA) ion implantation with ion beam assisted deposition (IBAD).

Combination of r.f. plasma and magnetron sputtering deposition process has been studied by Chan et al. (2011), A. Mahmood et al. (2000) and Liu et al. (2002). A hydrogenated diamond-like carbon (DLCH) with a copper dopant (Cu/a-C:H) was deposited on glass substrate under various Ar to CH<sub>4</sub> gas mixture. The advantage of using such system is the low substrate temperature allowing the use of various temperature-sensitive substrates. Other modification and customization of relevant

hybrid system includes the use of unbalanced magnetron sputtering combined with inductively coupled r.f. PECVD to form molybdenum-doped DLC thin films studied by Ji et al. (2008). The system consists of pulse bias assisted r.f. inductively coupled plasma chemical vapour deposition unit and medium frequency unbalanced magnetron sputtering unit (Ji et al., 2008). Besides that, combined magnetron PECVD and sputtering deposition technique have been developed to adopt the process pressure of the conventional PECVD and sputtering process which work under different deposition pressure (Ji et al., 2008). Hard and brittle metal oxide can be coated to soft and elastic polymer substrates by combining these two processes.

The hybrid r.f. PECVD/sputtering setup used by T. Ghodselahi et al. (2008) shown in Figure 2.1 (c) resembles the one used in this work. They have used this so called co-deposition of r.f. sputtering and r.f. PECVD method to deposit nanoparticle Cu/C composite films (Ghodselahi et al., 2008). Acetylene ( $C_2H_2$ ) gas and Cu target were used as precursor gas and target, respectively (Ghodselahi et al., 2008).  $C_2H_2$  was used as both reactive and bombarding gas in this r.f. plasma system. They studied the deposition process by changing the deposition pressure at constant power regime. The change in deposition pressure to lower value causes the physical sputtering mode to take over the r.f. PECVD deposition process.

## **2.2 Review on Properties of Hydrogenated Amorphous Carbon Thin Films**

a-C:H thin films are of keen scientific interest since the 70's until recent years due to their unique tunable structure and properties (Schwan et al., 1996). They have been deposited in various ways to produce a wide range of film properties (Valentini et al., 2001). These include chemical inertness, extreme hardness, optical transparency, low friction coefficient, good thermal conductivity, good electrical insulation and even

exhibit high photoluminescence (PL) efficiency (Liao et al., 2002; Liu et al., 1997; Rusli et al., 1995; Tomasella et al., 2001; von Keudell et al., 2002). These properties make them promising candidates for various applications such as protective and optical coatings, planarization layers for device fabrication and light-emitting devices (Liao et al., 2002; Liu et al., 1997; Tomasella et al., 2001).

Hydrogen (H) plays a major role in determining the film properties (Marins, 2011; Silinskas et al., 2008). H mainly passivates dangling bonds in such films. In  $sp^2$  rich films, the incorporation of H saturates  $\pi$  bonds and thus promotes  $sp^3$  bonding. At high H concentration this results in films with high energy gap,  $E_g$  (Awang et al., 2006; Dieguez Campo et al.; Maître et al., 2005). Different hydrogen content,  $C_H$  and chemical bonding configurations would likely modify a-C:H film structures, changing it from hard DLCH films to soft polymer-like carbon (PLCH) films (Awang et al., 2006). These can be effectively controlled by manipulating the deposition parameters and techniques used (Awang et al., 2006; Neyts et al., 2007; Ritala et al., 2008; Silinskas et al., 2008; Valentini et al., 2001). Numerous investigations have been carried out to understand the films growth, structural and optical properties by various analytical instruments.

### **2.2.1 Growth Rate of Hydrogenated Amorphous Carbon Thin Films**

Hydrocarbon source can be chosen from different gases such as  $CH_4$ ,  $C_2H_2$ , ethylene and benzene (Deng et al., 2011). Among this,  $CH_4$  is typically used. From the  $CH_4$  discharge, methyl ( $CH_3$ ) is a predominant species which are generated in the plasma (Guo et al., 2011; Liu et al., 1997; Tomasella et al., 2001; von Keudell et al., 2002). It is very important to understand the role of  $CH_3$  radicals and ions since they play an important role in the growth of a-C:H thin films (Liao et al., 2002). Deposition

parameters such as r.f. power, gas flow rate and deposition pressure strongly influence the impact energy of the ions impinging the surface of the substrate (Awang et al., 2006; Maréchal et al., 1998; Ryu et al., 2000; Silinskas et al., 2008; Viana et al., 2010).

A good example which explains the growth kinetics of these films is seen from the work of Cavalotti et al. (2004) which investigate the deposition and etching of thin solid films by weakly ionized plasma and relate the physical events and chemical reactions. They also discuss the influence of ion bombardment on the morphological and chemical evolution of the deposited films (Cavallotti et al., 2004). The discussion could be summarized into two phases. The first phase is related to the concentration, energy and reactivity of produced molecules, radicals, ions and electrons in the gas phase. The second phase occurs close to the film surface and involves the ion bombardment which has a significant impact on the surface chemistry.

Details on growth mechanism at the film surface have been elaborated by Neyts et al. (2007). Various processes occur at the film surface throughout the growth of a-C:H thin films are shown in Figure 2.2.

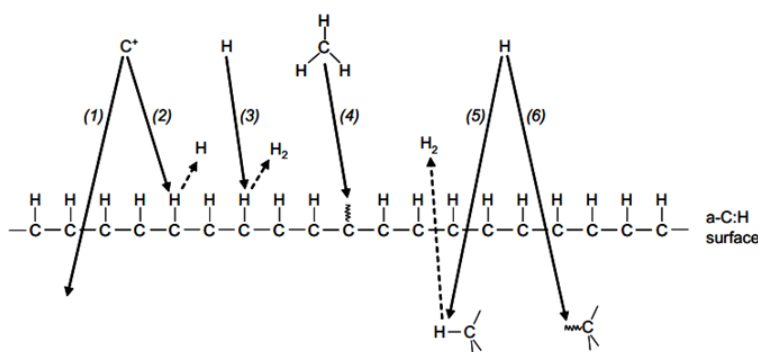


**Figure 2.2:** Schematic diagram of the deposition process in a-C:H film growth involving (1) ion subplantation, (2) creation of surface dangling bond by ion impact, (3) creation of surface dangling bond by H-abstraction, (4) radicals passivating the surface dangling bond, (5) H-abstraction from subsurface C-H bonds, (6) H repassivating subsurface dangling bonds (Neyts et al., 2007).

The diagram also illustrates the role of H atoms for film growth. Using r.f. PECVD method allows not only ions but also neutral species (radicals) to take part in the growth process (Neyts et al., 2007).

Chemical reaction at the surface of the films determines the sticking coefficient of neutral species and thus influences the growth rate of the films (Cavallotti et al., 2004; Neyts et al., 2007).  $\text{CH}_3$  radicals cannot passivate directly into surface bonds but can react with the surface if dangling bonds are present. The dangling bond can be created by H radicals from the plasma.

H concentration in the plasma also influences the growth of the films (Higa et al., 2006). Synergism between H atoms and  $\text{CH}_3$  radicals is very important in determining the growth rate of the films (Neyts et al., 2007). H is responsible for two different effect as it can increase or decrease the growth rate by H etching effect if excessive H is applied (Awang et al., 2006; Deng et al., 2011; Goswami et al., 2008; Neyts et al., 2007; S. Yang et al., 2009).

### **2.2.2 Structural Properties of Hydrogenated Amorphous Carbon Thin Films**

The structure of a-C:H was not fully understood until a structural model was developed by Robertson et al (1995, 1996). Numerous researchers refer to these studies in order to analyze structural properties of a-C:H thin films specially when characterized by Raman spectroscopy. Fourier transform infrared (FTIR) spectroscopy can be used to study the structural properties in term of chemical composition and bonding.

a-C:H can be classified into four groups which consist of graphite-like a-C:H (GLCH), tetrahedral hydrogenated carbon (ta-C:H), DLCH and PLCH (Casiraghi, Ferrari, et al., 2005; Casiraghi, Piazza, et al., 2005). The classification can be simplified as shown by the ternary phase diagram for H-free and a-C:H thin films in Figure 2.3. Among them, GLCH contain the lowest  $C_H$  of less than 20 % and high  $sp^2$  clustering and  $sp^2$  content. The energy gap,  $E_g$  is typically under 1 eV. a-C:H with highest  $C_H$  of 40 to 60 % can be classified as PLCH. These films have approximately 70 % of H terminated  $sp^3$  bond. DLCH have intermediate  $C_H$  of 20 to 40 %. These films have low overall  $sp^3$  content but contain higher C-C  $sp^3$  compared to PLCH. Their  $E_g$  ranges from 1 to 2 eV. ta-C:H falls within the category of DLCH but with significant C-C  $sp^3$ . This content can be as high as 70 % even when  $C_H$  is regulated at 25 %. The  $E_g$  can reach up to 2.3 eV.

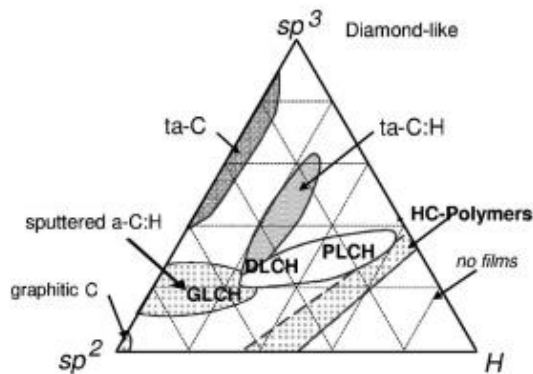


**Figure 2.3:** Ternary diagram illustrates four classes of a-C:H (Casiraghi et al. 2005).

Some studies also found another class consisting of highly hydrogenated GLCH (GLCHH) (Casiraghi, Ferrari, et al., 2005). This class is unusual, but can be obtained when films are deposited by PECVD in  $CH_4$  and  $H_2$  environment (Casiraghi, Ferrari, et al., 2005). Raman parameter for this film show GLCH characteristics but has higher PL background. The  $C_H$  is greater than 20 % (Casiraghi, Ferrari, et al., 2005).



Typical Raman spectra for GLCHH compared to GLCH and PLCH are shown in Figure 2.4. It is apparent that structural properties of a-C:H are directly dependent on  $sp^2$ ,  $sp^3$  and  $C_H$ .

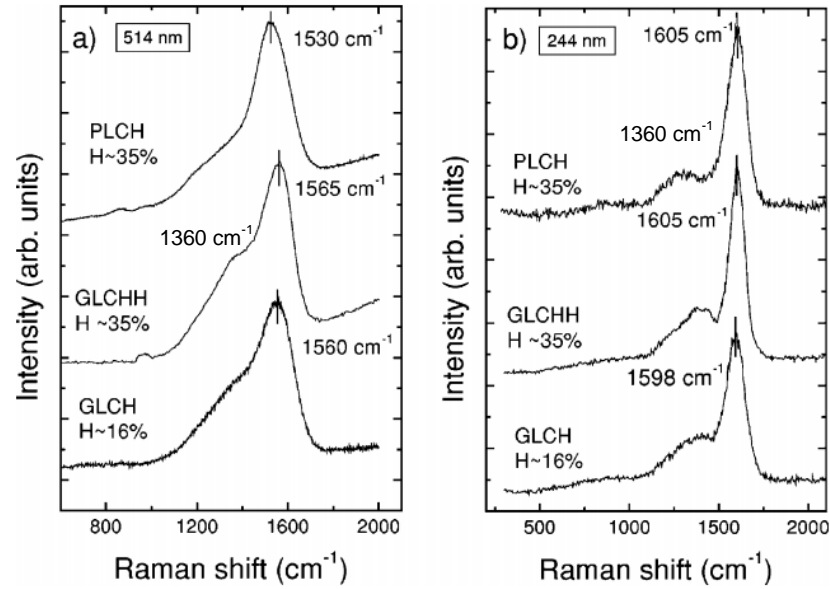


**Figure 2.4:** Typical Raman spectra for different types of a-C:H thin films (Casiraghi, Ferrari, et al., 2005).

All a-C:H thin films exhibit similar Raman spectra within the range of 800 to 2000  $cm^{-1}$  region. For both visible excitation of 514 nm and ultra violet (UV) excitation of 244 nm, the spectra mainly consist of two peaks centered at around 1360 and 1560  $cm^{-1}$  which are assigned to the so-called D and G peaks, respectively. The D peak is a disorder-induced band and is due to the breathing modes of  $sp^2$  atoms in rings, while the G (Graphite) peak is due to the bond stretching of all pairs of  $sp^2$  atoms in both rings and chains (Buijnsters et al., 2009; Deng et al., 2011; Silinskas et al., 2008; Veres et al., 2008). In the case of visible excitations, both D and G peak are due to  $sp^2$  sites which shows that the Raman spectra are dominated by these  $sp^2$  sites (Casiraghi, Ferrari, et al., 2005; Ferrari et al., 2003). For UV laser source, an additional peak found at approximately 1060  $cm^{-1}$  can be observed. This peak corresponds to the T peak

associated to C-C  $sp^3$  vibrations. Higher PL background can overshadow the D and G peaks as illustrated in Figure 2.5.

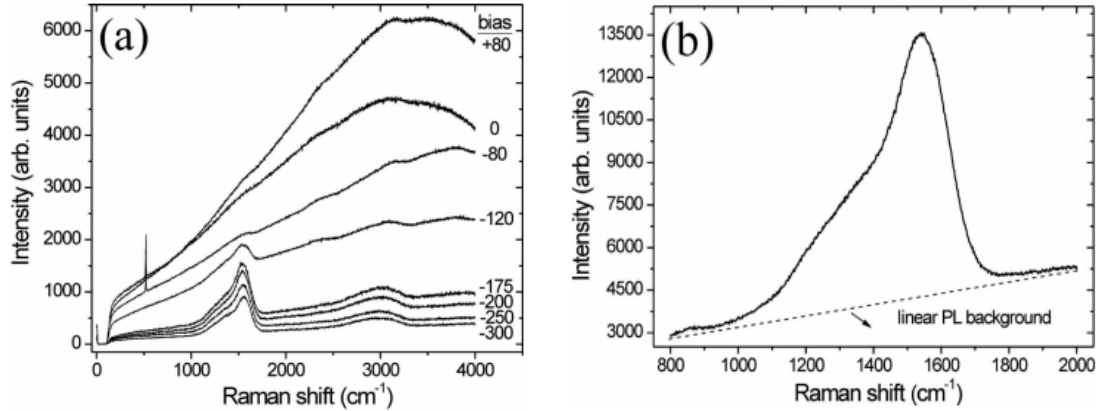


**Figure 2.5:** Typical Raman spectra with significant PL background (Buijnsters et al. 2009).

Additional peaks apart from the D and G should also be considered. This include a peak located at  $1180\text{ cm}^{-1}$  attributed to  $sp^3$ -rich phase (Schwan et al., 1996) and a peak at  $1150\text{ cm}^{-1}$  related to  $sp^3$ -C with some  $sp^2$  contributions (Chu et al., 2006).

On the other hand, auxiliary gases like H can greatly affect the structure of a-C:H films in such a way that it links the amount and configuration of the  $sp^2$  phase with the  $sp^3$  content (Casiraghi, Ferrari, et al., 2005; Deng et al., 2011). H can also affects the structure of the films by decreasing the  $sp^2$ -C bonds and increase the C-H bonds due to the higher probability of passivating dangling bonds which otherwise would form C-C bonds (Silinskas et al., 2008).

High  $C_H$  in a-C:H would typically exhibit high PL background in Raman measurement (Buijnsters et al., 2009) as shown in Figure 2.5. The dotted line in Figure 2.5 (b) shows the interpolation of the PL background from the Raman spectra.  $C_H$  can be estimated from this interpolation using an approximation listed in Equation 2.1.  $C_H$  is calculated using the ratio between the slope ( $m$ ) of the fitted linear background and the height of the G band ( $H_G$ ) measured in micron,  $m/H_G$  (Casiraghi, Ferrari, et al., 2005a; Casiraghi, Piazza, et al., 2005; Xie et al., 2010).

$$C_H \text{ (at \%)} = 21.7 + 16.6 \log \left\{ \frac{m}{H_G} [\mu\text{m}] \right\} \quad \text{..... (Equation 2.1)}$$

Alternatively,  $C_H$  can also be calculated from FTIR spectroscopy. Typically, the FTIR spectra of a-C:H will exhibit a broad absorption band at around 2600 to 3300  $\text{cm}^{-1}$  which is attributed to various C-H vibration modes (Son et al., 2001). A typical C-H band in this region is shown in Figure 2.6.

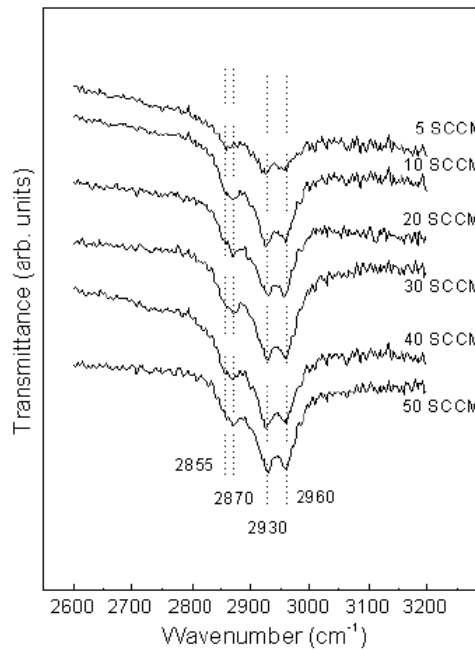


**Figure 2.6:** Typical FTIR spectra within the range of 2600 to 3200  $\text{cm}^{-1}$  which assigned to C-H stretching modes (Son et al. 2001).

This absorption band is made up of several overlapping peaks. This includes the peaks at 2855, 2870, 2930 and 2960  $\text{cm}^{-1}$  associated to  $\text{sp}^3\text{-CH}_2$  (symmetric),  $\text{sp}^3\text{-CH}_3$  (symmetric),  $\text{sp}^3\text{-CH}_2$  (asymmetric) and  $\text{sp}^3\text{-CH}_3$  (asymmetric), respectively. Additionally,  $\text{sp}^2\text{-CH}_2$  and  $\text{sp}^2\text{-CH}$  bonding peaks can be found at 2950  $\text{cm}^{-1}$  and 3000  $\text{cm}^{-1}$ , respectively (Son et al., 2001).

To analyze the FTIR spectra, they are normalized to the film thickness and deconvoluted using Gaussian fitting to obtain the total integrated area under the spectra. The relative hydrogen content,  $C_H$  is estimated using the relation

$$C_H = \frac{A}{N_C} \int \frac{\alpha(\omega)}{\omega} d\omega \quad \dots\dots\dots \text{(Equation 2.2)}$$

where  $\int \frac{\alpha(\omega)}{\omega} d\omega$  is the integrated intensity of the C-H absorption band at approximately 2900  $\text{cm}^{-1}$ .  $A$  is the proportionality constant for this C-H mode. The value of  $A$  used for this work is  $1.35 \times 10^{21} \text{ cm}^{-2}$  (Huang et al., 2002; Liu et al., 1997a).  $N_C$  is the atomic density of carbon atoms in diamond which is taken as  $1.76 \times 10^{23} \text{ cm}^{-3}$ . The absorption coefficient at wavenumber  $\omega$ ,  $\alpha(\omega)$  was normalized to the film thickness.

### 2.2.3 Energy Gap and Photoluminescence Emission Properties of Hydrogenated Amorphous Carbon Thin Films

According to structural model of a-C:H, these films are made of  $\text{sp}^2$  hybridized C atoms which form cluster in chain or rings (Füle et al., 2006). This forms the basis of the so-called cluster model whereby these  $\text{sp}^2$  bonded clusters are embedded in the amorphous  $\text{sp}^3$  matrix (Füle et al., 2006; Robertson, 1995; Rusli et al., 1996). The  $\text{sp}^3$  phases create the  $\sigma$  valence and  $\sigma^*$  conduction-band states, separated by a band gap in

the order of 6 eV. The lower optical gap is contributed by the  $\pi$  to  $\pi^*$  states which is made up of the  $sp^2$  phases in the films (Gupta et al., 2006). The size and configuration of  $sp^2$  clusters control the band gap (Robertson, 1996) and hence the optical properties.

In addition, photoluminescence (PL) emission is also related to the band gap of these films (Adamopoulos et al., 2004). Since the band gap is controlled by the  $sp^2$  configurations, PL occurs from the excitation and recombination of electron hole pairs which takes place within these  $sp^2$  clusters (Marchon et al., 1997; Rusli et al., 1995). Among others,  $C_H$  gives significant influence on the PL properties of the films (Deng et al., 2011). Introduction of H into the films helps saturates non-radiative recombination center thus producing stronger PL emission (Buijnsters et al., 2009; Casiraghi, Ferrari, et al., 2005; Marchon et al., 1997). PL intensity also tends to increase with  $C_H$  which may be due to longer localization of electron hole pair in its own cluster (Adamopoulos et al., 2004). While PL efficiency can be quenched when the  $E_g$  is narrowed, the narrowing of the  $E_g$  may not necessary decrease it since it may occur due to quantum confinement effect which would effectively increase PL efficiency.

### **2.3 Review on Properties of Amorphous Silicon Carbon Thin Films**

a-SiC films exhibit many noble properties such as high hardness, high thermal conductivity, good radiation resistance, good biocompatibility, improved high temperature stability and chemical inertness (Chung et al., 2008; Li et al., 2007; Mishra et al., 2007; Rashid et al., 2013; S. Lin, 2002; Swain, 2006; Swain and Dusane, 2006). Incorporation of Si into a-C:H has been reported to reduce film stress while maintaining the hardness, friction and wear (Rashid et al.; Shi et al., 1999). The Si doping also enhances corrosion resistance properties of amorphous carbon (Papakonstantinou et al., 2002; Rashid et al.). Potential applications include solar cells, photoluminescent

materials, optoelectronic devices and also high temperature engineering materials (Ahmed et al., 2011; Lien, 2011; Rashid et al.).

### **2.3.1 Growth Rate of Amorphous Silicon Carbon Thin Films**

Growth rate of a-SiC thin films strongly depends on the deposition method employed. There is various deposition techniques employed in the formation of a-SiC thin films. One of the popular methods is the r.f. PECVD. For this method, the growth rate can be easily controlled by varying certain deposition parameters such as r.f. power, deposition pressure and reactant gas ratio (Aida et al., 1996; Ambrosone et al., 2002; Xu, 2005; Yu et al., 2004). In most work, this method uses Si based gas source such as  $\text{SiH}_4$  and  $\text{S}_2\text{H}_2$  (Shi et al., 1999; Swain and Dusane, 2006). Summonte et al. (2004) reported the increase of growth rate with the increase in  $\text{SiH}_4$  flow rate. Racine et al. (2001) however obtained the trend in deposition rate that is opposite to the previous report, whereby the growth rate decreases with increasing  $\text{SiH}_4$  gas source. They believed this may be caused by lower incorporation efficiency of Si compared to C, higher etching or sputtering reaction of weaker Si-C bonds compared to C-C bonds (Racine et al., 2001). However, one of the most significant disadvantages of this method is the use of these highly toxic gases. Alternatively, it has been reported that the use of solid amorphous or crystalline Si sources can enhance the film formation and therefore increase the deposition rate of these films (Gupta et al., 2006; Lee et al., 2004).

Employing sputtering technique can meet the demand of eliminating the use of  $\text{SiH}_4$  for the deposition process. In sputtering process, ion bombardments are predominantly carried out by heavy ions typically Ar. Compare to H, Ar ion bombardment creates high surface defect density since the reaction between Si target and Ar ions only involves simple collisions (Umezu et al., 2002). If hydrocarbon gas

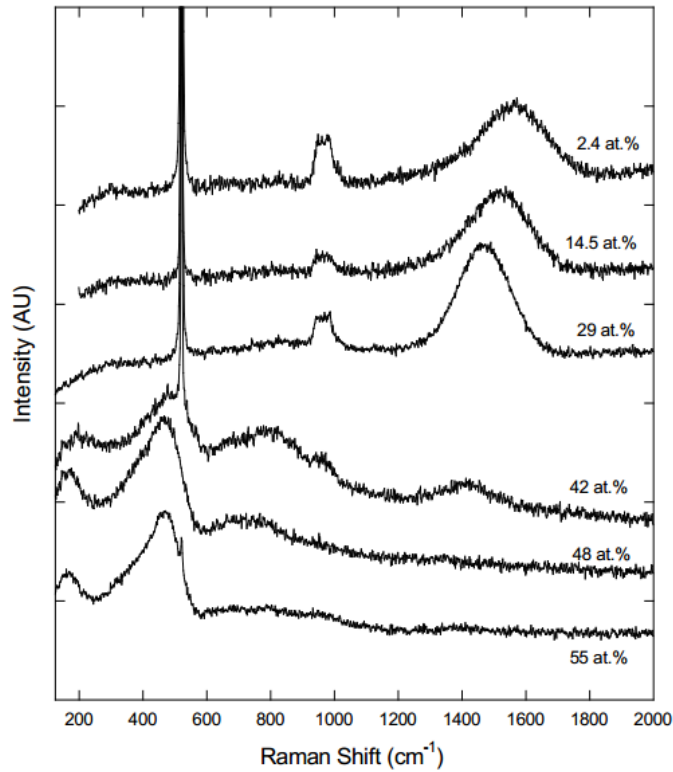
such as  $\text{CH}_4$  is discharged simultaneously with the Ar, this will create a reactive sputtering process which will further influence the deposition of the films (Gupta et al., 2006).

Ion bombardment is the main factor affecting the film grown from sputtering process and can be enhanced by applying high r.f. power (Aida et al., 1996). Apart from that, r.f. power would greatly influence the dissociation and ionization of hydrocarbon precursor and sputtering gas. Along with the r.f. power, varying the deposition pressure may also improve the density of the ions in the plasma (Aida et al., 1996). As a result, a much higher flux of energetic ions are imposed onto the substrate. Effect of deposition pressure at low r.f. power is less significant since the ionization process is low at this power range (Aida et al., 1996). It should be noted that the collision of Ar ions do not contribute to the film composition whereby they only distribute their kinetic energy towards the target.

### **2.3.2 Structural Properties of Amorphous Silicon Carbon Thin Films**

Raman spectroscopy is a well-known technique to detect both amorphous and crystalline C and Si phases. A number of recent research have employ this technique to study the structural characteristics of this films such as that of Ward et al. (2004) in the characterization of SiC monofilaments produced by CVD technique. Raman spectroscopy is able to identify small amount of C and Si that might be difficult for electron techniques. In terms of the C phases, ultra violet Raman (325 nm) can provide information for both  $\text{sp}^2$  and  $\text{sp}^3$  phases in the material (Adamopoulos et al., 2004). In the same way, Raman spectroscopy can detect and identify crystalline and amorphous Si phases in the film. Figure 2.7 shows typical Raman spectra for a-SiC films composed of various C and Si phases. These spectra show the D and G band within the range of

1000 to 1600  $\text{cm}^{-1}$  attributed to the presence of various  $\text{sp}^2$  and  $\text{sp}^3$ -C phases, and also the Si phase in the range of 150 to 1000  $\text{cm}^{-1}$ . Sharp protruding peak at 520  $\text{cm}^{-1}$  is ascribed to the optical phonon mode of crystalline silicon. Amorphous Si gives characteristic of broad band at around 480  $\text{cm}^{-1}$ .



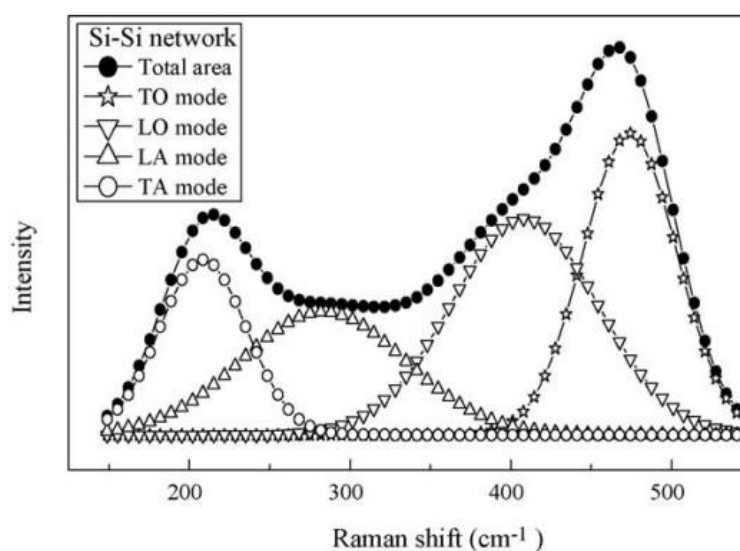
**Figure 2.7:** Raman spectra of a-SiC films composed of various Si content (Shi et al., 1999).

Figure 2.7 also illustrates variation in spectra for different Si and C composition in SiC films ranging from Si-rich to C-rich films (Shi et al., 1999). Swain (2006) obtained almost the same characteristics with increase in  $\text{S}_2\text{H}_2$  flow rate. c-Si substrate may exhibit background peak consisting of sharp first and second order Si peak at 520 and 950  $\text{cm}^{-1}$ , respectively (Cheng et al., 2008; Chew, 2002). For Si-rich a-SiC films, the broad a-Si spectra which comprises of Si-Si network may overlapped with the substrate signal. This broad a-Si spectra are the results of the superimpose of



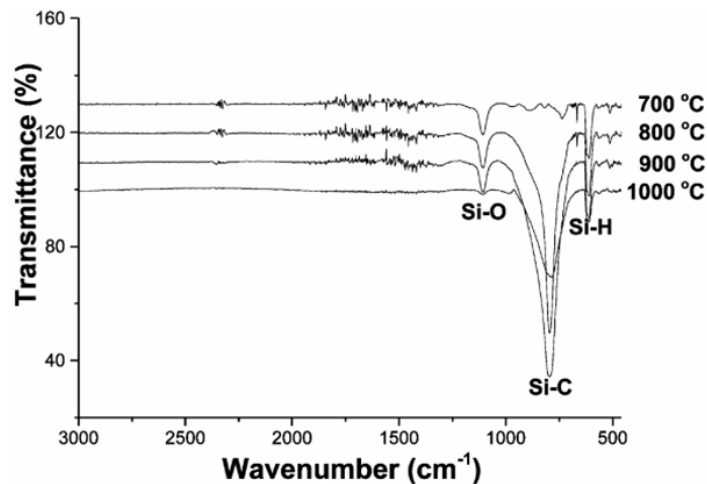
various peak at around 150, 300, 380 and 950  $\text{cm}^{-1}$  assigned to transverse acoustic (TA), longitudinal acoustic (LA), longitudinal optical (LO) and transverse optical (TO), respectively (Swain and Dusane, 2006). Films with intermediate Si and C content typically exhibit Raman spectra at around 650 to 1000  $\text{cm}^{-1}$  as shown in Figure 2.7 (Chew, 2002; Shi et al., 1999; Swain and Dusane, 2006; Swain and Dusane, 2007). This so called SiC band which assigned to SiC vibrational mode can be detected for the films with significant C concentration (Yu et al., 2004).

Figure 2.8 shows a typical deconvoluted spectrum in this region. A significant prominent TO peak suggest a significant ordering in atomic ring structure in the Si-Si network (Swain and Dusane, 2007). On the other hand, C-rich a-SiC films generally display a broad peak ranging from 1300 to 1500  $\text{cm}^{-1}$ . An additional peak at 1400  $\text{cm}^{-1}$  may be seen due to the presence of C bonded to Si or H atoms (Swain, 2006).



**Figure 2.8:** Typical deconvoluted peak of Si-Si network for a-SiC:H thin films (Swain and Dusane, 2007).

FTIR analysis can be used to support the information obtained from Raman spectroscopy. Typical FTIR spectra for SiC thin films are shown in Figure 2.9. The main features of the spectra include the peak at around 800 and 1100  $\text{cm}^{-1}$ . The absorption peak at approximately 790  $\text{cm}^{-1}$  is attributed to Si-C stretching mode (Cheng et al., 2008; Jung, 2003; Kumbhar et al., 2001; Li et al., 2011; Sha et al., 2005). Si-O stretching vibration can be observed at 1100  $\text{cm}^{-1}$  (Jung, 2003; Sha et al., 2005). Some researchers relate this peak to oxygen contamination during or after the deposition process (Li et al., 2011; Lin, 2002; Sundaram et al., 2000; Yu et al., 2004). Additionally, peak at 840  $\text{cm}^{-1}$  which assigned to Si-O-Si stretching vibrations can also be detected as reported by Dohi et al. (2002).



**Figure 2.9:** FTIR spectra of SiC thin films (Jung et al. 2003).

### 2.3.3 Photoluminescence Emission Properties of Amorphous Silicon Carbon Thin Films

The origin of PL is closely related to the structural properties of the films. The optical properties of the films can be tuned by manipulating the compositional ratio of C to Si in the films (Xu et al., 2005). PL in Si-rich hydrogenated a-SiC is similar to that of C-free hydrogenated a-Si films (Robertson, 1996). C content strongly influences the PL

intensity and peak position for such film (Coscia et al., 2008; Hu et al., 2004). By using the a-C:H framework as was discussed in Section 2.2.3, the PL mechanism of C-rich a-SiC can be interpreted by attributing it to the radiative recombination of photoexcited electron-hole pairs within  $sp^2$  clusters (Cheng et al., 2008; Robertson, 1996). PL can be quenched with the presence of non-radiative recombination centers (Cheng et al., 2008; Robertson, 1996) from paramagnetic Si dangling bonds (Robertson, 1996). PL of C-rich SiC is temperature independent and is not quenched by relatively high paramagnetic defect (Robertson, 1996). Indeed, PL efficiency correlates poorly with the paramagnetic defect densities (Robertson, 1996). Furthermore, Hu et al. (2004) suggested that this PL emission is related to the radiative recombination originated from defect state. Si-C bonds and H atoms can effectively passivate the Si dangling bonds and enhance PL intensity (Coscia et al., 2008; Huran et al.).

From the work carried out by Anis et al. (2007) a relationship between PL emission and  $E_g$  of the films was studied. The shift in peak position was related to the change in  $E_g$ . A broad PL spectra consisting of two or more overlapping peaks suggest that the films are multiphase in structure (Kumbhar et al., 2001). Kumbhar et al. (2001) relate the double band features of PL spectra to mixed phase structure of  $sp^3$ -C embedded in SiC matrix. Xu et al. (2005) also obtained multiband PL spectrum which can be attributed to the recombination process through localized states in a-SiC structures. There are also reports that suggest the PL emission is governed by the existence of Si-O bonds (Kassiba et al., 2002; Xu et al., 2005).

## CHAPTER 3

### EXPERIMENTAL SETUP

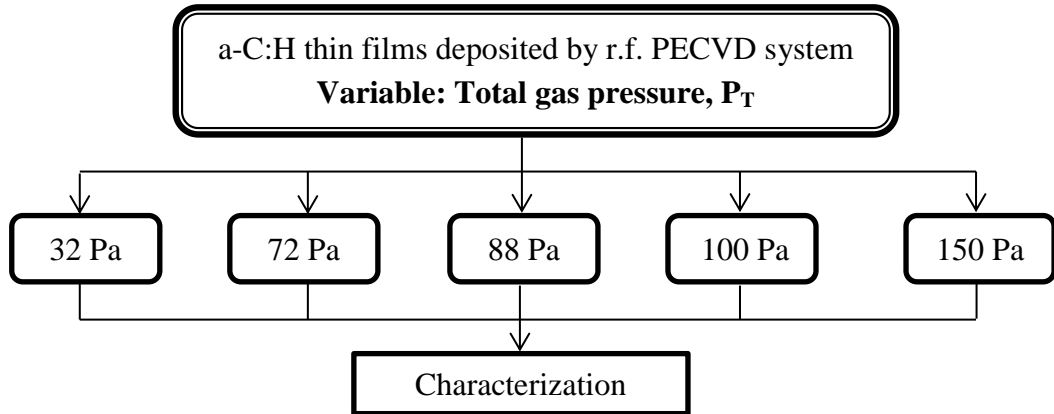
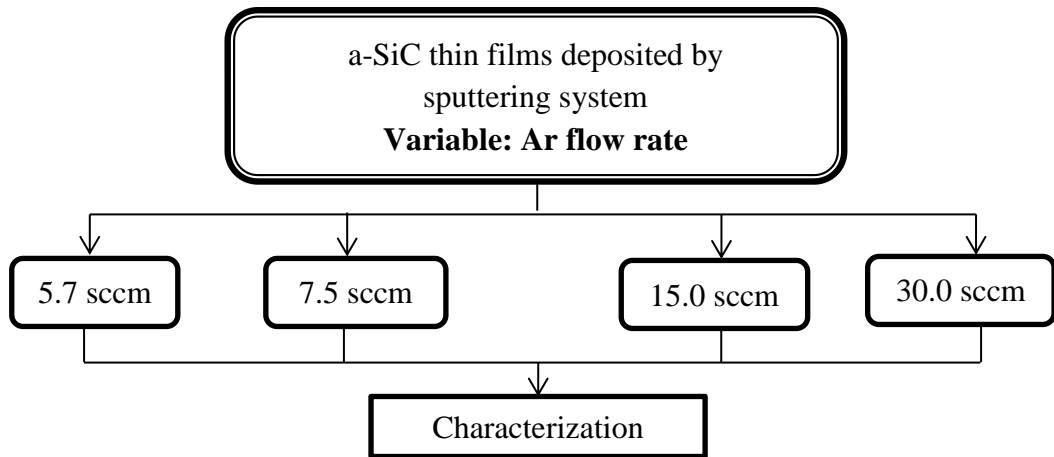
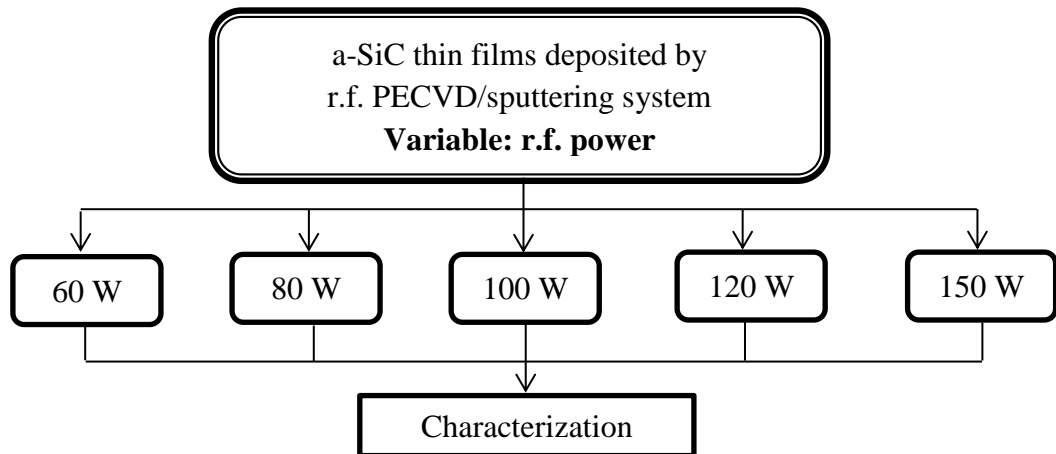
#### 3.0 Chapter Outline

Radio frequency plasma enhanced chemical vapour deposition (r.f. PECVD) is one of the most well established techniques in producing thin films. However, in this research project, a modification of the conventional r.f. PECVD system was adopted. The system was upgraded by inserting an r.f. sputtering setup into the conventional system in order for both techniques to work simultaneously and thus combines the advantages of r.f. PECVD and r.f. sputtering techniques. The advanced system is named hybrid r.f. PECVD/sputtering system.

This chapter mainly consists of two aspects. The first aspect focuses on the hybrid r.f. PECVD/sputtering system, which combines the strengths of each independent technique and at the same time minimizing their negative impacts. The second aspect describes the sample preparation procedures and measurement technique involved in the characterization of these thin films. Figure 3.1 summarized the sample preparation variables of this research work.

#### 3.1 Deposition System Setup

Generally, hybrid r.f. PECVD/sputtering system comprises of two different techniques which are implemented in the same system, causing them to share almost similar design, equipment and experimental setup. Figure 3.2 shows the home-built hybrid r.f. PECVD/sputtering system in the laboratory.

**SET 1****SET 2****SET 3****Figure 3.1:** Summary of sample preparation variables.

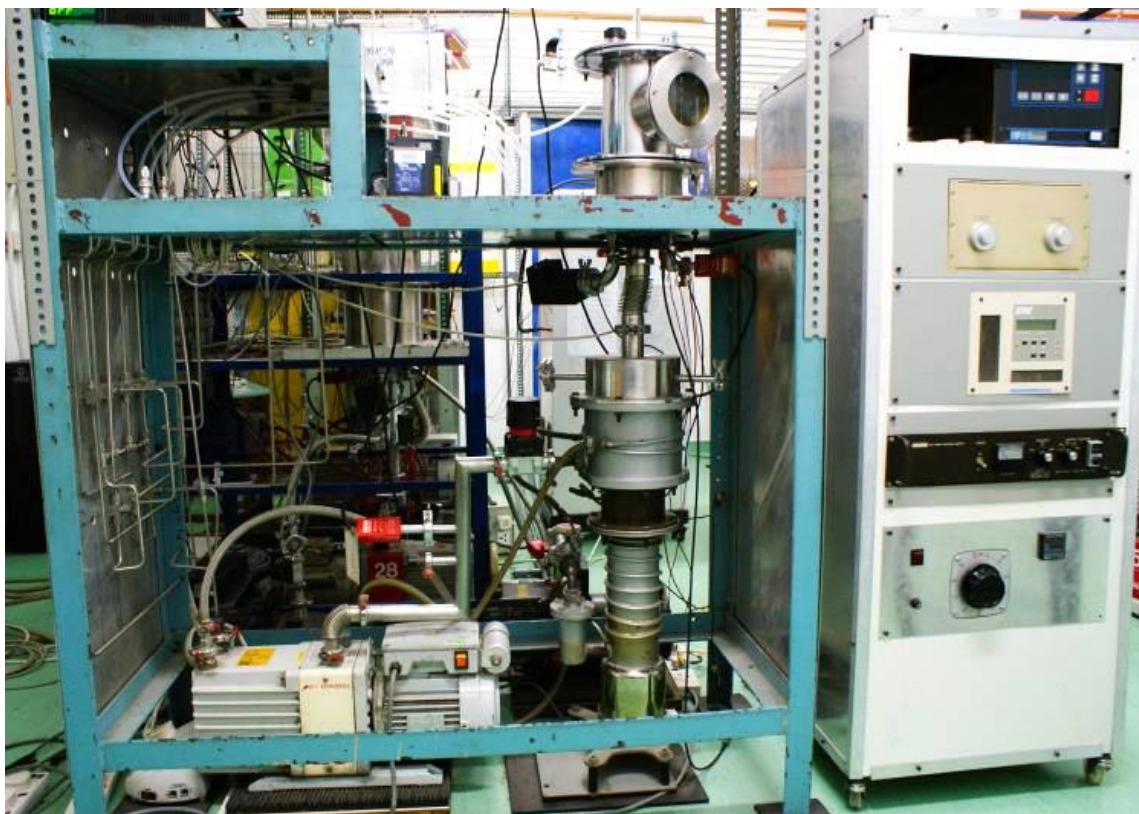


**Figure 3.2:** Home-built r.f. PECVD/sputtering deposition system.

The schematic representation of the system is shown in Figure 3.3. The hybrid system involves an insertion and modification on the reaction chamber which will be explained later in this chapter. The deposition system mainly consists of three major parts which are the evacuation subsystem, the gas distribution subsystem and the electrical subsystem. All of these subsystems are connected directly to the reaction chamber. The evacuation subsystem contains of a rotary pump for a low vacuum pumping and a diffusion pump to achieve high vacuum. The diffusion pump is water-cooled and is connected to another rotary pump which acts as a backing pump. The gas lines and the pressure controller make up the gas distribution subsystem, whereas the electrical subsystem includes the r.f. and heater power supplies, temperature controller and bias voltage source.

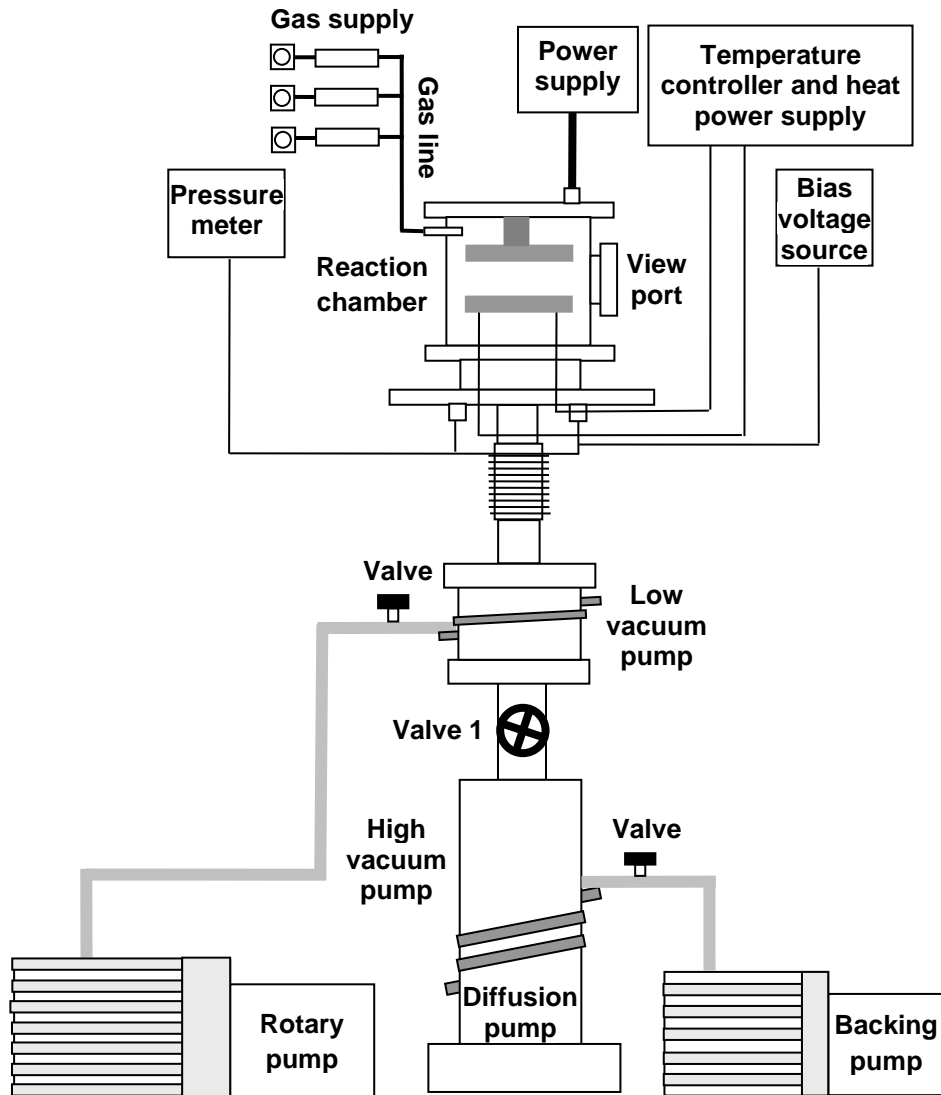


**Figure 3.3:** Schematic diagram of r.f. PECVD/sputtering deposition system.

### 3.1.1 The Evacuation Subsystem

The evacuation subsystem is used to sustain a vacuum condition and maintain a controlled environment therefore reducing the impurities that may contaminate the films during and after deposition. This subsystem helps in maintaining the required deposition pressure during the deposition process. The evacuation subsystem consists of three vacuum pumps which comprises of an Edwards E2M28 and Edwards E2M8 rotary oil pumps and an Edwards P603 oil diffusion pump. In the early stage of the

pumping process, the rotary pump will operate in the viscous region (fore and roughing pump) allowing the pressure to go down to  $10^{-3}$  mbar.

The diffusion pump is connected at the bottom of the whole system and is backed by an Edwards E2M8 rotary oil pump. The diffusion pump or high vacuum pump will take over the pumping process in the molecular flow region to further decrease the chamber pressure down to  $10^{-5}$  mbar. This will assure that the chamber will achieve the lowest possible pressure in order to reduce contamination. The pumping process is also carried out with the valves of the gas lines fully opened to ensure no leakage is present.

### **3.1.2 The Gas Distribution Subsystem**

Suitable gas composition is needed in order to deposit specific samples. This can be achieved by mixing different gases such as methane ( $\text{CH}_4$ ), hydrogen ( $\text{H}_2$ ) and Argon ( $\text{Ar}$ ). These gases are supplied from the gas tank into the reaction chamber through the gas lines. The gas is prevented from back-flowing by using one way valve placed at specific location along the gas line. Gas regulators for each gas tank are needed to control the gas flow in the gas lines and the pressure is kept at 5 PSI. The specified gas flow rates are controlled by the mass-flow controllers (MFCs). Each flow rates is limited by the maximum range allowed by the MFC. Aalborg MFC has maximum flow rates of 60 and 200 standard cubic centimetres per minute (sccm) for  $\text{CH}_4$  and  $\text{H}_2$  precursor gases, respectively. For  $\text{Ar}$  gas, the maximum flow rate set by Aera FC770AC MFC is 300 sccm.



### **3.1.3 The Electrical Subsystem**

The electrical subsystem comprises of r.f. power supply to generate the plasma from gas discharge, feedthrough for grounding or voltage bias supply, and the temperature controller connecting both the heater and thermocouple to maintain the substrate temperature during the deposition process.

An industrial standard 13.56 MHz r.f. regulator (ENI model, No:4CG-6B) is used to power the system. It is connected to the chamber through a manual tuning impedance matching network (model MMN600/Pi) which is used to increase the power dissipation, preventing any reverse power and protect the r.f. generator. The heater and thermocouple is connected to a temperature controller (model Taishio TS 501), which regulates the temperature at given set point. The temperature is directly measured on glass substrate placed on the holder. Care was taken to ensure proper isolation of the thermocouple tip with the holder itself.

### **3.1.4 The Reaction Chamber**

A description of the reaction chamber for both r.f. PECVD and hybrid r.f. PECVD/sputtering systems will be explained in this section. The reaction chamber plays the most important role in the deposition system as it connected to all the subsystems involve in the deposition system. The reaction chamber is also the location for the substrates and where the chemical reaction takes place. The reaction chamber is designed so that the plasma discharge will be generated between top and bottom electrodes. As shown in Figure 3.4(a) and 3.4(b), the reaction chamber is generally composed of three parts which comprise of the top cover plate, the main chamber and base chamber.

The main chamber is made from stainless steel with dimension of 18.4 cm high, 0.5 cm thick and 13.4 cm in diameter. The main chamber, the top cover plate and base chamber are secured together. The upper part of the main chamber is screwed to the lower part of the top cover plate, while the lower part of the main chamber is screwed to the upper part of the base chamber. To prevent gas leakage and to sustain the low pressure condition inside the chamber, the upper part of the main chamber is grooved by 20.5 cm in diameter to fit in a 0.5 cm thick Viton O-ring.

The differences between both r.f. PECVD and hybrid r.f. PECVD/sputtering systems involve mainly at the top cover plate and the position of electrical subsystem connections as displayed in Figure 3.4(a) and Figure 3.4(b).

Figure 3.4 (a) shows the schematic diagram of the home-built r.f. PECVD system consisting of parallel plate electrode configuration. Teflon is used to isolate the stainless steel bottom and top electrodes from the base chamber and top plate, respectively to avoid short circuitry. Teflon stud is made not only to isolate the base chamber from the substrate holder, but it is also designed with different height to vary the substrate distance between top and bottom electrodes. The top electrode is powered and also acts as the showerhead for gas feed while the bottom electrode is grounded. This bottom electrode also acts as the substrate holder where the heater and thermocouple are attached. a-C:H were deposited using this system at different total gas pressure,  $P_T$  with fixed flow rate ratio of  $CH_4$  and  $H_2$  at 1 to 5 sccm, respectively as reference.

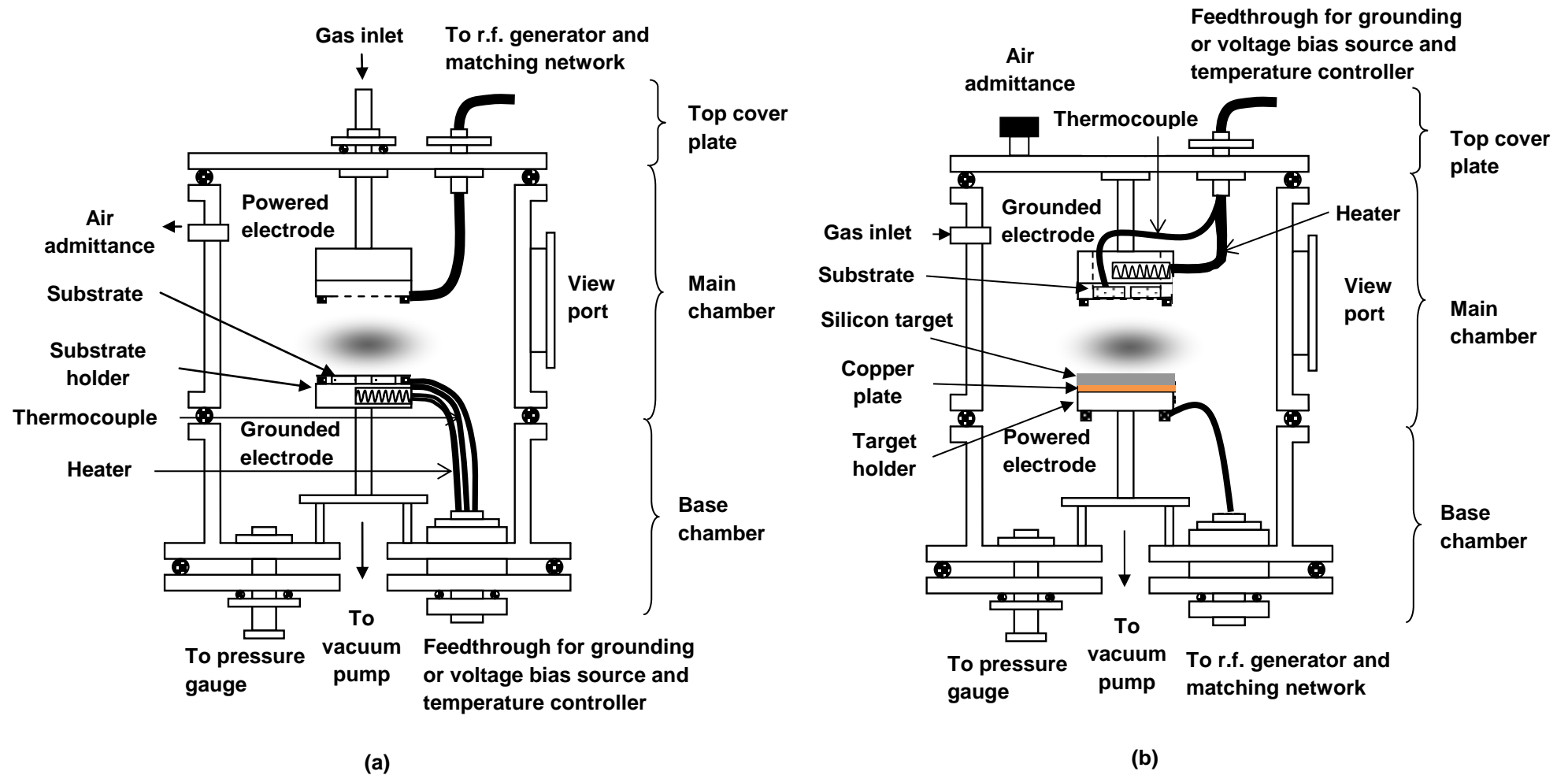


**Figure 3.4:** The schematic diagram of reaction chamber of (a) home-built r.f. PECVD and (b) home-built hybrid r.f. PECVD/sputtering system.

Figure 3.4(b) represents the schematic diagram of the home-built hybrid r.f. PECVD/sputtering system. Basically, the additional components for r.f. sputtering setup only involved the insertion of sputtering target. A pure amorphous silicon (a-Si) target (99.999%) is used. In contrast with the simpler r.f. PECVD system, the a-Si target is placed at the bottom electrode replacing the position of substrate holder as in the r.f. PECVD system. The bottom electrode held the a-Si sputtering target with diameter of 10 cm and thickness of 3 cm. The silicon target is glued on a copper bottom plate by epoxy kit. Also, this target is now the powered electrode. Consequently, the top electrode acts as the substrate holder and thus also eliminates the use of a showerhead in feeding the gasses into the system. The gas is fed into the chamber via a gas inlet on the chamber walls. This substrate holder inserted with a cylindrical heater is also grounded. The thermocouple is used to measure the temperature. Using this system amorphous silicon carbon (a-SiC) thin films were deposited at different Ar flow rate ratio and r.f. power. Detailed descriptions and information on the deposition parameters are provided in Section 3.4.

## **3.2 Pre-deposition Preparation**

Substrate preparation needs to be carried out prior to thin film deposition process. This is to ensure that the samples produced shows good adhesion. The use of glove and tweezers are compulsory at all times.

### **3.2.1 Substrate Cleaning Procedure**

p-type crystal silicon c-Si (111), quartz and glass substrates were used in this work. Optical properties were measured for samples deposited on quartz and glass substrate, while the chemical bonding and structural properties were determined for films deposited on c-Si substrates. These substrates need to be cleaned to ensure that the

surface is free from any contaminants. The contaminants usually encountered are finger print, oil, lint, manufacturing and packaging residual and airborne particulate matter. The degree of cleanliness needed, the type of contaminant on the substrate's surface and the type of substrate will determine the cleaning technique that should be applied.

### **3.2.1 (a) Silicon Substrate Cleaning Process**

c-Si substrates were initially rinsed in deionized (DI) water to remove the contamination during the cutting process. The substrates were immersed in  $\text{H}_2\text{O}:\text{H}_2\text{O}_2:\text{HCl}$  solution with ratio of 6:1:1 for 10 minute. They were then rinsed in DI water. The process was continued by immersing the substrates in  $\text{H}_2\text{O}:\text{H}_2\text{O}_2:\text{NH}_4\text{OH}$  with ratio of 5:1:1 and rinsing them with DI water once again. The same process of immersing and rinsing were repeated by using  $\text{H}_2\text{O}:\text{HF}$  with ratio of 10:1. These acids were used to dissolve and convert oxides and grease on the surface of the substrate into water soluble compound. After the final rinsing process, the substrates were dried in a stream of nitrogen gas. Since c-Si substrates are easily oxidized, they need to be used right after the cleaning process.

### **3.2.1 (b) Quartz and Glass Substrate Cleaning Process**

The substrates were immersed in a beaker containing a detergent solution of Decon ® Neutracon soap mixed with DI water. The beaker were then immersed into an ultrasonic bath and agitated for 15 minutes. Ultrasonic was used to create abrupt vibration on the surface of the substrate by shock wave stirring action in the cleaning solvent. The strong vibrations dissolve and carry away the impurities from the surface of the substrates. This technique can also remove gross dirt from the cutting process and residual oil. The substrates were then rinsed with DI water to remove remaining soap water. Later, they were rinsed in acetone and ethanol to remove any residual

contaminant. Finally, the substrates were rinsed in the DI water. A flow of nitrogen was used to dry the substrates.

### **3.2.2 Amorphous Silicon (a-Si) Target Cleaning Procedure**

The amorphous Silicon (a-Si) target was cleaned by ultrasonification in DI water to remove dirt on the surface. The target was not treated as c-Si substrates because the chemical reagents used may damage or causes it to be brittle. Finally, a flow of nitrogen was used to dry the target.

## **3.3 Operation of the Deposition System**

Successful and save deposition depend on proper operation of the r.f. PECVD system. Pre and post-deposition operations are just as crucial as the deposition process itself. Pre-deposition is related to the chamber cleaning and pumping process. The pumping process ensures that the system is well sealed to avoid leakage and to make sure that the chamber pressure and other parameters are stable during the deposition process. Post deposition process involves the removal of excess gases involved in the deposition process.

### **3.3.1 Pre-deposition Procedure**

The substrates and reaction chamber were clean thoroughly prior to substrate loading and system pumping. To remove dirt and coatings from previous deposition process, wet sand paper was used to scour stains on the inner wall of the stainless steel chamber. The chamber was then wiped with acetone to remove excess contaminants and oil. Once cleaned, substrates were loaded onto the holder. These substrates were held in place using a stainless steel mask. Schematic diagram of the stainless steel mask

is shown in Figure 3.5. A step profile could be formed for the measurement of film thickness, as the mask does not expose the whole substrate.

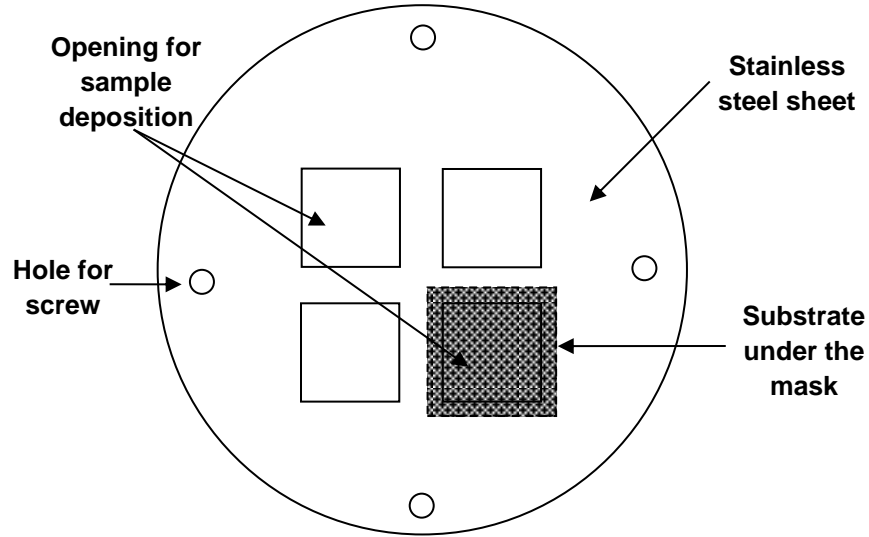


**Figure 3.5:** Top view of stainless steel mask.

The pumping process was carried out using the roughing and high vacuum pumps as explained in Section 3.3.1. The pumping process was initiated to evacuate the system down to  $10^{-3}$  mbar. After this pressure was obtained, the valve connected to the gas line was opened to evacuate the channel along the gas lines. This detects any leakage along the gas lines. During this time the diffusion pump was warmed up for 30 minutes. To attain high vacuum, the valve connected to the rotary pump was closed and the high vacuum valve was slowly opened. The system was pumped down to a base pressure of  $10^{-5}$  mbar. A typical roughing pressure of  $\sim 5 \times 10^{-3}$  mbar by rotary pump and base pressure of  $\sim 5 \times 10^{-5}$  Pa were routinely achieved.

Once the base pressure had been reached and the system had been pumped down for sufficient time, high vacuum valve was closed and the rotary pumps valve was fully opened again. The substrates were then heated up to the required temperature of 100°C.

### 3.3.2 Deposition Procedure

Once the system had been pumped down and the substrate temperature had been reached, the precursor gases were allowed to flow into the chamber. In this work, CH<sub>4</sub>, H<sub>2</sub> and Ar were used. The flow rates were controlled using MFC. The gases were allowed to flow into the chamber for at least 5 minutes in order to ensure that the flow rates were stable. The chamber pressure was controlled by adjusting the rotary pump valve.

Prior to the actual deposition, the substrates or a-Si target was pre-treated using H or Ar plasma, respectively. The pre-treatment parameters are provided in Section 3.4.1 and 3.4.2. The second process was the films deposition process. The r.f. PECVD and hybrid r.f. PECVD/sputtering system were used to deposit the a-C:H and a-SiC thin films, respectively. The following sections describe the conditions and parameters used to deposit different sets of films in this work.

#### 3.3.2 (a) *Deposition Parameters for Hydrogenated Amorphous Carbon Films Deposited by Radio Frequency Plasma Enhanced Chemical Vapour Deposition System*

The a-C:H films were deposited using the r.f. PECVD system from the discharge of pure CH<sub>4</sub> and H<sub>2</sub> on quartz and c-Si (111) substrates. Prior to the deposition process H<sub>2</sub> gas was introduced into the chamber at flow rate of 50 sccm and H<sub>2</sub> plasma was ignited at r.f. power of 50 W for a treatment time of 10 minutes to remove impurities on the substrate surface. Details of the parameters used are listed in Table 3.1.



**Table 3.1:** Parameters applied during Hydrogen treatment process.

Gas sources	H <sub>2</sub>
Flow rate (sccm)	20
Deposition time (min)	10
r.f. power (W)	40
Treatment pressure (Pa)	80

Five sets of films were deposited by increasing the CH<sub>4</sub> and H<sub>2</sub> gas flow rates while keeping the flow rate ratio fixed at 1:5. The deposition pressure increased accordingly with the increase in the gas flow rates as tabulated in Table 3.2. Other deposition parameters including substrate temperature, r.f. power, electrode distance and deposition time were kept constant at 100 °C, 60 W, 4 cm and 90 min, respectively. Details of the a-C:H deposition parameters are summarized in Table 3.3.

**Table 3.2:** Total gas pressure, P<sub>T</sub> relative to CH<sub>4</sub>:H<sub>2</sub> flow rate ratio.

CH <sub>4</sub> :H <sub>2</sub> flow rate ratio (sccm)	Total gas pressure, P <sub>T</sub> (Pa)
5:25	32
10:50	72
20:100	88
25:125	100
30:150	150

**Table 3.3:** Deposition parameters used to deposit a-C:H thin films.

Gas sources	CH <sub>4</sub>	Ar
Flow rate ratio (sccm)	1	5
Deposition time (min)	90	
r.f. power (W)	60	
Substrate	Si, Quartz	
Deposition temperature (°C)	100	
Distance between top and bottom electrode (cm)	4	

### 3.3.2 (b) Deposition Parameters for Hydrogenated Amorphous Silicon Carbon Films Deposited by Hybrid Radio Frequency Plasma Enhanced Chemical Vapour Deposition/Sputtering System

Prior to the deposition, the a-Si target was treated in 150 sccm of Ar plasma for one hour to remove any surface contaminants. Detail of the parameters used is summarized in Table 3.4.

**Table 3.4:** Parameters applied for Argon treatment.

Gas sources	Ar
Flow rate (sccm)	150
Deposition time (min)	60
r.f. power (W)	50
Treatment pressure (Pa)	40

Two different conditions were carried out in order to study a-SiC thin films by using the hybrid r.f. PECVD/sputtering deposition system. The conditions are as stated below:

- (i) Sputtering of a-Si target coated with a-C:H and silicon oxide ( $\text{SiO}_x$ ) layers by pure Ar.

This was done to study the effect of Ar flow rates on the sputtering of a-Si target coated with a-C:H and  $\text{SiO}_x$  layers. Four sets of a-Si-C thin films were deposited on c-Si substrate at fixed r.f. power of 100 W. The effect of Ar flow rates was studied by applying different Ar flow rates of 5.7, 7.5, 15 and 30 sccm. The deposition pressure increased correspondingly to the variation in the flow rates as shown in Table 3.5 while the details of the deposition parameters are shown in Table 3.6.

**Table 3.5:** Deposition pressure relative to Ar flow rate.

Ar flow rate (sccm)	Deposition pressure (Pa)
5.7	10
7.5	10
15	13
30	34

**Table 3.6:** Deposition parameters for deposition of a-SiC thin films: Effect of Ar flow rates.

Gas sources	CH <sub>4</sub>	Ar
Deposition time (min)	180	
r.f. power (W)	100	
Substrate	Si	
Deposition temperature (°C)	100	
Distance between top and bottom electrode (cm)	4	

- (ii) Sputtering of a-Si target coated with of a-C:H and SiO<sub>x</sub> layers by a mixture of CH<sub>4</sub> and Ar gases.

Effect of r.f. power on the properties of a-SiC thin films was then studied with the flow rates of CH<sub>4</sub> to Ar gases were fixed at ratio of 1 to 7.5 sccm. The choice of the flow rates were subjected to the range of the MFCs used. The minimum limit for CH<sub>4</sub> MFC only allowed the ratio setting of the said values. Five sets of a-SiC films were deposited for this study. Detail information on a-SiC deposition parameters in this study are summarized in Table 3.7.

**Table 3.7:** Deposition parameters for deposition of a-SiC thin films: Effect of r.f. power.

Gas sources	CH <sub>4</sub>	Ar
Flow rate ratio (sccm)	1	7.5
Deposition time (min)	180	
r.f. power (W)	60, 80, 100, 120, 150	
Substrate	Si, Quartz	
Deposition temperature (°C)	100	
Distance between top and bottom electrode (cm)	4	
Deposition pressure (Pa)	1	

It should be noted that the sputtering was carried out on the target coated with a-C:H and SiO<sub>x</sub> layers. This a-C:H layer was the residual coating obtained from the CH<sub>4</sub> plasma discharge of earlier deposition while SiO<sub>x</sub> layer was formed from oxidation passivation of a-Si target. Taking advantage of the residual film on the target, this coating was not removed but used instead to enhance the incorporation of C in the formation of the Si and C deposition.

### 3.3.3 Post-deposition Procedure

Once the deposition was completed, the r.f power and the gas flow were turned off. The valve of the rotary pump was then fully opened to evacuate the chamber of the reaction gases. The chamber was pumped continuously while allowing the system and the films in particular, to cool down to room temperature.

## 3.4 Characterization Techniques

In this work, the films were characterized to obtain the growth rate, structural, surface morphology, chemical bonding, chemical compositions, optical properties, and PL emission properties. The growth rate was determined from thickness measurement by means of surface profilometer. The structural properties were studied by Raman

spectroscopy. Fourier transform infrared (FTIR) spectroscopy and Auger electron spectroscopy were employed to determine the chemical bonding and elemental compositions, respectively (Frach et al., 2010). The optical properties were investigated by using Ultra-violet-near infrared (UV-Vis-NIR) spectroscopy and PL spectroscopy was used to study PL of the deposited films. Detail descriptions of all the characterization techniques involved will be explained in the following sections.

### 3.4.1 Surface Profilometer

Surface profilometer was used to measure the film thickness along step heights created from the edge of the film. The variation of thickness allowed the growth rates of the films to be studied in terms of the different deposition parameters. A mechanical surface profilometer (KKA Tencor P-6) used in this study equipped with special tips of 2  $\mu\text{m}$  diamond stylus was used as shown in Figure 3.6.

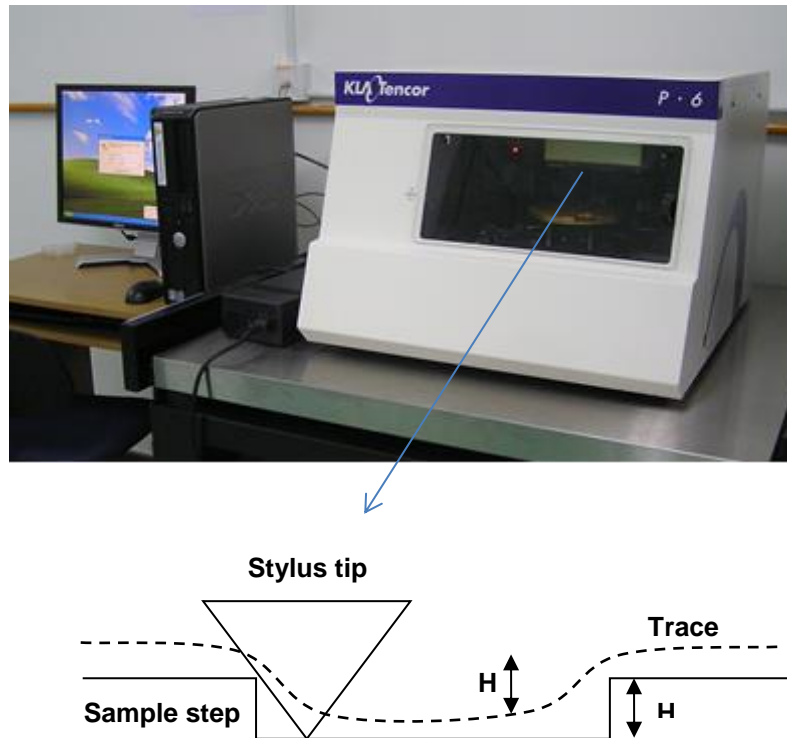


**Figure 3.6:** Mechanical surface profilometer (KKA Tencor P-6) and its stylus tip.

The stylus was in contact with the films and can be scanned up to 150 mm vertically and laterally. The thickness was measured as the displacement of the stylus across the step heights and allowed direct measurement. Figure 3.7 shows a typical topological graph obtained from this surface profilometer.

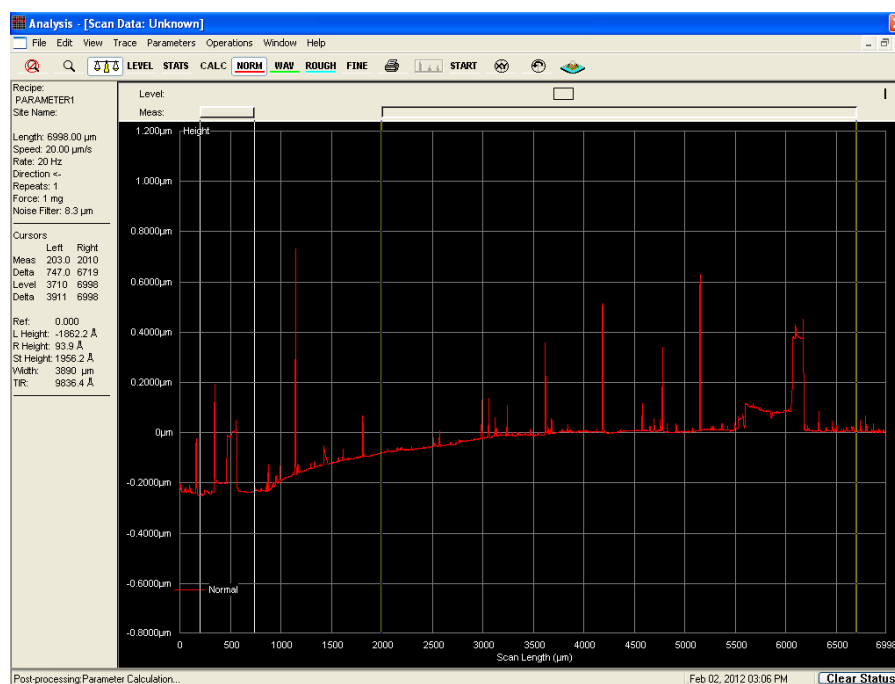


**Figure 3.7:** The step edge of a deposited thin film displayed by profilometer, representing the thickness of the films.

### 3.4.2 Fourier Transform Infrared Spectroscopy

FTIR spectra were recorded using Perkin Elmer 2000 system in transmission mode within the range of 400 to 4000  $\text{cm}^{-1}$ . The spectral resolution used was 8  $\text{cm}^{-1}$ . Figure 3.8 shows the Perkin Elmer 2000 system used in this work.



**Figure 3.8:** FTIR spectrometer (Perkin Elmer 2000 system).

When the films were scanned over a wide wavenumber range, the corresponding spectra obtained allowed different bonding in the films to be identified. The transmission spectra can be converted to absorption coefficient ( $\alpha$ ) and normalized by the film thickness according to the equation below

$$\text{Absorption coefficient } (\alpha) = \frac{\ln(\frac{100}{T})}{d} \dots\dots\dots (\text{Equation 3.1})$$

where T is the transmission of the films detected in percentage and d is the thickness of the measured films in nm.

Figure 3.9 shows a typical FTIR absorption spectra for a-C:H and a-Si-C thin films and the assigned peaks. The wavenumbers and their corresponding assignments are listed in Table 3.8.

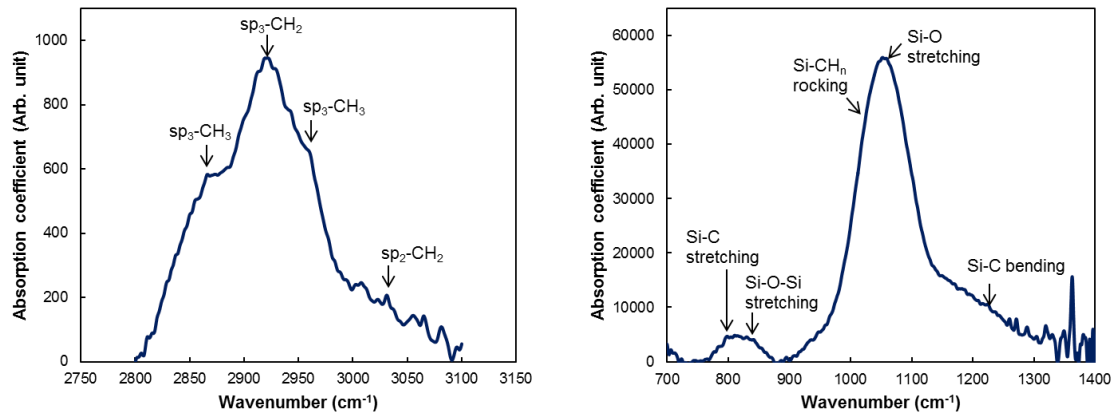


**Figure 3.9:** Typical FTIR spectra obtained from a-C:H and a-SiC thin films.

**Table 3.8:** Chemical bonding at specific range of wavenumbers (Deng et al. 2011; Higa et al. 2006; Liu et al. 1997; Yoon et al. 2000).

Wavenumber (cm <sup>-1</sup> )	Assignments
<b>a-C:H</b>	
2870/2875	sp <sup>3</sup> -CH <sub>3</sub> (symmetrical)
2850/2920/2930	sp <sup>3</sup> -CH <sub>2</sub> (asymmetrical)
2960	sp <sup>2</sup> -CH <sub>3</sub> (asymmetrical)
3000/3050	sp <sup>2</sup> -CH
<b>a-SiC</b>	
800	Si-C stretching
840	Si-O-Si stretching
1020	Si-CH <sub>n</sub> rocking
1050	Si-O stretching
1230	Si-C bending

Another important parameter which can be calculated from the FTIR spectra is the relative hydrogen content,  $C_H$ .  $C_H$  was determined from the C-H bonds concentration estimated from the integrated intensity at about 2900 cm<sup>-1</sup> by using the relation

$$n_H = \frac{A}{N_C} \int \frac{\alpha(\omega)}{\omega} d\omega \quad \dots\dots\dots \text{(Equation 3.2)}$$



The integrated intensity of C-H absorption band was obtained from the fitted area under the curve of the band, performed using OriginPro 8.1 program. This and other corresponding fitting is necessary since the raw data involved a number of overlapping peaks and may even be dominated by a certain amount of PL background. This technique uses a standard Gaussian fitting which allows elimination of PL background and individual peaks to be obtained and analyzed. From this the intensity, height, FWHM and area of the individual peak can be obtained. Example of a fitted FTIR peak is shown in Figure 3.10.

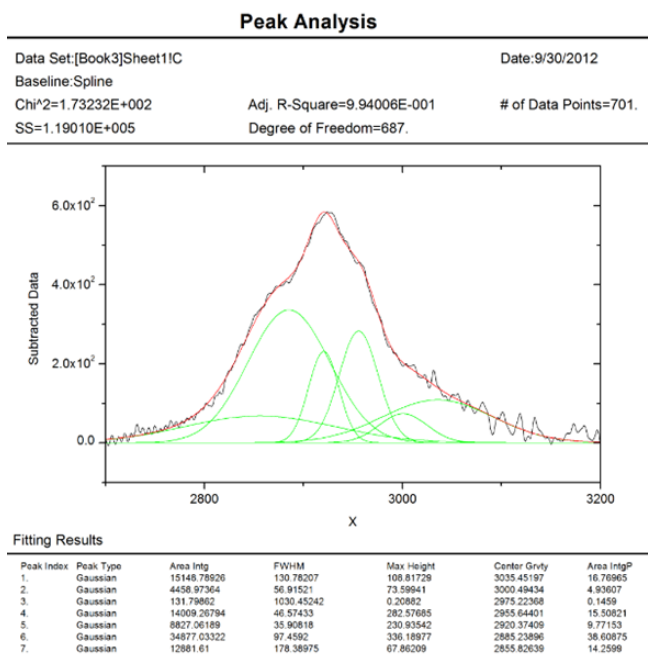


**Figure 3.10:** Final information gained from curve fitting by OriginPro 8.1.

### 3.4.3 Ultra Violet-Near Infrared Spectroscopy

Optical measurements were carried out using a Jasco V-570 Uv-Vis-NIR spectrometer. The spectrometer is shown in Figure 3.11. The measurement was carried out in transmission and reflectance modes within a scanning range of 250 nm to 2500 nm wavelength. From these measurements, the energy gap of the films was calculated.



**Figure 3.11:** Jasco V-570 Uv-Vis-NIR spectrometer.

Figure 3.12 is a representation of the propagation of light through a thin film sample. When a beam of light with wavelength,  $\lambda$  is incident onto a transparent film, its initial intensity,  $I_0$  reduces to  $I_T$  due to light reflectance,  $I_R$  and absorption  $I_A$ . This is described by Equation 3.3.

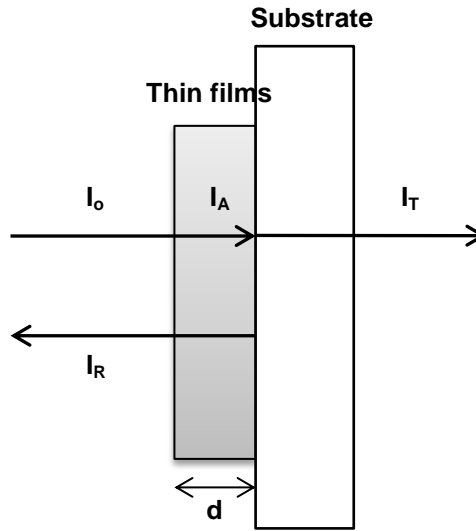


**Figure 3.12:** Reflectance, transmittance and absorption of light by the deposited thin films.

$$I_o = I_T + I_A + I_R \quad \dots\dots\dots \text{(Equation 3.3)}$$

The absorption coefficient,  $\alpha$  was determined from both the transmittance and reflectance spectra. According to Lambert-Beer's law, this is given by Equation 3.4

$$\text{Absorption coefficient}(\alpha) = \frac{1}{d} \ln \left( \frac{100-R(\%)}{T(\%)} \right) \quad \dots\dots\dots \text{(Equation 3.4)}$$

where T, R and d are the transmission and reflectance in percentage, and thickness of the sample, respectively.

Optical energy gap,  $E_{Tauc}$  of a-C:H films were obtained from the corresponding Tauc's plot which could be determined from the Tauc's relation as prescribed in Equation 3.5

$$(\alpha E)^{\frac{1}{2}} = B^{\frac{1}{2}} (E - E_{Tauc}) \quad \dots\dots\dots \text{(Equation 3.5)}$$

where  $\alpha$ ,  $E$  and  $B$  is the absorption coefficient, photon energy and Tauc coefficient, respectively.

From these calculations, a graph of  $(\alpha E)^{\frac{1}{2}}$  against  $E$  was plotted. The value of  $E_{\text{Tauc}}$  was determined from the intersection of the extrapolated linear region onto the energy axis. On the other hand, the value of  $E_g$  can be obtained from the graph of absorption coefficient,  $\alpha$  versus energy,  $E$ .  $E_g$  is the band gap which corresponds to an absorption coefficient,  $\alpha$  at  $10^4 \text{ cm}^{-1}$ . Examples of these extrapolations are shown in Figure 3.13.

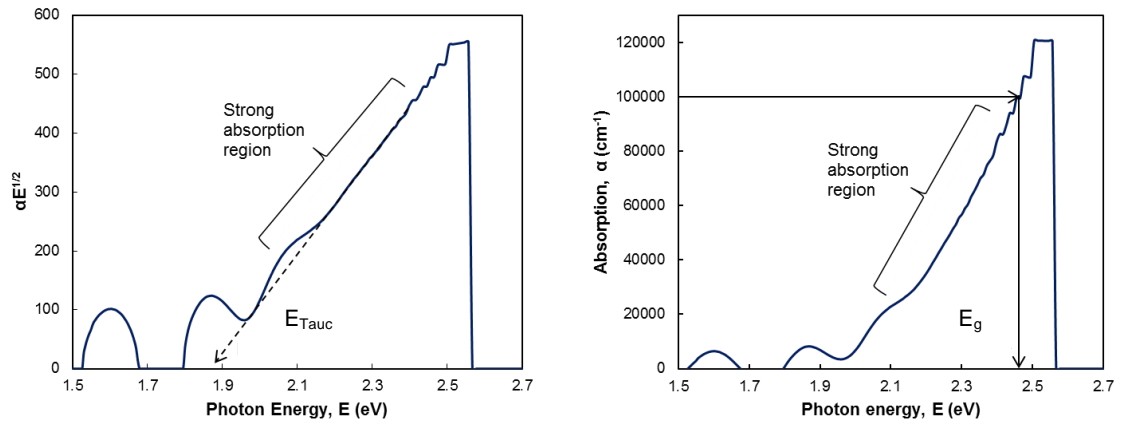


**Figure 3.13:** Extrapolation of  $\alpha E^{1/2}$  versus  $E$  to obtain  $E_{\text{Tauc}}$  and optical absorption edge of  $E_g$ .

#### 3.4.4 Raman Spectroscopy

Raman scattering spectra were obtained by using Renishaw inVia Raman spectrophotometer coupled with Leica DMLM microscope as shown in Figure 3.14. The spectra were obtained for samples deposited on c-Si substrate within the range of  $100$  to  $1800 \text{ cm}^{-1}$  by using  $\text{Ar}^+$  laser source with excitation wavelength of  $325 \text{ nm}$ . Stronger Raman signal can be obtained by using this wavelength rather than the conventional  $514.5 \text{ nm}$  helium (He) cadmium laser source since the intensity of Raman scatter is proportional to  $1/\lambda^4$ . The interaction between the monochromatic light from

the laser source and the molecule of the films will cause the molecule to vibrate, rotate and form other low frequency transitions. Raman spectroscopy though fairly recent, emerged as an important analytical tool due to its sensitivity, richness in information and non-destructive behavior. Raman is sensitive to symmetric bonds and backbone structures.



**Figure 3.14:** Raman and Photoluminescence spectroscopy.

The Raman effects is a process whereby a sample that has been irradiated by a laser source scattered most of the radiation at a wavelength that is shifted from the original laser wavelength. The changes in the energies of the excited and emitted photons are identified as a Raman shift. It occurs only as a small portion or the total excited energy compared to other processes such as Rayleigh scattering that may scattered at the same wavelength as the laser source. Both processes can be summarized in Figure 3.15.

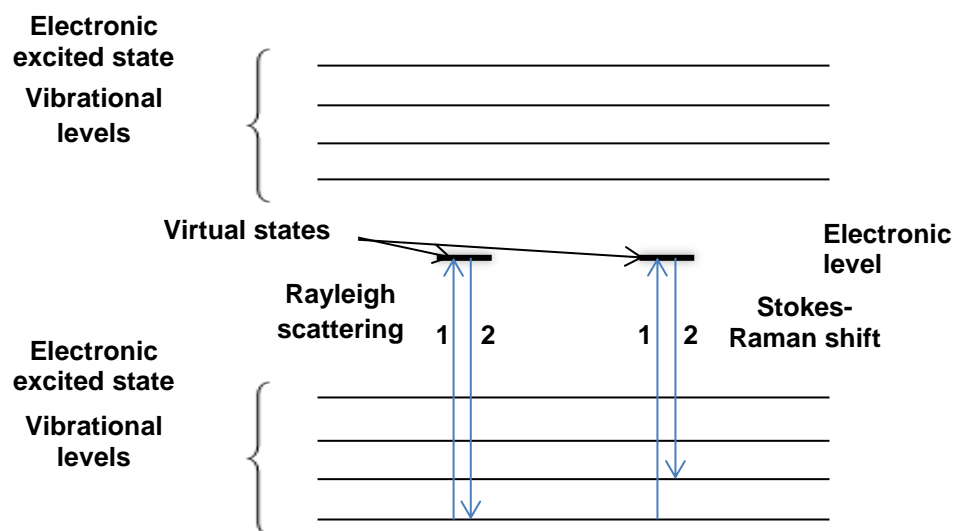


**Figure 3.15:** Energy level diagram of Rayleigh scattering and Stokes-Raman shift.

Numerous information related to structure and chemical identity of the molecules can be obtained from the position and intensity of the peaks in the spectra. A very strong Raman shift can be detected for stretching vibration of C double and triple bonds, and aromatic group with symmetric vibration such as benzene ring. Phase transition from amorphous to crystalline structure can also be detected based on the emitted spectra. Table 3.9 records the different phases of Si and C structure and its corresponding Raman shift. Due to the overlapping of some of these peaks, it is necessary to deconvolute the Raman spectra. This was done in a similar way to that of FTIR Gaussian fitting.

**Table 3.9:** Assignments of Raman shift of a-C:H a-SiC films taken from (Shi et al.1999; Swain and Dusane 2007; Wang et al. 2002).

Wavenumber (cm <sup>-1</sup> )	Assignments
	Carbon Network
1390	D band (disordered clusters for sp <sup>2</sup> coordinated C)
1440	C network attached with Si
1490	Semicircle ring stretch vibration of benzene or condensed benzene rings
1600	G band (graphite-like) structure
	Silicon Network
150	Transverse acoustic (TA) of the amorphous silicon mode
300	Longitudinal optical (LO) of the amorphous silicon mode
380	Transverse optical (TO) of the amorphous silicon mode
480	TO branch from the contribution of the amorphous silicon
520	TO branch from the contribution of the crystal silicon substrates
970	2 <sup>nd</sup> order Raman band
650 to 1000	Si-C bond

### 3.4.5 Photoluminescence Spectroscopy

PL spectra were obtained by using Renishaw inVia PL spectrophotometer coupled with Leica DMLM microscope. The instrument used is the same as that used for Raman measurement. Ar<sup>+</sup> laser was used as the excitation source operating at a wavelength of 325 nm. The PL emission of the samples deposited on c-Si substrate was scanned within the range of 100 to 1000 cm<sup>-1</sup>.

Brief PL mechanism can be described as follows: When photon is incident on a material, their electrons absorb a certain amount of energy and are excited to higher energy states. This process is called photon excitation. However, they eventually lost their energy and decay to lower energy state to overcome their non-equilibrium state. This process is called PL as the luminescence (light) emitted is contributed by photon.

### 3.4.6 Auger Electron Spectroscopy

The chemical composition and depth profile of the films was determined by Auger Electron Spectroscopy (Frach et al., 2010) equipped with ion etching. JAMP-9500F Field Emission Auger Microprobe as shown in Figure 3.16 was used for this purpose.



**Figure 3.16:** JAMP-9500F Field Emission Auger Microprobe.

AES is an extensively used chemical composition analytical technique. It is most sensitive to low atomic number elements except H or He. This measurement is based on the Auger process which is initiated by ejection of an electron from an inner shell which creates a core hole. This is normally done by bombarding the films with high energy electron within the range of 3 to 20 keV. Resulting ejected electron has sufficient energy to form photoelectron and a hole in the core shell. The ionized atom then relaxes and releases some amount of energy. The energy released from this process resulted in two phenomena which are typically known as X-Rays and Auger Electron. The electron which relaxes and falls to the ground state to fill the vacancy at the core shell in the order of descending binding energy is called Auger electron. These processes are illustrated in Figure 3.17.



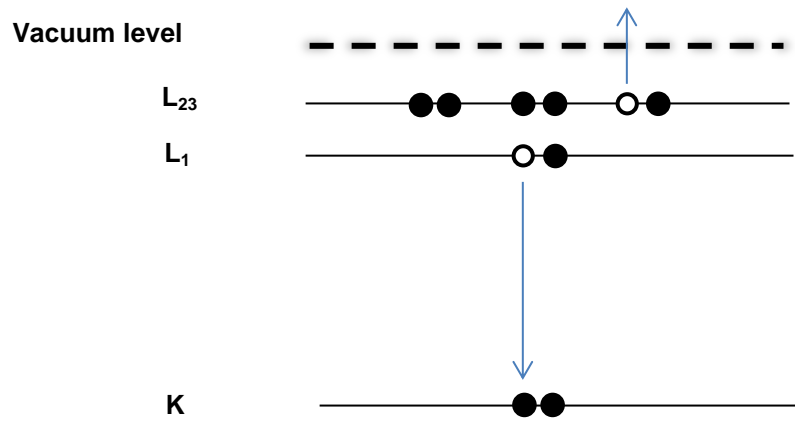


**Figure 3.17:** Energy level diagram of Auger process.

Additionally, measurement of depth profile was also carried out in this research work. This process was accomplished by periodically sputtering the material during intervals of composition measurements.  $\text{Ar}^+$  ion beam was used as a sputtering source. The etching rate used was 0.247 nm/sec. The depth profiling was carried out until the substrate had been reached. The mechanism is illustrated in Figure 3.18.

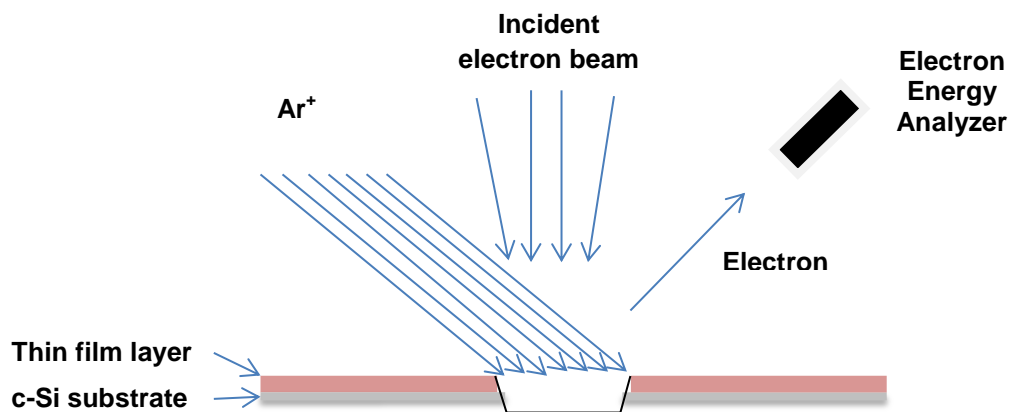


**Figure 3.18:** Depth profile mechanism of AES.

## CHAPTER 4

### RESULTS AND DISCUSSION

#### 4.0 Chapter Outline

This chapter focuses on the deposition and characteristics of the three sets of films prepared. The first set was prepared by the home-built radio frequency plasma enhanced chemical vapour deposition (r.f. PECVD), where the effect of total gas pressure,  $P_T$  on the properties of the hydrogenated amorphous carbon (a-C:H) films deposited were studied. The second set was to study the effect of argon (Ar) flow rate on the properties of films deposited by r.f. sputtering of amorphous silicon (a-Si) target. The last set of film was deposited using the hybrid r.f. PECVD/sputtering system. For these set, the a-Si target was sputtered by Ar ions in  $CH_4$  gas discharge atmosphere. The effects of r.f. power on the structural and photoluminescence (PL) properties of the films were investigated.

It is noted that the a-Si target already has a layer of a-C:H formed by methane ( $CH_4$ ) discharge during earlier depositions; and  $SiO_x$  layer that was formed when dangling bonds at the surface were passivated by oxygen atoms when exposed to the atmosphere.

#### 4.1 Hydrogenated Amorphous Carbon Films Prepared by Plasma Enhanced Chemical Vapour Deposition

In this section, the structural and optical properties of a-C:H thin films prepared by r.f. PECVD were investigated.  $CH_4$  gas was used as the precursor gas and hydrogen ( $H_2$ ) gas was added to act as a diluent gas. These gases were introduced continuously into the reactor chamber at a fixed flow rate.

The motivation of this part of the work is to investigate how the  $P_T$  of precursor gas,  $\text{CH}_4$  and diluent gas,  $\text{H}_2$  influence the growth rate, structure and PL properties of the a-C:H films. The a-C:H films were deposited at various  $P_T$  by changing the flow rates of  $\text{CH}_4$  and  $\text{H}_2$  while maintaining the  $\text{CH}_4$  to  $\text{H}_2$  flow rate ratio at 1:5. The deposition pressure in this work is the  $P_T$  in the reaction chamber with the pumping speed maintained at a constant rate. The  $P_T$  was registered by a Piranni gauge at the highest pumping rate with the valves fully opened. Detailed deposition parameters for this set of films are tabulated in Tables. 3.1 to 3.7.

#### 4.1.1 Growth Rate of Hydrogenated Amorphous Carbon Thin Films

Figure 4.1 shows to the growth rate of the films as a function of  $P_T$ . The growth rate was calculated by dividing the film thickness with the deposition time. The film growth rate can be divided into three variation of growth with respect to  $P_T$ .

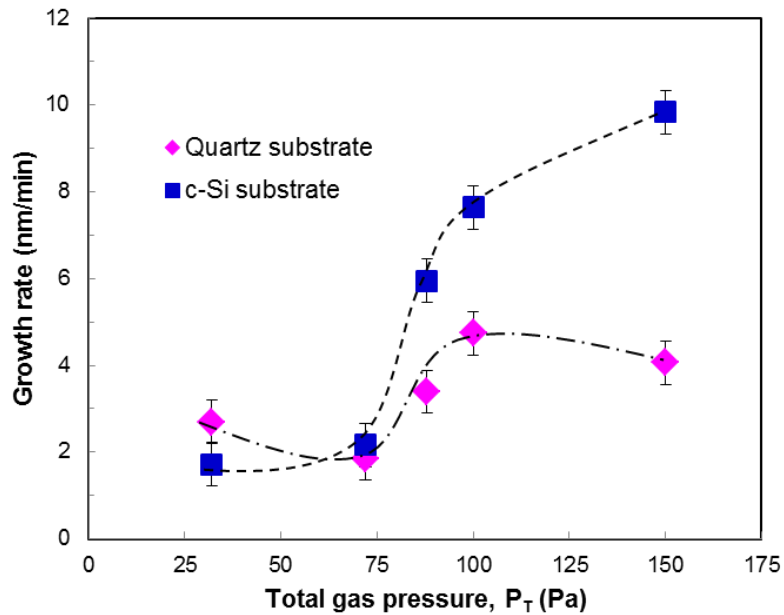


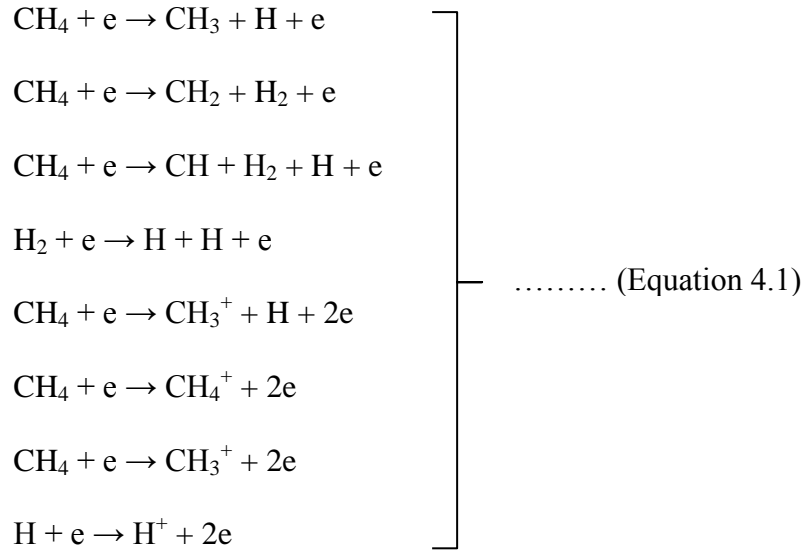
**Figure 4.1:** Growth rate of a-C:H films deposited on c-Si and quartz substrate at different total gas pressure,  $P_T$ .

The first phase of film growth at  $P_T$  of 32 and 72 Pa show no dependence on the  $P_T$  for films on crystal silicon (c-Si) substrate while for the film grown on quartz substrate, a slight decrease was observed when  $P_T$  was increased to 72 Pa. In the second phase of film growth within the  $P_T$  range of 88 and 100 Pa, a drastic change in growth rate with increase in  $P_T$  was observed. The films grown on c-Si generally showed higher increase in growth rate compared to the films grown on quartz substrates. In the third phase, the growth rate of the film on c-Si continues to increase with increase in  $P_T$  to 150 Pa but at a significantly slower rate. In contrast, within the same phase the film grown on quartz showed a slight decrease in growth rate with increase in  $P_T$ .

The main contributing factor in the low deposition rate was the low concentration of gases which limits the amount of available species for reactions and the film growth to occur. Low residence time for the radicals in the plasma due to the low concentration of  $CH_4$  and  $H_2$  gases lowers the probability for secondary gas phase reactions to occur between the radicals and excess molecules. This allows only primary gas phase reaction to occur and resulted in lower number of growth radicals and H atoms reaching the substrates and subsequently lowering the growth rates. The energetic hydrocarbon,  $CH^+$  ion bombardments on the growth surface also do not encourage the growth rate.

Secondary gas phase reaction is a reaction whereby the radicals, mainly  $CH_3$  and H, atoms produced from dissociation and ionization of  $CH_4$  and  $H_2$  during the primary gas phase reaction starts to interact and collide with excess molecules or with other radicals (Awang et al., 2006).

The reaction follows the sequences as listed below (Mutsukura et al., 1992; Rhallabi et al., 1991; Tachibana et al., 1984)



Increase in growth rate of a-C:H films grown by r.f. PECVD is typically contributed by increase in the number of hydrocarbon radicals especially methyl ( $\text{CH}_3$ ) growth radicals and hydrogen (H) atoms reaching the growth sites (von Keudell et al., 2002). The second phase of the film growth with respect to  $P_T$  could be the result of increased collision frequency of radicals produced through dissociation of gas molecules with excess gas molecules since the gas concentration was higher and there were more precursors available for reaction to occur. The flow rate ratios of  $\text{CH}_4:\text{H}_2$  of 20:100 and 25:125 sccm produced the  $P_T$  of 88 and 100 Pa respectively. The increase in collision frequency resulted in the increase in the number of  $\text{CH}_3$  growth radicals and H atoms reaching the substrates. This led to the enhancement in growth rate for this phase.

The faster increase in growth rate with  $P_T$  for the films on c-Si compared to the films deposited on quartz substrate was due to the presence of Si dangling bonds on the c-Si substrates which acted as growth sites for a-C:H growth. The absence of initial nucleation sites on quartz substrates may cause the slower increase in growth rates for

the films grown on this substrate. At the same time,  $H_2$  helps in forming the chemisorption sites for the film growth and this process is better on Si than on quartz substrate since the former possess high concentration of H terminated bonds (von Keudell et al., 2002). The H atoms through H etching effects also create nucleation sites for diffusion of  $CH_3$  radicals to increase the film growth rate.

Apart from the increase in the number of radicals suited for the growth at high flow rates, the increased presence of H radicals makes H etching effects on the film surface become significant. Excessive H atoms at the growth sites resulted in strong etching for C-C  $sp^2$  bonds and eventually decrease the growth rate (Deng et al., 2011; Silinskas et al., 2008). This substantially decelerated the growth rate of the film. The increase in H etching effect is believed to be due to the presence of higher H collision frequency rather than higher impingement energy of H atoms on the film surface. Although the H etching effect is similar on films deposited on both c-Si and quartz substrate, it seems to be more significant for latter. This suggests that the films deposited on c-Si substrate have higher structural order, with lower concentration of weak C-H bonds.

#### **4.1.2 Structural Properties of Hydrogenated Amorphous Carbon Thin Films**

Structure characteristics of a-C:H films was determined by non-destructive Raman spectroscopy (Deng et al., 2011; Goswami et al., 2008; Guangwei Guo et al., 2011; Marchon, 1997; Park et al., 2004). Raman scattering spectra of a-C:H films deposited at different  $P_T$  are shown in Figure 4.2.

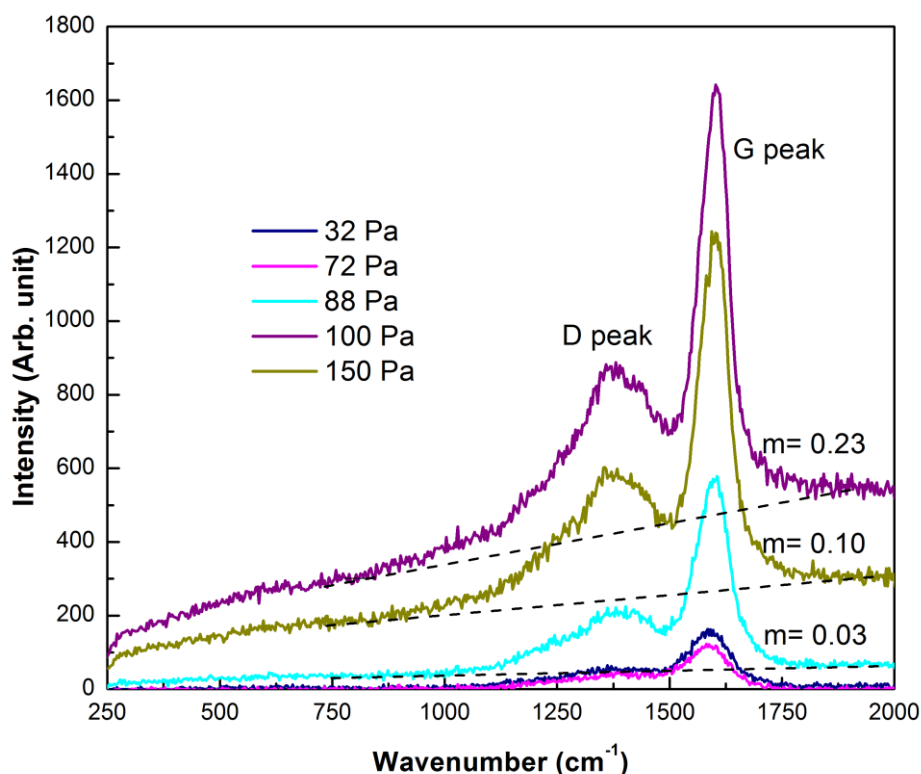


**Figure 4.2:** Raman spectra of a-C:H films deposited at different total gas pressure,  $P_T$ . Dashed line shows slanting background of Raman spectra which indicate the photoluminescence (PL) of films, where  $m$  is the slope of PL.

The Raman spectra of these a-C:H films showed the typical broad asymmetric peak in the range of 1200-1700  $\text{cm}^{-1}$ . This broad asymmetric peak was contributed by the presence of a mixed phase of  $\text{sp}^2$  and  $\text{sp}^3$  C-C bonds in the film. The feature of the Raman spectra in Figure 4.2 is typical for amorphous carbon (a-C) films whereby in the structure,  $\text{sp}^2$  bonded carbon clusters are embedded in  $\text{sp}^3$  amorphous matrix (Pandey et al., 2007).

IR absorption studies focused on the region at approximately 2900  $\text{cm}^{-1}$  corresponding to the vibration modes of various  $\text{sp}^2$  and  $\text{sp}^3$  C-H bonds. The relative hydrogen content,  $C_H$  determined from the C-H bonds concentration was estimated from the integrated intensity at about 2900  $\text{cm}^{-1}$  as was described in Chapter 3. The

plots of the absorption bands of a-C:H prepared in this region as a function of  $P_T$  are presented in Figure 4.3.

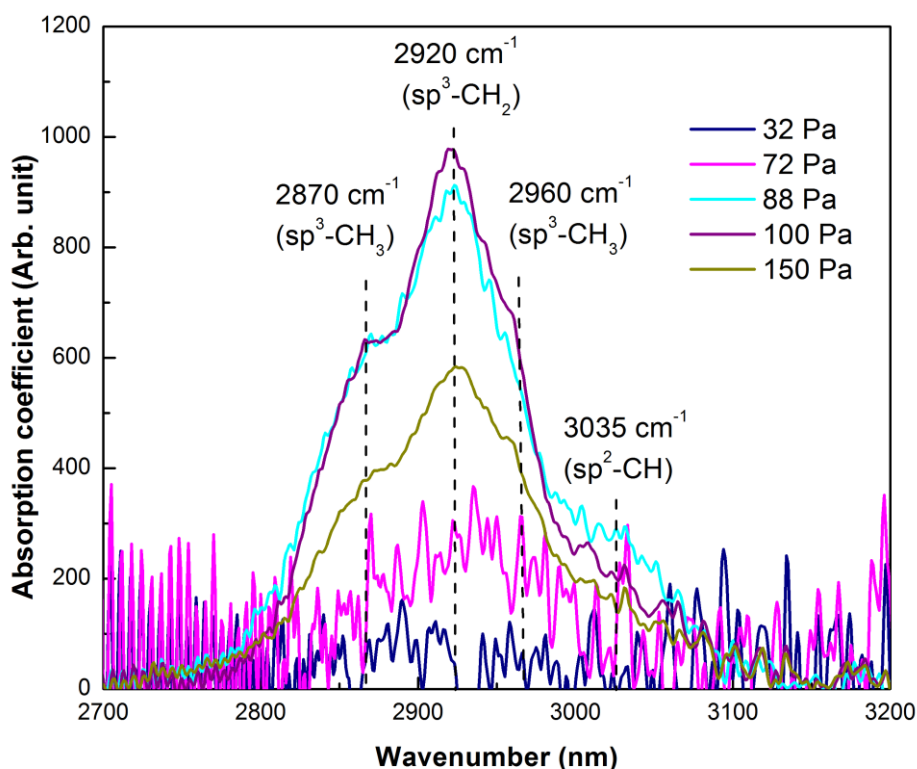


**Figure 4.3:** FTIR absorption spectra of C-H<sub>n</sub> vibrational bands of a-C:H films deposited at different total gas pressure,  $P_T$ .

Qualitative estimation on the amount of H bonded  $sp^2$  and  $sp^3$  was carried out by deconvolution of individual peak that was interpolated within the asymmetric CH<sub>x</sub> absorption band. Among them, the peak at 2920 cm<sup>-1</sup> is the most intense peak followed by the peak at 2870 and 2960 cm<sup>-1</sup> which corresponds to the  $sp^3$  hybridized carbon sites of  $sp^3$ -CH<sub>2</sub>, asymmetric  $sp^3$ -CH<sub>3</sub> and symmetric  $sp^3$ -CH<sub>3</sub> respectively (Deng et al., 2011).  $sp^2$ -CH absorption peak can only be clearly seen for films deposited at higher  $P_T$ . Figure 4.3 also alluded that the  $sp^3$ -CH were more dominant than  $sp^2$ -CH. This implied that the H atoms showed higher preference to bond with  $sp^3$ -C compared to  $sp^2$ -C bond sites (Deng et al., 2011) in the film structure. Quantitative analysis on the C<sub>H</sub> calculated



from the background slope of the Raman band in Figure 4.2 and the FTIR absorption band assigned to the  $sp^2$ -CH and  $sp^3$ -CH bonding modes in Figure 4.3 were also carried out and illustrated in Figure 4.4.

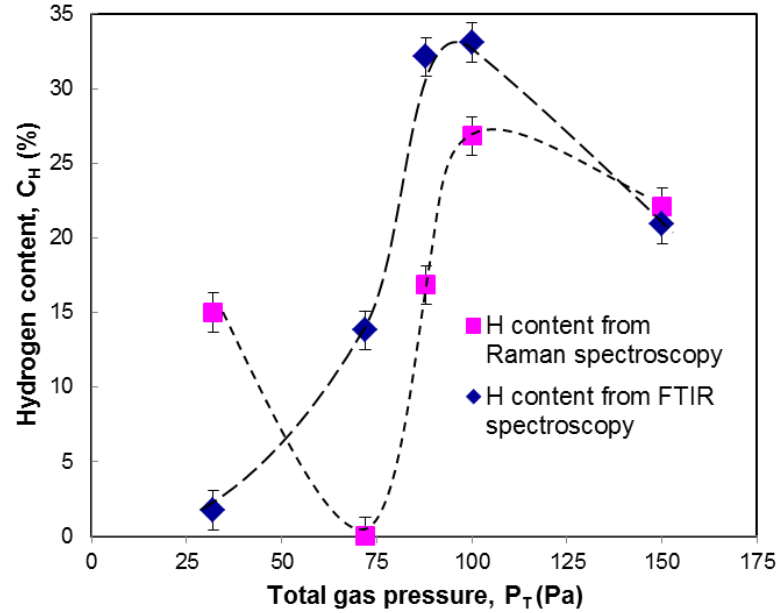


**Figure 4.4:** Hydrogen content,  $C_H$  of films deposited at different total gas pressure,  $P_T$ .

The  $C_H$  was estimated by analyzing the PL background of Raman spectra as identified by the dotted line depicted in Figure 4.2.  $C_H$  was obtained from the ratio between the slope ( $m$ ) of the fitted linear background and the height of the G band ( $H_G$ ) measured in micron,  $m/H_G$  (Casiraghi, Ferrari, et al., 2005; Casiraghi, Piazza, et al., 2005; Xie et al., 2010) as given in Equation 4.2.

$$C_H \text{ (at \%)} = 21.7 + 16.6 \log \left\{ \frac{m}{H_G} [\mu\text{m}] \right\} \dots\dots\dots \text{(Equation 4.2)}$$

The values of calculated  $C_H$  from FTIR and Raman spectra are shown in Figure 4.4. From the calculations, generally  $C_H$  increased with increase in  $P_T$ . The  $C_H$  obtained are within the range of 3 to 31 %. In the first growth phase region, where  $P_T$  is 32 and 72 Pa, the  $C_H$  showed reversed trend when calculated using these two techniques. This may be due to the fact that the  $C_H$  calculated from the Raman spectra include all the H atoms present in the film regardless of the atoms they were bonded to whereas the  $C_H$  calculated from IR spectra only include the H atoms bonded to C atoms only. This explained the higher  $C_H$  for film prepared at highest  $P_T$ . Furthermore, C. Casiraghi et al. (2005) emphasize that Equation 4.2 is not valid for films with  $C_H$  less than 20 %. In the next two growth regions, both techniques showed similar trends with regards to the  $C_H$  of the films, though the  $C_H$  bonded to C atoms was higher for the films deposited at the second growth phase region of  $P_T$  of 72 to 100 Pa. In this region the  $C_H$  increased significantly with increase in  $P_T$ . When the  $P_T$  was increased to 150 Pa, both films showed a noticeable decrease in  $C_H$ . These results showed that  $C_H$  calculated from Raman and FTIR were comparable.

The smaller number of H atoms reaching the substrate and more energetic  $CH^+$  ion bombardments (Xie et al., 2010) as was earlier discussed for the case of the low deposition rates might contribute to the low  $C_H$  measured from FTIR spectroscopy. Small amount of gases introduced into the chamber also resulted in the presence of low concentration of ions and radicals, therefore resulting in the stronger bombardment effect. This also contributed to the decrease in formation of C-H bonds in the films.

$C_H$  for films grown at 88 to 100 Pa was increased since larger number of ions and hydrocarbon radicals were produced with higher concentration of reactant gases. Methane,  $CH_4$  mainly produced three types of neutral particles, namely CH,  $CH_2$  and

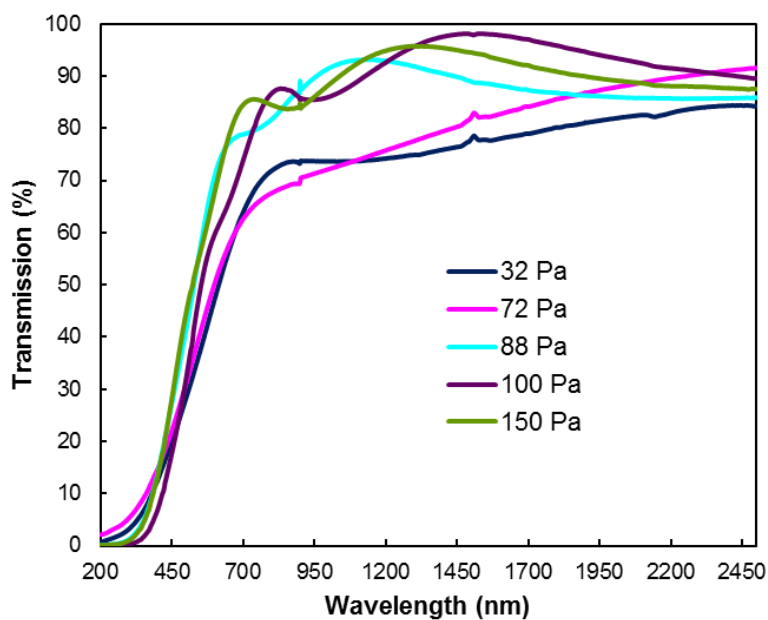
$\text{CH}_3$  (Yoon et al., 2000). The density of radicals and ions colliding with each other increases with the operating pressure of the vacuum chamber. Furthermore the chamber was fed with more diluent gas, H at these operating pressures. H atoms can form dangling bonds which act as nucleation sites that favour film growth and enhance  $\text{C}_\text{H}$ . H species can either decrease or increase the H content in the films (Guo et al., 2011). This is due to the competition between recombination of H species with dangling bonds resulting in the increase in  $\text{C}_\text{H}$ , and breaking of C-H bonds by H atoms to form  $\text{H}_2$  molecules followed by desorption causing  $\text{C}_\text{H}$  to decrease. The more dominant process is determined by the amount of H species present in the plasma (Guo et al., 2011; Viana et al., 2010; Yang et al., 2009). Apparently, in the case shown in Figure 4.4, the diffusion of H atoms onto the dangling bonds is the more dominant process thus suggesting that the presence of H atoms in the plasma for these films was high and the C-H bonds formed are strong enough which results in the breaking of C-H bonds less dominant.

At higher pressure of 100 to 150 Pa, synergisms between the  $\text{CH}_3$  and H atoms seem to slightly increase the growth rates of the films as shown in Figure 4.1. Less H atoms were incorporated into the film structure at 150 Pa resulting in the reduction of  $\text{C}_\text{H}$  in the film. The slow increase in growth rate and the lower  $\text{C}_\text{H}$  in this film showed that H etching effects is more dominant at this  $P_\text{T}$  since the number of H atoms reaching the substrates was significantly larger.

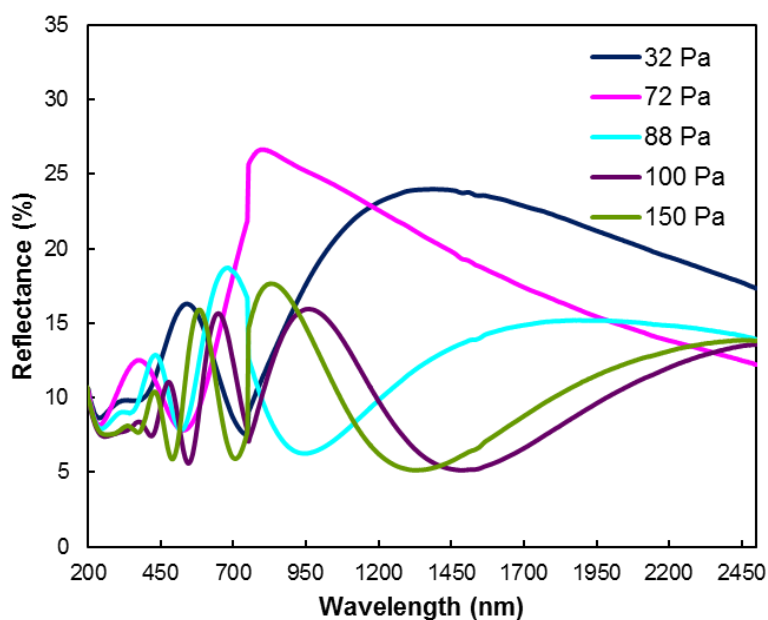
#### 4.1.3 Optical Energy Gap of Hydrogenated Amorphous Carbon Thin Films

The optical transmission and reflection spectra of the a-C:H films deposited at different  $P_\text{T}$  were measured using ultraviolet-visible-near infrared (UV-Vis-NIR)

spectrophotometer in the wavelength range between 190 to 2500 nm as shown in Figure 4.5(a) and 4.5(b), respectively.



(a)



(b)

**Figure 4.5:** Transmission (a) and reflection (b) spectra of a-C:H thin films.

The optical energy gaps (Dieguez Campo et al., 1998) of the films were obtained from these spectra at photon energy when the absorption coefficient,  $\alpha$  is equal to  $10^4 \text{ cm}^{-1}$ . This energy represents the minimum amount of energy for electron transition from maximum of extended state in the valence band to the minimum of extended state of conduction band.

The variation of  $E_g$  with respect to  $P_T$  in Figure 4.6 was studied. The relationship between the structural properties and growth rate of the films to the  $E_g$  were analyzed. The  $E_g$  increases to a highest value of 2.12 eV at 100 Pa and decreases slightly with further increase in  $P_T$ . Together with the plot showing the variation of  $C_H$  with  $P_T$  in Figure 4.4 which showed similar trend with  $P_T$ ,  $E_g$  could be said to be almost directly dependent on  $C_H$ . The growth rate of the films deposited on quartz substrate shown in Figure 4.1 also showed similar trend suggesting that  $E_g$  values of the films grown on this substrate were also almost directly dependent on the growth rate.

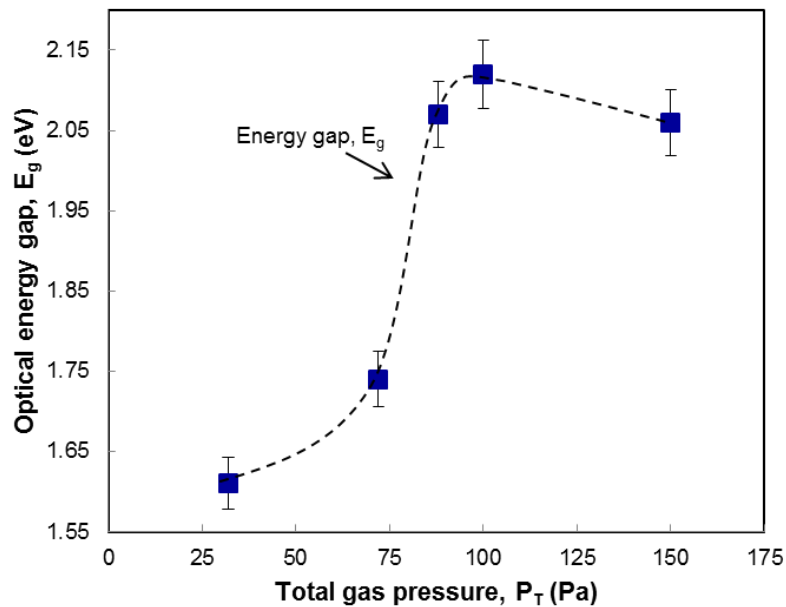


**Figure 4.6:** Energy gap,  $E_g$  variation of a-C:H films deposited at different total gas pressure,  $P_T$ .

In this section, the results showed that the increase in  $P_T$  markedly influence the  $E_g$  values of the films. This parameter also influences the  $C_H$  in the a-C:H films. The higher optical energy gap of the films deposited at higher  $P_T$  was shown to be due to the higher number of bonded  $C_H$  in the films. H atoms passivate the unsaturated bonds in the amorphous structure of a-C:H films, thus decreasing the defect states. This then decreases the absorption in the tail state region and consequently increases the  $E_g$  value (Alves et al., 2001). An increase in bonded  $C_H$  also saturates the  $\pi$  bonds thus promoting the  $sp^3$  hybridization over  $sp^2$  (Awang et al., 2006). By altering the  $sp^2$  fraction in the film, the  $E_g$  value of the films was increased due to incorporation of H atoms in the film structure. H atoms help to promote and stabilize the  $sp^3$ -C configuration in the film (Rusli et al., 1995).

#### **4.1.4 Photoluminescence Emission Properties of Hydrogenated Amorphous Carbon Films**

Figure 4.7 can be useful to elucidate the PL emission for the entire films. Significant PL emissions in the a-C:H films studied in this work were observed only from the films grown at  $P_T$  of 88, 100 and 150 Pa. The PL emission intensity was obviously enhanced for films deposited at  $P_T$  of 100 and 150 Pa. Low PL emission at 2.1 eV was exhibited by films grown at the lowest  $P_T$  of 32 and 72 Pa. The PL emission intensity increased with increasing  $P_T$  and had shifted towards higher energy of 2.4 eV. A broad, low PL emission was observed in the infrared region of energy 1.5 eV from the films deposited at 100 and 150 Pa.

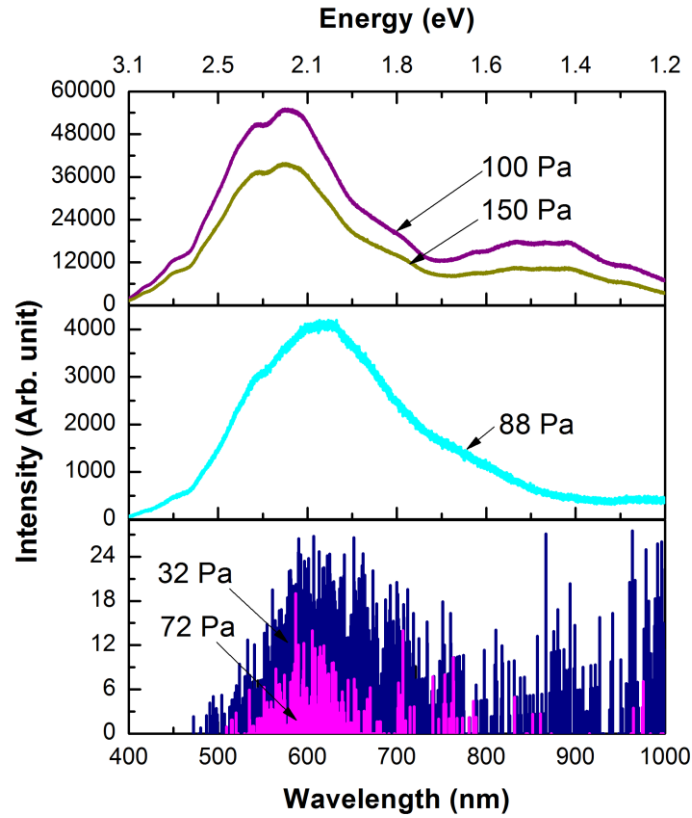


**Figure 4.7:** Variation of photoluminescence (PL) spectra of a-C:H films prepared at various total gas pressure,  $P_T$ .

From the Figure 4.7 and plots in Figures 4.6 and 4.4, it was observed that the PL intensity increases correspondingly with the increase in  $E_g$  and  $C_H$ . The results also show that PL emission intensity is highest for the films with the G peak position blue shifted above the graphite band limit of  $1580\text{ cm}^{-1}$ . This shift could therefore be related to the significant presence of the  $sp^2$  clusters in these films. These  $sp^2$  clusters introduce defect states which normally act as non-radiative recombination centers (Marchon et al., 1997; Robertson, 1996; Xie et al., 2010). However, the high PL emission produced by the films is due to passivation of the dangling bonds on these  $sp^2$ -C sites by H atoms resulting in these sites transforming to become radiative recombination centers producing the PL emission in the films (Rusli et al., 1995). This is confirmed by the higher  $C_H$  in these films as shown in Figure 4.4. The PL emission energy appears to

correspond to the  $E_g$  of the films suggesting that PL emission in these films was due to the band to band transition.

#### 4.1.5 Summary

This part of the work presents the investigation on the effects of  $P_T$  on the surface morphology, structure and optical properties of a-C:H films deposited by r.f. PECVD technique from the discharge of  $CH_4$  and  $H_2$ , at fixed  $CH_4$  to  $H_2$  flow rate of 1:5. The film growth rate has produced three phases of growth with respect to the  $P_T$ . The low residence time of the radicals and molecules in the chamber, and the energetic ion bombardments on the growth surface at  $P_T$  of 32 and 72 Pa produces almost no change to the growth rate and  $E_g$ . Significant increase in growth rate was observed in the second growth phase involving films grown at  $P_T$  of 88 and 100 Pa. The approach towards equilibrium between the film growth and  $H_2$  etching effects by the  $CH_3$  radicals and  $H$  atoms has produced the significant increase in growth rate and  $C_H$ . The  $H_2$  etching effects however become dominant, thus slowing down the growth process resulting in the slow decrease in the growth rate of the films on the c-Si and quartz when  $P_T$  increases to 150 Pa.

The obvious transformation of the film structure can be observed in the second phase of the film growth (72 to 100 Pa). This may be due to the increase in the flow rate of  $CH_4$  and  $H_2$  gases that was introduced into the chamber which simultaneously increases the  $P_T$  of the deposition process.

Passivation of the dangling bonds in the defect states by  $H$  atoms enhanced the growth rate, widened  $E_g$ , blue shifted the PL emission peak and enhanced the PL emission intensity. Thus, the work showed that  $H$  terminated  $sp^2$ -C sites acted as the



reactive recombination centers for PL emission in the films. The PL produced by these films is through band to band transition mechanism.

## 4.2 Effect of Argon Flow Rate on the Properties of Films Produced by r.f. Sputtering Process

The hybrid r.f. PECVD/ sputtering system consists of two main parts that is the r.f. PECVD and r.f. sputtering systems. In the previous section, the r.f. PECVD system was tested by depositing a-C:H films from the discharge of methane ( $\text{CH}_4$ ) and hydrogen ( $\text{H}_2$ ) at different total gas pressure,  $P_T$ . Films with controllable structural and optical properties were grown by changing the  $P_T$ . In this section, the r.f. sputtering part is tested by growing films sputtered from amorphous silicon (a-Si) target. The a-Si target however has a layer of a-C:H and silicon oxide ( $\text{SiO}_x$ ) covering the surface. The a-C:H layer was formed during earlier deposition when  $\text{CH}_4$  gas was discharged in the plasma while the  $\text{SiO}_x$  layer was formed at the surface due to passivation of Si dangling bonds when the target was exposed to the atmosphere after each deposition process.

The Ar flow rate is an important parameter influencing the properties of the films deposited by sputtering of the a-Si target. The growth rate, structural and photoluminescence (PL) emission properties were studied with respect to the Ar flow rate. The deposition pressure increases correspondingly according to the Ar flow rate. The r.f. power was fixed at 100 W for all depositions. The other deposition parameters of the films studied in this section is tabulated in Table 3.6. The films prepared by this deposition technique were predicted to consist of mixed phases of a-C:H, a-SiC, a-Si, and  $\text{SiO}_x$ . However, the a-SiC and a-C:H phases were comparatively very small since these phases were formed from the sputtering of the layer of a-C:H covering the a-Si target formed during earlier depositions.

#### 4.2.1 Effect of Argon Flow Rate on Growth Rate of the Deposited Thin Films

Figure 4.8 depicts the change of the film growth rate deposited at Ar flow rates of 5.7, 7.5, 15 and 30 sccm.

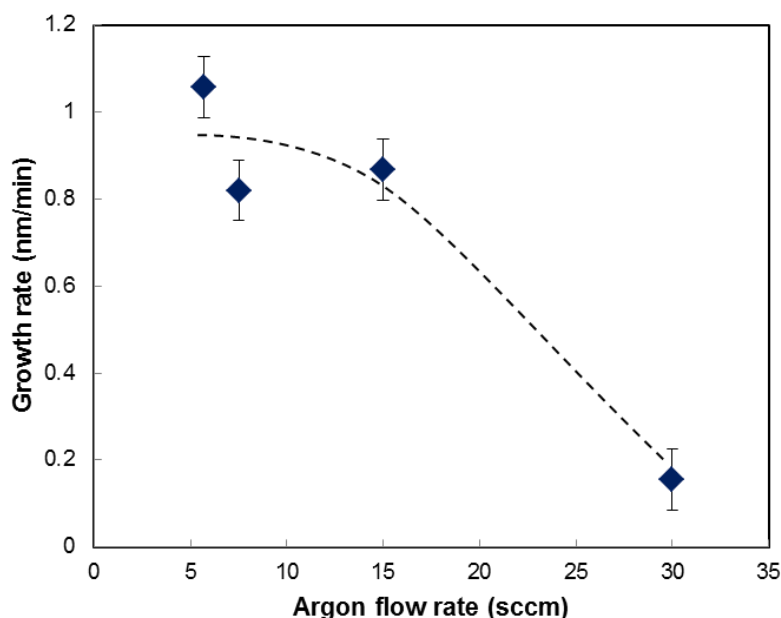


**Figure 4.8:** Variation of the growth of deposited films as a function of Argon (Ar) flow rate.

The deposition pressure increases correspondingly with increasing Ar flow rate as tabulated in Table 3.5. The variation of the growth rate implies that Ar flow rate gives direct impact to the growing process of the films due to the significant decrease in growth rate with increasing Ar flow rate.

Low Ar flow rates up to 15 sccm resulted in a slow decrease in growth rate. On the other hand, an increase in Ar flow rate to 30 sccm resulted in a steep decrease in the growth rate. Low concentration of Ar ions in the chamber resulted in more energetic Ar ions moving towards the a-Si target due to lower frequency collision with other Ar atoms present in the chamber. Correspondingly, an increase in Ar flow rate resulting in

decrease of the growth rate of the films due to low energetic Ar ions sputtering the target.

#### **4.2.2 Effect of Argon Flow Rate on Structural Properties of the Deposited Thin Films**

Elemental compositions within the film structure were determined using Auger electron spectroscopy (Frach et al., 2010). This technique is one of the most used techniques to investigate the elemental composition and status of the deposited thin films (Lei et al., 2000).

Auger depth profiling analysis was carried out to obtain information on the distribution of elemental atoms present within the film structure below the surface of the films. The relative concentration of the main atoms present in the films studied in this work as obtained from the Auger depth profiling is illustrated in Figure 4.9. The three main atomic components present in the films are carbon (C), oxygen (O) and silicon (Si). The C content is the lowest for all the films followed by Si and O. The spectra show that the films have uniform composition distributions within the depth of the films except at the surface of the films deposited using Ar flow rates of 5.7, 7.5, and 10 sccm. In these films, relative C atomic composition showed a sudden increase while the relative O atomic composition showed a sudden drop.

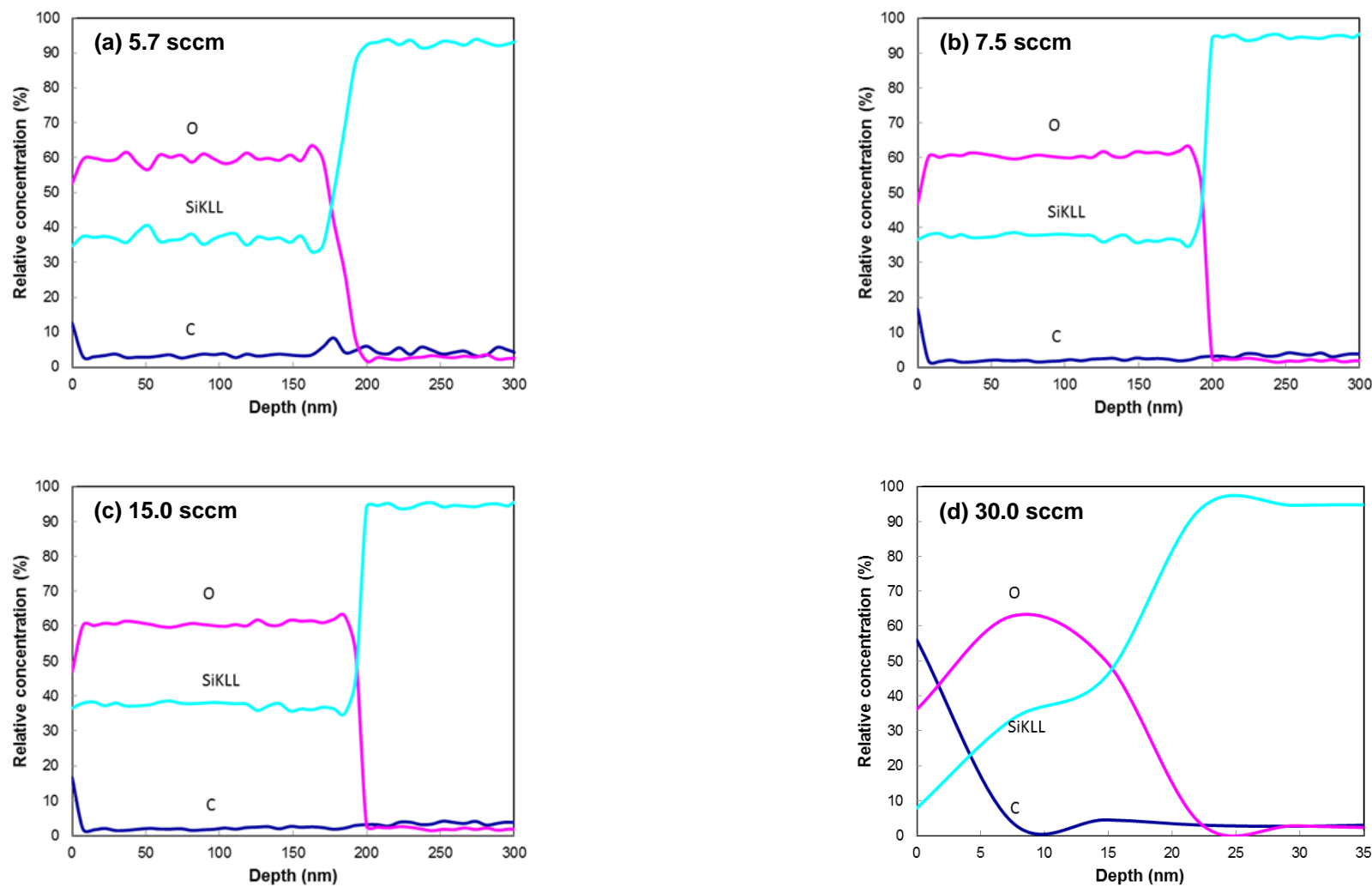


**Figure 4.9:** Variation of the growth of deposited films as a function of Argon (Ar) flow rate.

This shows that all these atoms originated mainly from the a-Si target. The surface target consists of O atoms which actively passivated the Si dangling bonds when the target was exposed to the atmosphere after the deposition process. The C atoms were incorporated into the a-Si target during earlier deposition of films where CH<sub>4</sub> gas was discharged by r.f. PECVD. The Ar and CH<sub>4</sub> gases acted as sputtering ion and C based precursor sources, respectively. Therefore, the C atoms were incorporated deeper into the target compared to the O atoms.

The more dominant O atoms present in the films showed that the a-Si target was covered by a significant layer of SiO<sub>x</sub> films and the C incorporation was very small relatively. During the deposition process, Ar ions also sputtered off atoms at the growth surface of the films and removed O and C atoms at a constant rate. However, when the r.f. power was turned off, the substrate temperature was not high enough to passivate the Si dangling bonds at the surface with O atoms but these Si dangling bonds readily bonded with the C atoms present at the growth sites. This explained the increase in relative concentration of C atoms at the surface of the films with respect to Si atoms. When the flow rate of Ar was increased to 30 sccm, sputtering rate was significantly reduced as only a thin layer of film was deposited. For this film, the surface effect where the C atom concentration was increased even higher than both Si and O atoms. The higher frequency of Ar ions bombardment on the surface created higher concentration of Si dangling bonds at the growth sites. Thus, when r.f. power was switched off, the C atoms present at the growth sites were quickly incorporated at surface of the film. This increased the relative C atoms concentration at the surface of this film.

To further confirm the surface effects during the deposition, the change of relative concentration for the expected elements present at the surface of the films for various Ar flow rate is shown in Figure 4.10. It can be seen here that Ar flow rates influenced the elemental composition strongly at the surface rather than the inner layer of the films. The relative concentration of C at the film surface increased with increase in Ar flow rate and reached a maximum for film deposited with Ar flow rate of 30 sccm.

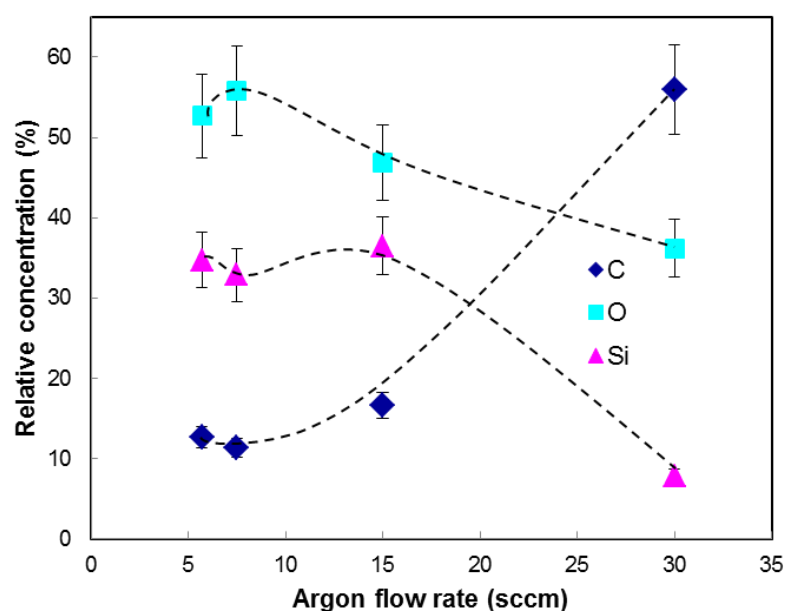


**Figure 4.10:** Relative concentration at the surface of the films relative to Ar flow rate.

The results suggested that the film compositions were independent of the Ar flow rate but significantly changed at the surface of the films. The C composition at the surface evidently increases with the increase in Ar flow rates as shown in Figure 4.10. The increase in relative C composition and relative decrease in elemental composition of Si and O showed that C atoms present at the growth sites were easily incorporated

into the film structure when r.f. power was turned off to passivate the Si dangling bonds.

Raman spectroscopy was employed to study the structural properties of the films. The existence of the mixed phases of a-Si and a-C:H phases in the films deposited by this process can be shown through analysis of Raman absorption band from the presence of Si-Si and C-C network in the films (Shi et al., 1999). The presence of the phases were expected based on the fact that the deposition process only involved Ar and no other gases which was used as the sputtering gas source during the deposition process. As mention earlier, the a-Si target was coated with a-C:H layer through earlier deposition process involving discharge of CH<sub>4</sub> in the chamber and SiO<sub>x</sub> layer through passivation of Si dangling bonds when target was exposed to the atmosphere. Otherwise, only a-Si phase was expected in these films.

Raman absorption spectra were taken within the range of 100 to 2000 cm<sup>-1</sup> as shown in Figure 4.11. Raman spectra exhibit various slopes,  $m$  due to the photoluminescence (PL) background. The value of the respective slope,  $m$  for each film is stated in the same figure. Strong PL is related to hydrogen (H) saturation of the non-radiative recombination centers, as was elaborated in Section 4.1.2.



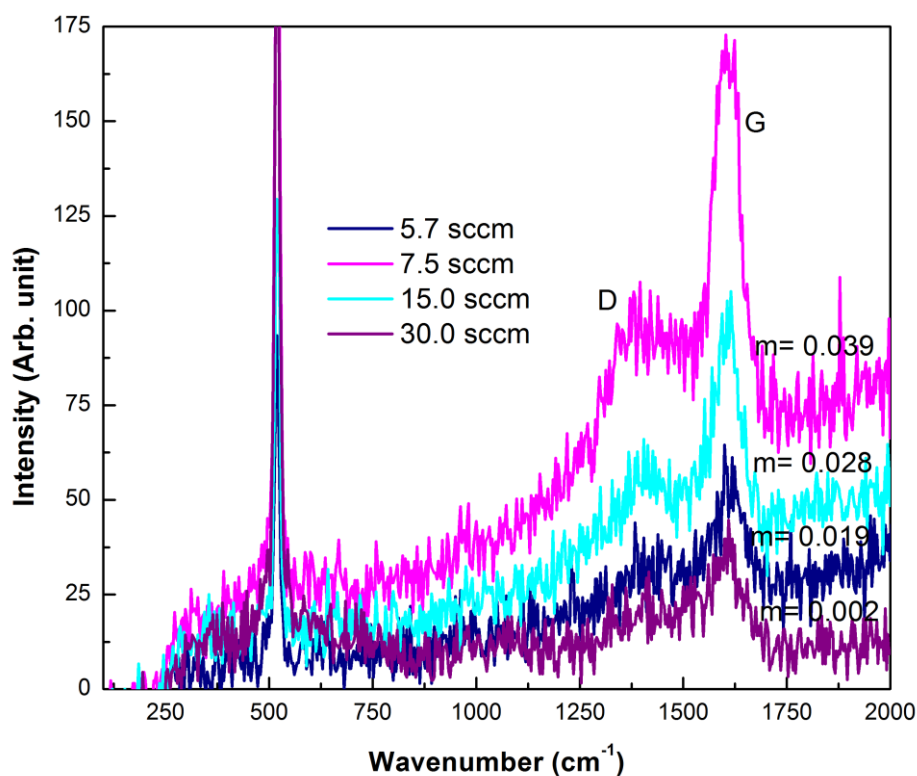


**Figure 4.11:** The whole range of Raman spectra for a-SiC thin films deposited at various Ar flow rate and their corresponding slope,  $m$ .

The overall Raman spectra were divided into two parts according to the bonding configurations of the films as shown in Figure 4.12 and 4.13. Figure 4.12 and 4.13 capture the Si-Si network regions and C-C networks region in the films, respectively. All the films studied exhibit the same spectra producing both the Si-Si and C-C network regions indicating that these films have mix phases of both a-Si and a-C:H phases.

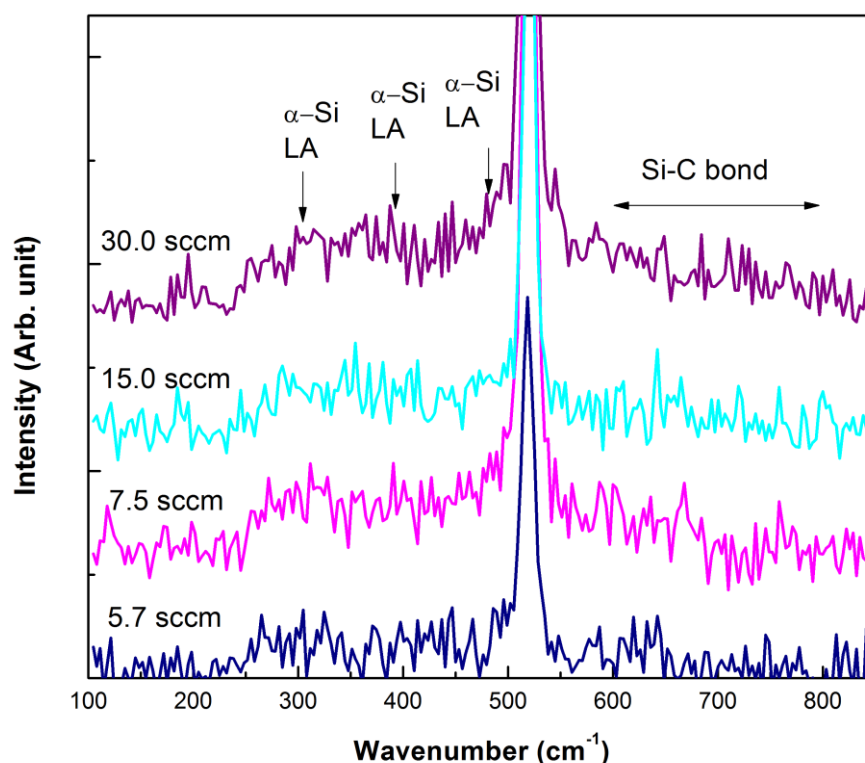


**Figure 4.12:** Raman spectra in the range of 100 to 850  $\text{cm}^{-1}$  which consists of several overlapping peaks indicating the existence of Si-Si network in the films.

The overlapping band at low wavenumber of 300, 380 and 480  $\text{cm}^{-1}$  assigned to the main features of Si-Si network that are produced by longitudinal acoustic (LA), longitudinal optic (LO) and transverse optic (TO) of a-Si, respectively. The presence of these overlapping bands suggested that all of the films were amorphous in structure (Swain and Dusane, 2007). The Si-C band should be detected at around 600 to 1000  $\text{cm}^{-1}$ . However, the Si-C absorption band was not observed due to the smaller Raman efficiency of the Si-C band compared to C-C and Si-Si band (Cheng et al., 2008).

Figure 4.12 also displays the Si-Si network which is produced by the a-SiC phase in the films and c-Si substrate. The Raman spectra in this region are quite featureless except for the c-Si peak at about 520  $\text{cm}^{-1}$  contributed by c-Si substrate

(Cheng et al., 2008; Shi et al., 1999; Swain and Dusane, 2006). The first order c-Si peak was so dominant such that the other peaks were suppressed.

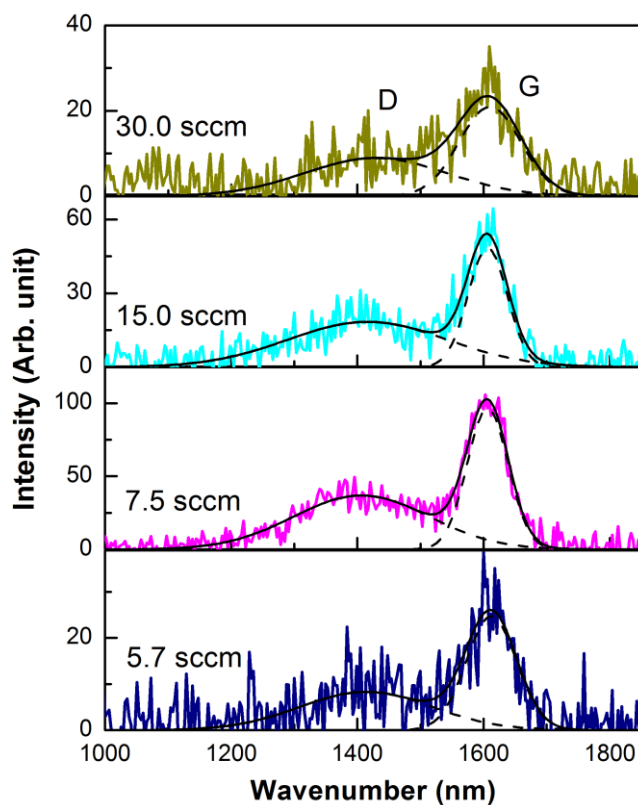


**Figure 4.13:** Raman spectra in the range of 1000 to 1800  $\text{cm}^{-1}$  which consists of D and G peak indicating the existence of C-C network in the films.

Figure 4.13 shows the Raman spectra in the range of 1000 to 1800  $\text{cm}^{-1}$  which represent the C-C network in the film structure (Cheng et al., 2008; Chew, 2002; Hu et al., 2004; Shi et al., 1999). The presence of this peak in the Raman spectra showed that the a-C:H phase in the films was quite significant especially for the film deposited at 7.5 sccm. This showed that the a-C:H layer on the target can produce a significant presence of a-C:H phase in the film structure.

Further study on the structural properties of the films was carried out by FTIR spectroscopy. The broad FTIR spectroscopy provides information concerning the chemical bonding and composition of two major vibration modes of Si-C stretching and Si-O stretching within the range of 650 to 1400  $\text{cm}^{-1}$  as can be seen in Figure 4.14. FTIR absorption spectra are mainly observed at approximately 800 and 1050  $\text{cm}^{-1}$ . They are typically assigned to Si-C stretching and Si-O stretching vibration absorption respectively (Dieguez Campo et al., 1998; Li et al., 2011; Sha et al., 2005). Several additional peaks expected in this region overlapped with the major peaks. The overlapping peaks consist of peaks located at 1020 and 1230  $\text{cm}^{-1}$  which correspond to Si-CH<sub>n</sub> rocking (Rusakov et al., 2001) and Si-CH<sub>n</sub> bending modes, respectively (Mori et al., 2006). There were also reports assigning the peak at 840  $\text{cm}^{-1}$  to Si-O-Si stretching vibration mode (Dohi et al., 2002; Khashan et al.).

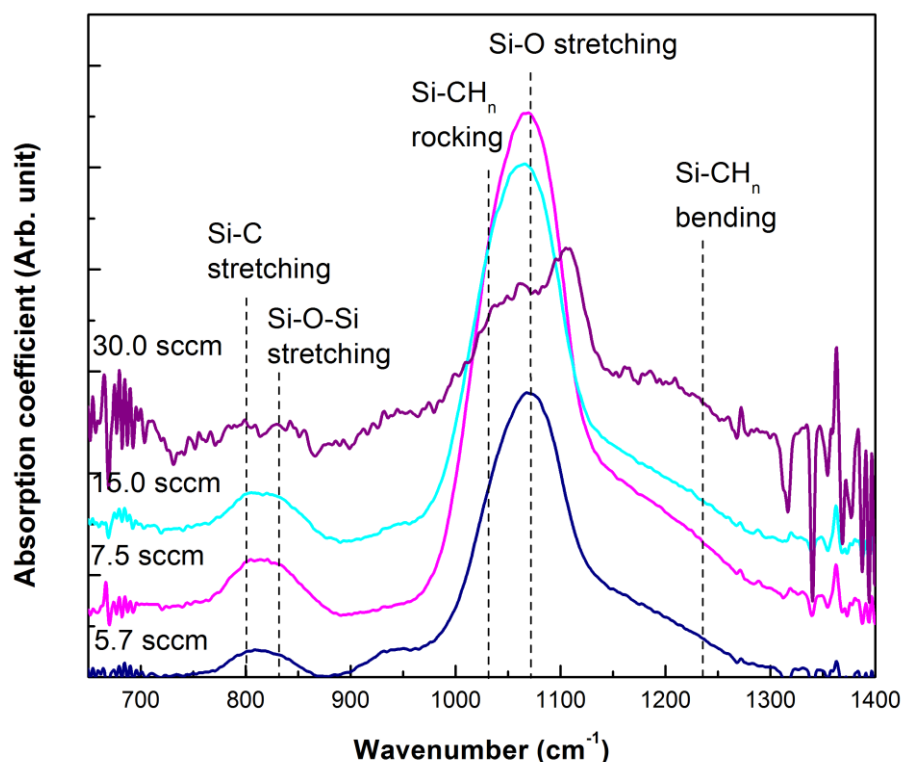


**Figure 4.14:** FTIR spectra of silicon carbon films deposited at different Ar flow rate showing the absorption band within the spectral range.

From Figure 4.14, it was observed that the presence of Si-O peak was most dominant in the spectra of all the films. However, this was expected since the AES results showed dominant presence of O atoms in the films. As mentioned earlier, the a-Si target surface was covered by a layer of  $\text{SiO}_x$  as O atoms have actively passivated the Si dangling bonds as soon as the target was exposed to the atmosphere. Rajagopalan et al. (2003) also showed similar observation regarding the existence of Si-O peak for their deposited films. The sputtering process has etched out all of the components on the a-Si target including the  $\text{SiO}_x$  layer on the surface of the target and the layer can be quite significant as shown by the results. SiC peaks were also observed in the films deposited using Ar flow rates of 5.7, 7.5 and 15 sccm when the sputtering rate was high. This shows that at low sputtering rate as produced during the deposition with Ar flow rate of 30 sccm failed to form Si-C phase in the film.

#### **4.2.3 Effect of Argon Flow Rate on Photoluminescence Properties of the Deposited Thin Films**

PL emission spectra of silicon carbon films deposited at different Ar flow rate are presented in Figure 4.15. He-Cd laser at UV-light wavelength of 325 nm was used as an excitation source. PL emission for substrate was scanned as a reference. All of the films showed similar features one major peak centered at around 600 nm and a minor peak at about 675 nm. From the spectra, the peaks positions remained the same for all films. PL emission increases with increasing Ar flow rate up to 7.5 sccm and decreases with further increase in Ar flow rate to 15 and 30 sccm. The PL emission intensities obviously showed strong dependence on the Ar flow rate.

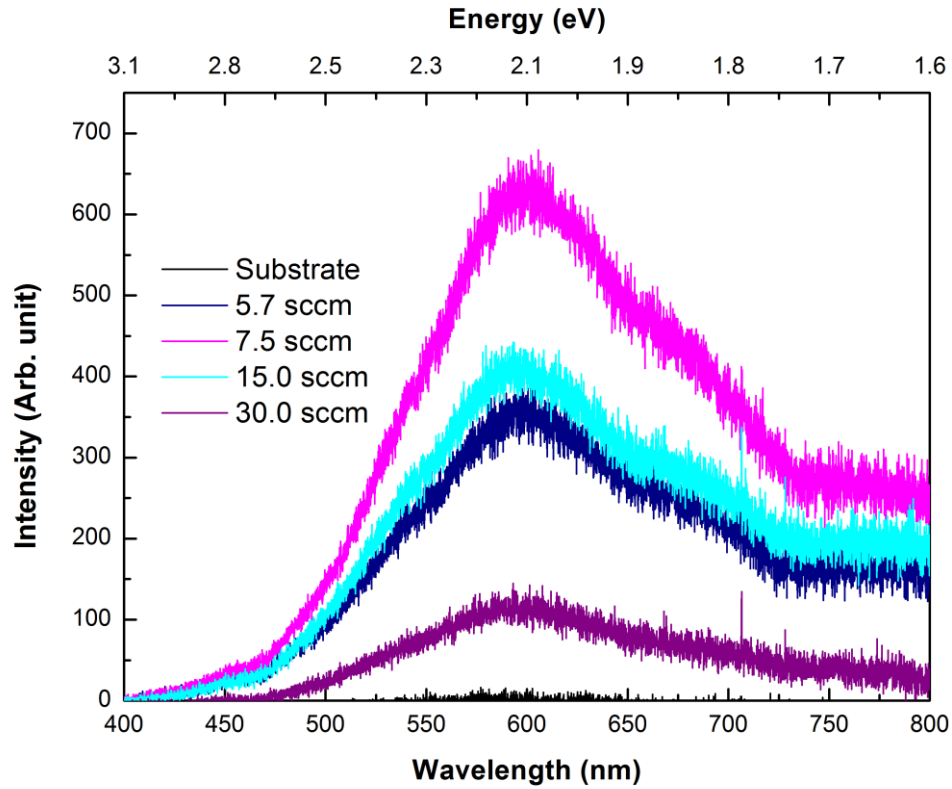


**Figure 4.15:** PL spectra of silicon carbon film deposited at different Ar flow rate.

The dominant effects of the presence of Si or C in a-SiC thin films on the PL emission properties have been widely studied by several researchers (Cheng et al., 2008). Some researchers showed that strong PL was exhibited by carbon-rich samples. H atoms passivate the  $sp^2$ -C bonds and these sites act as radiative recombination centers for PL emission due to quantum confinement effect. The presence of the  $sp^2$ -C clusters within a-C:H, a-Si:H, SiC and  $SiO_x$  phases in the film structure may be the origin of the broad PL emission band in these films. As shown in Figures 4.13 and 4.14, the presence of a-C:H and  $SiO_x$  phases was most dominant in the film deposited at Ar flow rate of 7.5 sccm. This shows that  $sp^2$ -C clusters embedded within the a-C:H and  $SiO_x$  phases contribute most to the PL emission in the films as these films produce the highest PL emission intensity.

#### 4.2.4 Summary

A set of films were deposited at different Ar flow rate of 5.7, 7.5, 15 and 30 sccm by means of r.f. sputtering component in the hybrid r.f. PECVD/sputtering system. The films were deposited on c-Si substrates by sputtering the a-Si target which was exposed to CH<sub>4</sub> discharge during previous deposition in the deposition chamber. Different flow rate of Ar introduced into the chamber controlled the film growth rate based on the bombardment energy of the Ar ions. The growth rate was highest at the lowest Ar flow rate of 5.7 sccm. Information related to elemental composition, structural properties, chemical bonding and optical properties of the films shows that the films consist of significant component of a-C:H and SiO<sub>x</sub> phases which contribute most to the PL emission from the film. The origin of PL emission in these films was deduced to be due to quantum confinement effects in the sp<sup>2</sup>-C clusters embedded within a-C:H and SiO<sub>x</sub> matrix.

### **4.3 Effects of r.f. Power on Amorphous Silicon Carbon Films Prepared by Hybrid PECVD/Sputtering Deposition System**

Previous work to assess and test separately the efficiency of the two main techniques involved in the newly designed hybrid r.f. PECVD/sputtering system was accomplished. In this section, the feasibility of combining both techniques to grow a-SiC films was investigated. The films were deposited by simultaneous sputtering of a-Si target in plasma discharge of CH<sub>4</sub> gas. The effects of r.f. power on the growth rate, structural and PL properties of a-SiC thin films were studied.

#### **4.3.1 Growth Rate of Amorphous Silicon Carbon Thin Films**

The film thickness and corresponding growth rate of the films deposited by r.f. PECVD were contributed by several factors dependent on the deposition parameter used. With respect to r.f. PECVD, the growth rate was strongly influenced by dissociation of the precursor gas, CH<sub>4</sub> followed by the secondary gas phase reactions (Awang et al., 2006). Hydrogen etching effects also influenced the film growth rates. Growth rate of the films deposited by r.f. sputtering was strongly influenced by the Ar flow rate as shown in the previous section. In this part of work, the two processes were operated simultaneously and the effects of r.f. power on the film properties were investigated.

Figure 4.16 presents the growth rate of a-SiC thin films deposited by hybrid PECVD/sputtering deposition system on c-Si substrate with respect to r.f. power. The deposition rate of the silicon carbon films increase drastically to a maximum when deposited at r.f. powers of 100 and 120 W and decrease steeply for the film deposited at r.f. power of 150 W.



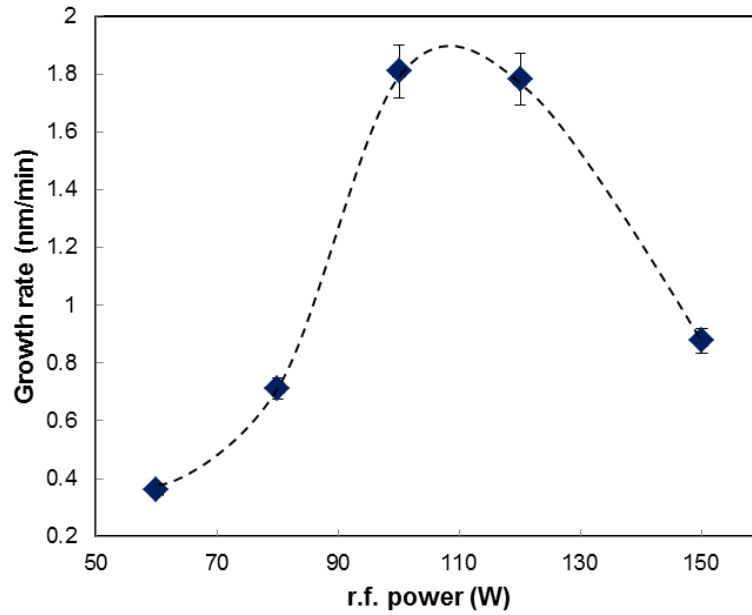
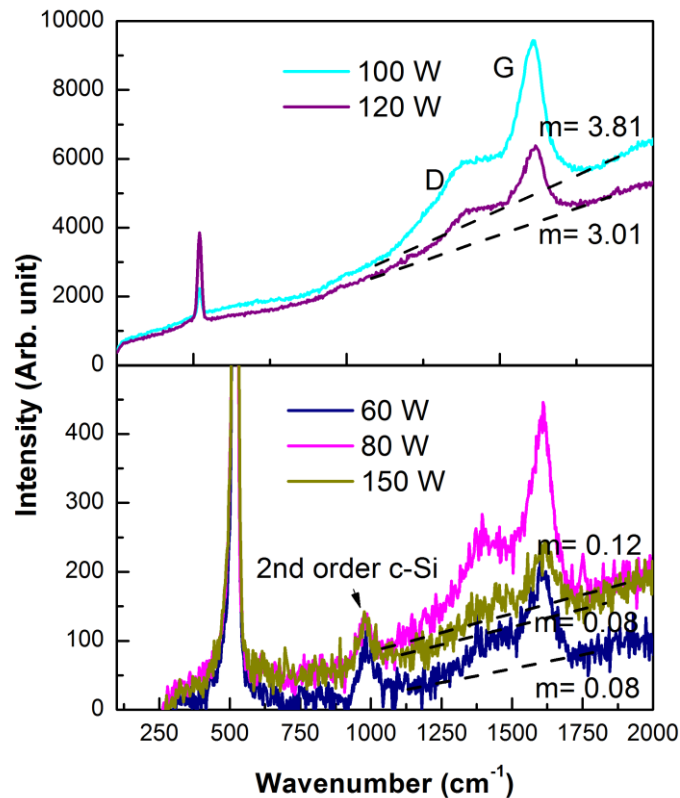


**Figure 4.16:** Growth rate of a-SiC thin films prepared by hybrid PECVD/sputtering deposition system.

The magnitude of r.f. power is shown to have strong influence on the growth rate of a-C:H films. The r.f. power dissociated the  $\text{CH}_4$  gas and ionized the Ar gas thus increasing the number of C based growth precursors and Ar ions in the chamber, respectively. The latter increased the bombardment effects on the a-Si target thus sputtered off higher concentration of Si atoms to be deposited on the substrates. These combined effects significantly increase the growth rate at 100 and 120 W. However, increase in r.f. power also produces sputtered off atoms from the growth surface of the films. This was expected to result in a competition between film growth and etching rates at the growth surface depending on whichever effect was more dominant. Obviously, the etching effect was more dominant at r.f. power of 150 W and this led to the decrease in the film growth rate.

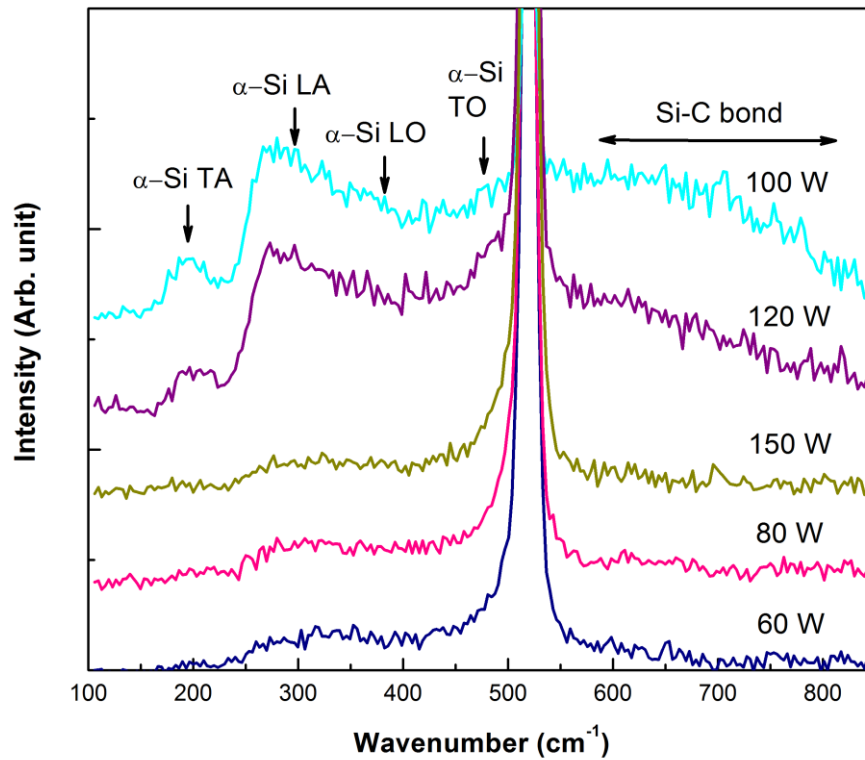
### 4.3.2 Structural Properties of Amorphous Silicon Carbon Thin Films

The Raman spectra within 100 to 1800  $\text{cm}^{-1}$  for films deposited at different r.f. power are presented in Figure 4.17. Significant PL background and their corresponding slopes,  $m$  are displayed in the same figure. The slope increased to a high value for the films deposited at r.f. powers of 100 and 120 W and decreased for film deposited at 150 W. This showed that the  $C_H$  in the films deposited at r.f. powers of 100 and 120 W was the highest and the trend was similar to the trend showed by the growth rate. The existence of Raman peak at around 100 to 850  $\text{cm}^{-1}$  and 850 to 1800  $\text{cm}^{-1}$  showed the existence of expected Si-Si and C-C network of a-SiC thin films respectively (Swain and Dusane, 2006).



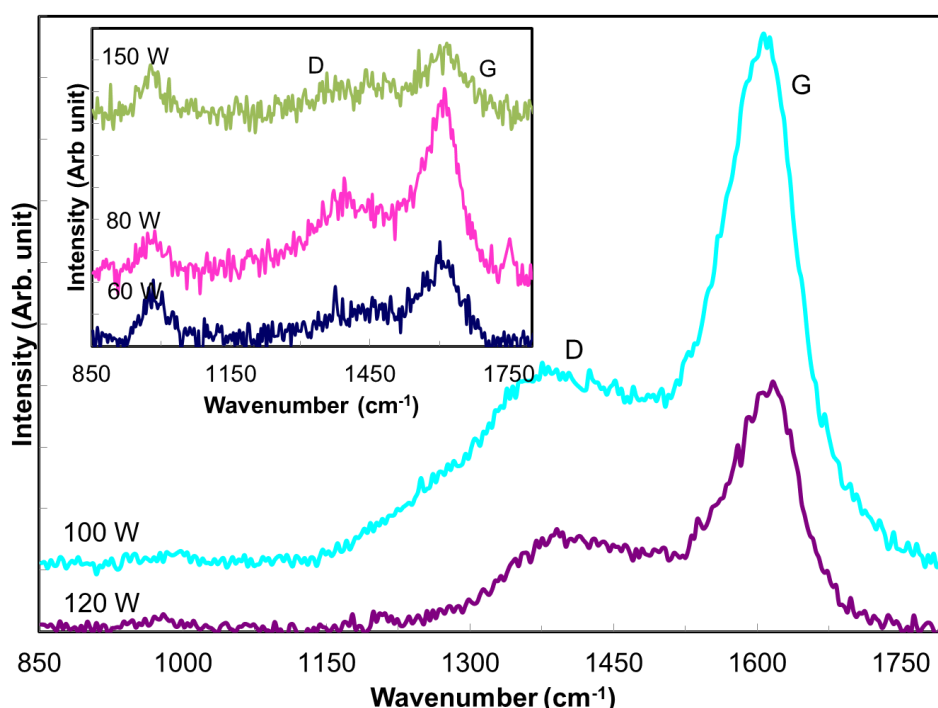
**Figure 4.17:** The whole range of Raman spectra for a-SiC thin films and their corresponding slope,  $m$ .

Figure 4.18 shows the Raman spectra in the region focused on the Si-Si network for all samples in the range of 100 to 850  $\text{cm}^{-1}$ . A broad absorption band produced by the overlapping of Si-Si transverse acoustic mode (TA) at 150  $\text{cm}^{-1}$ , Si-Si longitudinal acoustic (LA) branch at 300  $\text{cm}^{-1}$ , Si-Si longitudinal optical (LO) mode at 380  $\text{cm}^{-1}$  and the transverse optical (TO) branch from the contribution of the amorphous silicon at 480  $\text{cm}^{-1}$  (Shi et al., 1999; Swain and Dusane, 2006; Swain and Dusane, 2007) are observed for the films deposited at 100 and 120 W. Appearance of broad peak between 600 to 800  $\text{cm}^{-1}$  as illustrated in Figure 4.18 indicates the presence of Si-C phase in the films (Swain and Dusane, 2006).



**Figure 4.18:** Silicon network of a-SiC thin films observed from Raman spectra in the range of 100 to 850  $\text{cm}^{-1}$ .

The strong protruding peak located at  $520\text{ cm}^{-1}$  in Figure 4.18 and the peak at  $950\text{ cm}^{-1}$  illustrated in Figure 4.19 correspond to the first and second order vibration of crystal silicon (c-Si) substrates respectively (Shi et al., 1999; Swain and Dusane, 2007). The appearance of the sharp protruding peak at  $520\text{ cm}^{-1}$  indicates that the films were very thin and very transparent and when excited by the ultra-violet (UV) laser wavelength of  $325\text{ nm}$ , the laser light penetrated right through the film and reached the substrate (Shi et al., 1999; Swain and Dusane, 2007).



**Figure 4.19:** Carbon network of a-SiC thin films observed from Raman spectra which was baseline corrected in the range from  $850$  to  $1800\text{ cm}^{-1}$ .

The results show that the films deposited at  $100$  and  $150\text{ W}$  had high growth rate and the a-Si and a-C:H phases were very dominant in these films. The  $\text{C}_\text{H}$  with the C-C network was also very high for these films. For the film deposited at  $150\text{ W}$ , the a-Si phase was almost insignificant but a-C:H phase was still significant. The bombardment on the growth sites effectively removed the a-Si phase at this high r.f.

power. Figure 4.19 shows the stacked C-C network obtained from Raman spectra in the range of 850 to 1800  $\text{cm}^{-1}$ . The insert in this figure shows the stacked C-C network for the films deposited at 60, 80 and 150 W which exhibited a very low intensity band compared to band produced by films deposited at 100 and 120 W.

Next, FTIR spectroscopy was used to study the bonding properties of the films. The FTIR spectra of the films prepared at different r.f. powers are presented in Figure 4.20. The presence of Si-C and Si-O stretching bonds in the films is represented by the peaks at the wavenumber of 800  $\text{cm}^{-1}$  (Wang et al., 2002) and 1050  $\text{cm}^{-1}$  respectively (Li et al., 2007; Sundaram et al., 2000).

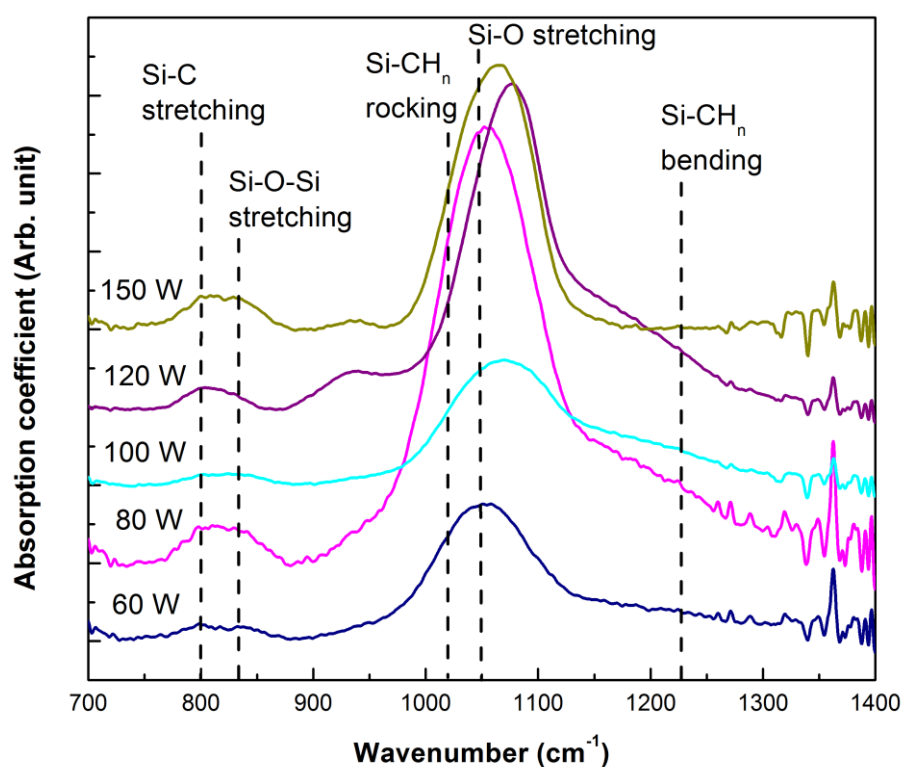


**Figure 4.20:** FTIR spectra of the silicon carbon films deposited at different r.f. power showing the absorption bands expected in silicon carbon films within the spectral range.

The peak at 800 to 840  $\text{cm}^{-1}$  is assigned to the overlapping of SiC transverse optical phonons (Dieguez Campo et al., 1998) at 800  $\text{cm}^{-1}$  and Si-O-Si stretching vibration mode at 840  $\text{cm}^{-1}$  (Dohi et al., 2002). The broad peak between 950 and 1250  $\text{cm}^{-1}$  are produced by the overlapping of several peaks namely Si-CH<sub>n</sub> rocking (Rusakov et al., 2001) at 1020  $\text{cm}^{-1}$ , Si-O stretching at 1050  $\text{cm}^{-1}$  (Sha et al., 2005) and Si-CH<sub>n</sub> bending at 1230  $\text{cm}^{-1}$  (Mori et al., 2006). It can be seen that the presence of Si-O bonds were very dominant in these films and the peak at 800 to 840  $\text{cm}^{-1}$  basically was dominated by Si-O-Si stretching band rather than Si-C stretching except for the film deposited at 120 W. The a-SiC phase in the films can be seen to consist of mainly hydrogenated amorphous silicon carbon (a-SiC:H) phases since the Si-CH<sub>n</sub> rocking and bending modes were quite significant in all the films. The SiO phase was quite significant in these films and this phase originated from the SiO layer in the initial part of the sputtering. From this result, it can be concluded that the films were multiphase in structure consisting of a-Si, a-SiC:H and a-C:H. The presence of the a-C:H phase was mainly confirmed by the Raman spectra.

#### 4.3.3 Photoluminescence Properties of Amorphous Silicon Carbon Thin Films

Figure 4.21 shows the room temperature PL emission spectra of the films deposited at different r.f. power excited by UV laser operating at wavelength 325 nm recorded in the wavelength range of 400 to 800 nm. The PL emission spectrum of c-Si substrate was seen to produce low intensity PL emission band centered at 604 nm possibly contributed by virgin oxide present on the surface. It can be seen that the presence of deposited films result in a shift in the PL emission peak to lower wavelength. The film deposited at 60 W produced PL emission blue shifted below 600 nm. This film mainly consisted of a-C:H phase and SiO phase as shown in Raman and FTIR results. The PL emission peak broadened with increase in r.f. power due to

increase in presence of a-C:H and SiO phases in the films. The PL intensity was also increased with increase in r.f. power especially for films deposited at 100 and 120 W. and dropped for the film deposited at r.f. power of 150 W. The high PL emission produced by films deposited at the 100 W was due to the dominant presence of a-C:H and a-SiC phases in the film as SiO<sub>x</sub> phase is smaller in this film as indicated by the FTIR spectrum. The PL emission peak was also narrower and was blue-shifted. The dominant presence of a-C:H and SiO phases in the film deposited at 120 W produced the high broad PL emission spectrum in this film.

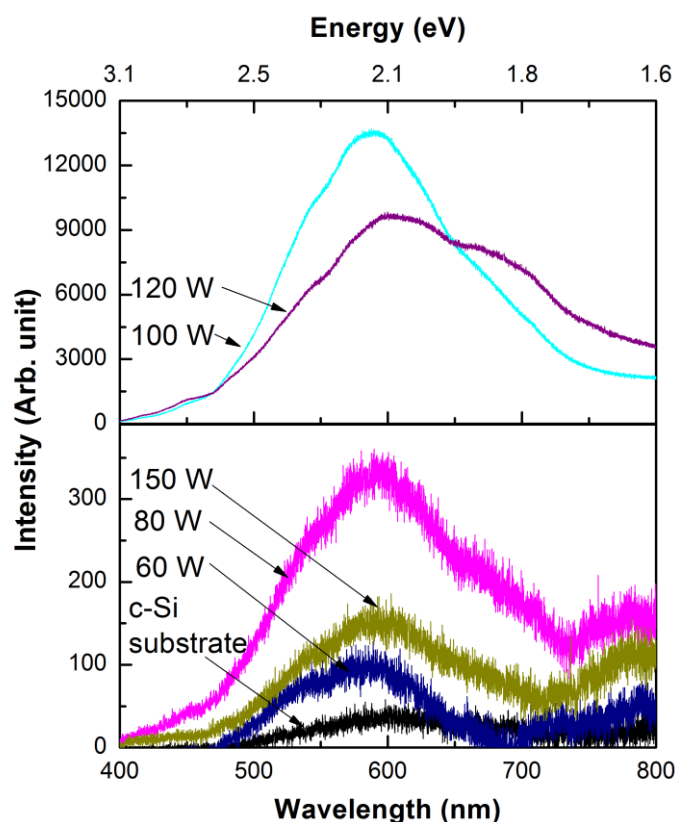


**Figure 4.21:** PL spectra of silicon carbon film deposited at different r.f. power.

The decrease in PL intensity for the films deposited at 150 W is consistent with decrease in C-C network intensity in Raman spectrum for this film. The PL emission in this film was mainly produced by the  $\text{SiO}_x$  phase in the film as it was red-shifted towards 600 nm. The results showed that PL emission in this films originated from the a-C:H and  $\text{SiO}_x$  phase in the films. This further confirmed earlier deduction that the origin of PL emission was from the  $\text{sp}^2$ -C clusters embedded in a-C:H and  $\text{SiO}_x$  matrix in the films due to quantum confinement effect.

#### 4.3.4 Summary

In this study, silicon carbon films have been deposited by sputtering of an amorphous silicon target in methane plasma discharge environment using a hybrid r.f. sputtering/PECVD system at different r.f. powers and the effects of r.f. power on the structural and PL properties of the films have been investigated. The films consisted of a mixed phase of a-Si, a-C:H and a-SiC which contained  $\text{sp}^2$ -C clusters embedded in the matrices of these phases. Effective diffusion of C based growth radicals from the methane discharge and incorporation of Si atoms from the sputtering process at r.f. power of 100 W resulted in film with high carbon incorporation resulting in the dominant presence of  $\text{sp}^2$  C content and Si-C bonds in the film. Strong PL emissions were produced at around 600 nm wavelength by the films with high C incorporation. The origin of the high intensity broad PL emission from the film deposited at 120 W however was produced through recombination processes within the  $\text{sp}^2$  C clusters embedded within a-C:H, a-SiC and  $\text{SiO}_x$  phases through quantum confinement effects mechanisms.



#### 4.4 Overall PL Emission Analysis

In this part of the work, an attempt was made to study the origin of PL emission produced by the three techniques namely the r.f. PECVD, r.f. sputtering and hybrid r.f. PECVD/sputtering techniques. The highest PL emission produced by each of these three techniques were studied and compared. Figure 4.22 shows the PL emission band normalized to the highest peak intensity of these films.

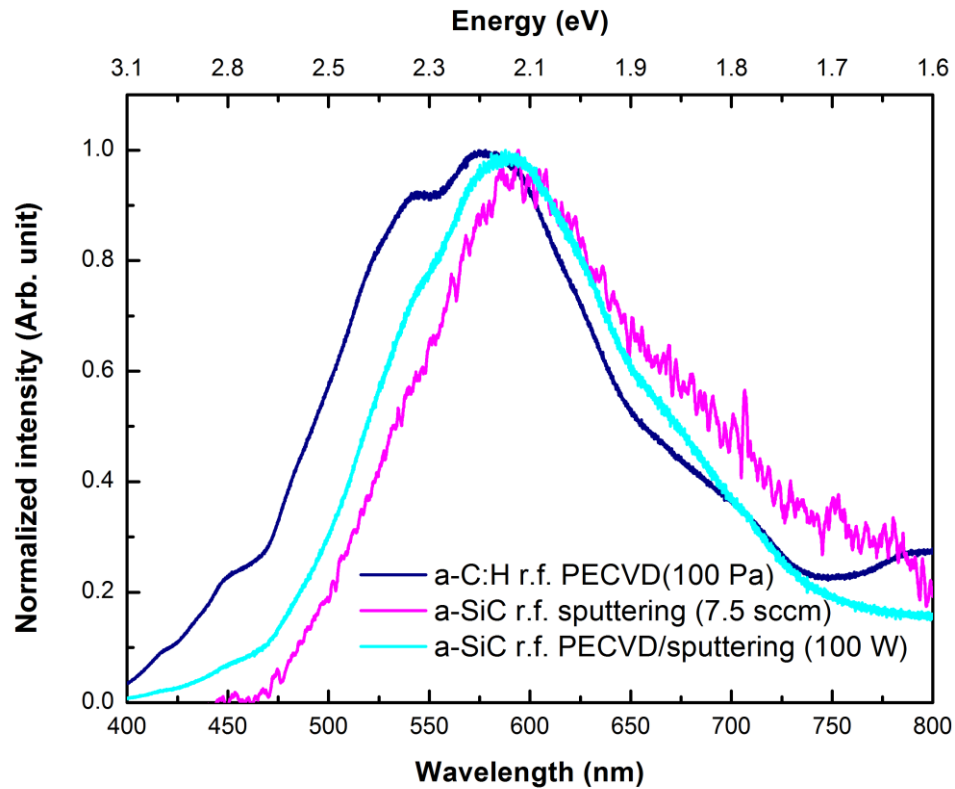


**Figure 4.22:** Normalized PL intensity of the highest PL emitted from three sets of films.

It can be seen that the peak position was shifted for each film deposited by three different techniques. The a-C:H film (100 Pa) exhibited PL emission with peak at 2.2 eV. This film was deposited from the r.f. discharge of  $\text{CH}_4$  diluted in  $\text{H}_2$  gas. The film deposited from the sputtering of a-Si target covered with a-C:H and  $\text{SiO}_x$  layers.(7.5 sccm) produce PL emission which was red shifted to 2.1 eV. The more dominant

presence of  $\text{SiO}_x$  phase in this film produced this PL emission. The film produced using the hybrid r.f. PECVD/sputtering technique (100 W) showed PL emission band at 2.15 eV contributed by the presence of a-C:H and  $\text{SiO}_x$  phases. These results showed that PL emission in these films are mainly contributed by the a-C:H and  $\text{SiO}_x$  phases in the film. The hybrid r.f. PECVD/sputtering system built for this work can therefore be used to tune the PL emission by changing the deposition parameters for future work.

## CHAPTER 5

### CONCLUSION AND FUTURE WORK

#### 5.1 Conclusion

The operation of a newly designed ‘environmental friendly’ hybrid r.f. PECVD/sputtering system was successfully tested. The structural and optical properties of the films deposited by the r.f. PECVD and r.f. sputtering components of hybrid r.f. PECVD/ sputtering system were studied in the first two parts of this work. This was then followed by the study on the properties of the films deposited by the hybrid r.f. PECVD/sputtering technique.

The films produced by r.f. PECVD from methane ( $\text{CH}_4$ ) mixed in hydrogen ( $\text{H}_2$ ) discharge mainly consisted of hydrogenated amorphous carbon (a-C:H) films. In this part of work, it was established that the  $\text{CH}_4$  and  $\text{H}_2$  gas pressures strongly influenced the growth rate, structural and photoluminescence (PL) properties of the films. Therefore, the  $\text{CH}_4$  to  $\text{H}_2$  flow rates ratio was not the determining factor influencing the film properties. The origin of PL emission in these films was through recombination process at the H terminated  $\text{sp}^2$ -C sites.

The films produced by r.f. sputtering of amorphous silicon (a-Si) target showed that the growth rate was strongly determined by the argon (Ar) flow rate. Low Ar flow rate of 15 sccm or lower produced high growth rate. The a-C:H and silicon oxide ( $\text{SiO}_x$ ) layers on the a-Si target produced films with a-Si, a-SiC:H and a-C:H phases. The a-C:H phases in the films contributed most to the PL emission of the film.

The r.f. power was shown to strongly influence the growth rate, structural and PL emission properties for the films deposited by the hybrid r.f. PECVD/sputtering technique. Higher r.f. power of 100 and 120 W enhance the film growth rate and increase the concentration of a-C:H, a-Si, a-SiC:H and SiO<sub>x</sub> phases in the films significantly. However, increasing the r.f. power to 150 W produces a reverse effect. This is due to the increase in Ar ion bombardment on the growth sites. PL emission was shown to have its origin from the a-C:H and SiO<sub>x</sub> phase in the films. The films deposited at 100 and 120 W which have the highest a-C:H and SiO<sub>x</sub> phase exhibited the highest PL emission intensity. The a-Si:H phase in the films showed no contribution to PL emission in the films.

The multiphase structure of the films was analyzed based on the PL emission of films produced by r.f. PECVD, r.f. sputtering and hybrid r.f. PECVD/sputtering techniques. The pure a-C:H films produced by r.f. PECVD exhibited high PL emission intensity at the shortest wavelength comparatively. The origin of PL emission in this film was through recombination process at the H terminated sp<sup>2</sup>-C sites. The film deposited from r.f. sputtering of a-Si target coated with a-C:H and SiO<sub>x</sub> layer produced PL emission which was red-shifted towards 2.1eV. This film consisted predominantly of SiO<sub>x</sub> phase from which the PL emission originated. The films produced from the hybrid r.f. PECVD/sputtering technique consisted of a-Si, a-C:H, SiC and SiO<sub>x</sub> phases. The PL emission originated from a-C:H and SiO<sub>x</sub> phase in the films producing a broad PL emission. In this work, it was established that the hybrid r.f. PECVD/sputtering system could be used to produce multiphase films where the PL emission can be tuned by controlling the concentration of a-C:H and SiO<sub>x</sub> phases in the films.

The hybrid r.f. PECVD/sputtering system developed for this work is still at its infancy. Further work needs to be carried out on the system to produce films with tunable PL emission properties. This can be done through improved control of the deposition pressure by introducing a mass flow controller for CH<sub>4</sub> and Ar with lower flow rate range and more efficient pumping systems. By introducing a shutter at the target, the concentration of a-C:H and SiO<sub>x</sub> phase in the film can be controlled. In this way, PL emission tuning can be more refined.

## References

- Adamopoulos, G., Robertson, J., Morrison, N., & Godet, C. (2004). Hydrogen content estimation of hydrogenated amorphous carbon by visible Raman spectroscopy. *Journal of Applied Physics*, 96(11), 6348-6352.
- Ahmed, S. F., Banerjee, D., Mitra, M. K., & Chattopadhyay, K. K. (2011). Visible photoluminescence from silicon-incorporated diamond like carbon films synthesized via direct current PECVD technique. *Journal of Luminescence*, 131(11), 2352-2358.
- Aida, M. S., & Rahmane, S. (1996). Measurement of the striking force of Ar ions on the substrate during sputter deposition of a-Si:H thin films. *Thin Solid Films*, 288(1-2), 83-85.
- Alexandrov, S. (1995). Remote PECVD: a route to controllable plasma deposition. *Le Journal de Physique IV*, 5(C5), 5-5.
- Alves, M. A. R., Rossetto, J. F., Balachova, O., da Silva Braga, E., & Cescato, L. (2001). Some optical properties of amorphous hydrogenated carbon thin films prepared by rf plasma deposition using methane. *Microelectronics Journal*, 32(9), 783-786.
- Ambrosone, G., Coscia, U., Ferrero, S., Giorgis, F., Mandracci, P., & Pirri, C. F. (2002). Structural and optical properties of hydrogenated amorphous silicon-carbon alloys grown by plasma-enhanced chemical vapour deposition at various rf powers. *Philosophical Magazine B: Physics of Condensed Matter; Statistical Mechanics, Electronic, Optical and Magnetic Properties*, 82(1), 35-46.
- Awang, R., Tong, G. B., Gani, S. M. A., Ritikos, R., & Rahman, S. A. (2006) The effects of deposition pressure on the optical and structural properties of d.c. PECVD hydrogenated amorphous carbon films. *Vol. 517* (pp. 81-84).
- Azis, A., & Rahman, S. A. (2007). Optical Characteristics of Hydrogenated Amorphous Silicon Carbide Films Prepared at Various Gas Flow Rate Ratios. *Japanese Journal of Applied Physics*, 46, 6530.
- Buijnsters, J., Gago, R., Jiménez, I., Camero, M., Agulló-Rueda, F., & Gómez-Aleixandre, C. (2009). Hydrogen quantification in hydrogenated amorphous carbon films by infrared, Raman, and x-ray absorption near edge spectroscopies. *Journal of Applied Physics*, 105(9), 093510-093517.
- Bullot, J., & Schmidt, M. (1987). Physics of amorphous silicon-carbon alloys. *physica status solidi (b)*, 143(2), 345-418.
- Casiraghi, C., Ferrari, A. C., & Robertson, J. (2005). Raman spectroscopy of hydrogenated amorphous carbons. *Physical Review B-Condensed Matter and Materials Physics*, 72(8), 085401.
- Casiraghi, C., Piazza, F., Ferrari, A. C., Grambole, D., & Robertson, J. (2005). Bonding in hydrogenated diamond-like carbon by Raman spectroscopy. *Diamond and Related Materials*, 14(3-7), 1098-1102.
- Cavallotti, C., Di Stanislao, M., & Carrà, S. (2004). Interplay of physical and chemical aspects in the PECVD and etching of thin solid films. *Progress in Crystal Growth and Characterization of Materials*, 48-49, 123-165.
- Cheng, Q., Xu, S., Long, J. D., Ni, Z. H., Rider, A. E., & Ostrikov, K. (2008). High-rate, low-temperature synthesis of composition controlled hydrogenated amorphous silicon carbide films in low-frequency inductively coupled plasmas. *Journal of Physics D: Applied Physics*, 41(5), 055406.

- Chew, K., Rusli, Yoon, S. F., Ahn, J., Ligatchev, V., Teo, E. J., Osipowicz, T., Watt, F. (2002). Hydrogenated amorphous silicon carbide deposition using electron cyclotron resonance chemical vapor deposition under high microwave power and strong hydrogen dilution. *Journal of Applied Physics*, 92(5), 2937.
- Chu, P. K., & Li, L. (2006). Characterization of amorphous and nanocrystalline carbon films. *Materials Chemistry and Physics*, 96(2-3), 253-277.
- Chung, C. K., Lai, C. W., Peng, C. C., & Wu, B. H. (2008). Raman inspection for the annealing induced evolution of  $sp^2$  and  $sp^3$  bonding behavior in sandwiched Si/C/Si multilayer. *Thin Solid Films*, 517(3), 1101-1105.
- Coscia, U., Ambrosone, G., & Basa, D. K. (2008). Room temperature visible photoluminescence of silicon nanocrystallites embedded in amorphous silicon carbide matrix. *Journal of Applied Physics*, 103(6).
- Deng, X. R., Leng, Y. X., Dong, X., Sun, H., & Huang, N. (2011). Effect of hydrogen flow on the properties of hydrogenated amorphous carbon films fabricated by electron cyclotron resonance plasma enhanced chemical vapor deposition. *Surface and Coatings Technology*, 206(5), 1007-1010.
- Dieguez Campo, J. M., Lenski, M., & Comes, F. J. (1998). Influence of gas phase chemistry on the properties of hydrogenated amorphous silicon and silicon-carbon alloys grown by HACVD. *Thin Solid Films*, 323(1-2), 115-125.
- Dohi, M., Yamatani, H., & Fujita, T. (2002). Paramagnetic defects in ultrafine silicon particles. *Journal of Applied Physics*, 91(2), 815-818.
- Ferrari, A., Rodil, S., & Robertson, J. (2003). Interpretation of infrared and Raman spectra of amorphous carbon nitrides. *Physical Review B*, 67(15), 155306.
- Frach, P., Gloess, D., Bartzsch, H., Taeschner, K., Liebig, J., & Schultheiss, E. (2010). Advanced key technologies for magnetron sputtering and PECVD of inorganic and hybrid transparent coatings. *Thin Solid Films*, 518(11), 3105-3108.
- Füle, M., Budai, J., Tóth, S., Veres, M., & Koós, M. (2006). Size of spatial confinement at luminescence centers determined from resonant excitation bands of a-C:H photoluminescence. *Journal of Non-Crystalline Solids*, 352(9-20 SPEC. ISS.), 1340-1343.
- Ghodselahi, T., Vesaghi, M. A., Shafiekhani, A., Baradaran, A., Karimi, A., & Mobini, Z. (2008). Co-deposition process of RF-Sputtering and RF-PECVD of copper/carbon nanocomposite films. *Surface and Coatings Technology*, 202(12), 2731-2736.
- Goh, B. T., Aspanut, Z., Muhamad, M. R., & Rahman, S. A. (2011). Optical properties and crystallinity of hydrogenated nanocrystalline silicon (nc-Si: H) thin films deposited by rf-PECVD. *Vacuum*.
- Goh, B. T., Kien, N. S., Ling, Y. S., San, W. C., & Rahman, S. A. (2012). Effect of energetic ion beam irradiation on structural and optical properties of a-Si:H thin films. *Thin Solid Films*.
- Goswami, R., Jana, T., & Ray, S. (2008). Transparent polymer and diamond-like hydrogenated amorphous carbon thin films by PECVD technique. *Journal of Physics D: Applied Physics*, 41(15), 155413.
- Guo, G., Tang, G., Wang, Y., Ma, X., Sun, M., Wang, L., & Yukimura, K. (2011). Structure and hardness of a-C:H films prepared by middle frequency plasma chemical vapor deposition. *Applied Surface Science*, 257(10), 4738-4742.
- Gupta, N. D., Longeaud, C., Chaudhuri, P., Bhaduri, A., & Vignoli, S. (2006). Some properties of amorphous carbon films deposited on the grounded electrode of a RF-PECVD reactor from Ar-CH<sub>4</sub> mixtures. *Journal of Non-Crystalline Solids*, 352, 1307-1309.

- Higa, A., Oshiro, T., Saida, Y., Yamazato, M., & Toguchi, M. (2006). Correlation between properties and hydrogen concentration of a-C:H films prepared by RF magnetron sputtering. *New Diamond and Frontier Carbon Technology*, 16(5), 245-253.
- Hu, Z., Liao, X., Diao, H., Kong, G., Zeng, X., & Xu, Y. (2004). Amorphous silicon carbide films prepared by H<sub>2</sub> diluted silane-methane plasma. *Journal of Crystal Growth*, 264(1-3), 7-12.
- Huang, X., Xu, J., Li, W., & Chen, K. (2002). Preparation of amorphous carbon films by layer-by-layer hydrogen plasma annealing method and their luminescence properties. *Thin Solid Films*, 422(1-2), 130-134.
- Huran, J., Kučera, M., Kobzev, A., Valovič, A., Balalykin, N., & Gaži, Š. Influence of substrate temperature on the photoluminescence properties of silicon carbide films prepared by ECR-PECVD.
- Jaskorzynska, B., & Wosinski, L. (2008). Silicon-based photonic crystals and nanowires. *Photonic Crystals: Physics and Technology*, 149-169.
- Ji, L., Li, H., Zhao, F., Chen, J., & Zhou, H. (2008). Microstructure and mechanical properties of Mo/DLC nanocomposite films. *Diamond and Related Materials*, 17(11), 1949-1954.
- Jun, X., Xiao-Hui, H., Wei, L., Li, W., & Kun-Ji, C. (2002). Photoluminescence of amorphous carbon films fabricated by layer-by-layer hydrogen plasma chemical annealing method. *Chinese Physics*, 11(5), 502.
- Jung, C. K., Lim, D. C., Jee, H. G., Park, M. G., Ku, S. J., Yu, K. S., Hong, B., Lee, S. B., Boo, J. H. (2003). Hydrogenated amorphous and crystalline SiC thin films grown by RF-PECVD and thermal MOCVD; comparative study of structural and optical properties. *Surface and Coatings Technology*, 171(1-3), 46-50.
- Jutarosaga, T., Seraphin, S., Smith, S. M., & Wei, Y. (2006). Effect of RF-PECVD synthesis conditions on the carbon nanotube growth. *Microscopy and Microanalysis*, 12(SUPPL. 2), 662-663.
- Kassiba, A., Makowska-Janusik, M., Bouclé, J., Bardeau, J. F., Bulou, A., & Herlin-Boime, N. (2002). Photoluminescence features on the Raman spectra of quasistoichiometric SiC nanoparticles: Experimental and numerical simulations. *Physical Review B - Condensed Matter and Materials Physics*, 66(15), 1553171-1553177.
- Kelly, P., & Arnell, R. (2000). Magnetron sputtering: a review of recent developments and applications. *Vacuum*, 56(3), 159-172.
- Khanis, N. H., Ritikos, R., Othman, M., Rashid, N. M. A., Gani, S. M. A., Muhamad, M. R., & Rahman, S. A. (2011). Effect of pre-deposited carbon layer on the formation of carbon nitride nanostructures prepared by radio-frequency plasma enhanced chemical vapour deposition. *Materials Chemistry and Physics*, 130(1), 218-222.
- Khashan, K. S., Awaad, A. A., & Mohamed, M. A. Effect on Rapid Thermal Oxidation process on Electrical Properties of Porous Silicon.
- Kumbhar, A., Patil, S. B., Kumar, S., Lal, R., & Dusane, R. O. (2001). Photoluminescent, wide-bandgap a-SiC:H alloy films deposited by Cat-CVD using acetylene. *Thin Solid Films*, 395(1-2), 244-248.
- Le Contellec, M., Richard, J., Guivarc'h, A., Ligeon, E., & Fontenille, J. (1979). Effects of the silicon-to-carbon ratio and the hydrogen content in amorphous SiC thin films prepared by reactive sputtering. *Thin Solid Films*, 58(2), 407-411.
- Lee, K. H., Baik, K., Bang, J. S., Lee, S. W., & Sigmund, W. (2004). Silicon enhanced carbon nanotube growth on nickel films by chemical vapor deposition. *Solid State Communications*, 129(9), 583-587.



- Lei, Y. M., Yu, Y. H., Cheng, L. L., Ren, C. X., & Zou, S. C. (2000). Auger electron spectroscopy study of SiC thin films deposited on silicon. *Vacuum*, 58(4), 602-608.
- Li, G., Zhang, J., Meng, Q., & Li, W. (2007). Synthesis of silicon carbide films by combined implantation with sputtering techniques. *Applied Surface Science*, 253(20), 8428-8434.
- Li, Z., Bian, J., He, H., Zhang, X., & Han, G. (2011). *The effect of relatively low hydrogen dilution on the properties of carbon-rich hydrogenated amorphous silicon carbide films*. Paper presented at the Journal of Physics: Conference Series.
- Liao, M., Feng, Z., Chai, C., Yang, S., Liu, Z., & Wang, Z. (2002). Violet/blue emission from hydrogenated amorphous carbon films deposited from energetic CH ions and ion bombardment. *Journal of Applied Physics*, 91, 1891.
- Lien, S. Y., Weng, K. W., Huang, J. J., Hsu, C. H., Shen, C. T., Wang, C. C., Lin, Y. S., Wu, D. S., Wu, D. C. (2011). Influence of CH<sub>4</sub> flow rate on properties of HF-PECVD a-SiC films and solar cell application. *Current Applied Physics*, 11(1 SUPPL.), S21-S24.
- Liu, S., Gangopadhyay, S., Sreenivas, G., Ang, S. S., & Naseem, H. A. (1997). Infrared studies of hydrogenated amorphous carbon (a-C:H) and its alloys (a-C:H,N,F). *Physical Review B*, 55(19), 13020-13024.
- Maître, N., Camelio, S., Barranco, A., Girardeau, T., & Breille, E. (2005). Physical and chemical properties of amorphous hydrogenated carbon films deposited by PECVD in a low self-bias range. *Journal of Non-Crystalline Solids*, 351(10-11), 877-884.
- Marchon, B. (1997). Photoluminescence and Raman Spectroscopy in Hydrogenated Carbon Films. *IEEE Transactions on Magnetics*, 33(5 PART 1), 3148-3150.
- Marchon, B., Jing, G., Grannen, K., Rauch, G. C., Ager, J. W., III, Silva, S. R. P., & Robertson, J. (1997). Photoluminescence and Raman spectroscopy in hydrogenated carbon films. *Magnetics, IEEE Transactions on*, 33(5), 3148-3150.
- Maréchal, C., Zeinert, A., Zellama, K., Lacaze, E., Zarrabian, M., & Turban, G. (1998). Correlation between surface morphology and optical properties for different types of hydrogenated amorphous carbon films grown by plasma enhanced chemical vapour deposition. *Solid State Communications*, 109(1), 23-28.
- Marins, N. M. S., Mota, R.P., Honda, R.Y., Nascente, P.A.P., Kayama, M.E., Kostov, K.G., Algatti, M.A., Cruz, N.C., Rangel, E.C. (2011). Properties of hydrogenated amorphous carbon films deposited by PECVD and modified by SF<sub>6</sub> plasma. *Surface and Coatings Technology*, 206(4), 640-645.
- Mishra, S. K., Shekhar, C., Rupa, P. K. P., & Pathak, L. C. (2007). Effect of pressure and substrate temperature on the deposition of nano-structured silicon-carbon-nitride superhard coatings by magnetron sputtering. *Thin Solid Films*, 515(11), 4738-4744.
- Mori, M., Tabata, A., & Mizutani, T. (2006). Properties of hydrogenated amorphous silicon carbide films prepared at various hydrogen gas flow rates by hot-wire chemical vapor deposition. *Thin Solid Films*, 501(1-2), 177-180.
- Motta, E. F., & Pereyra, I. (2004). Amorphous hydrogenated carbon-nitride films prepared by RF-PECVD in methane-nitrogen atmospheres. *Journal of Non-Crystalline Solids*, 338-340(0), 525-529.
- Mutsukura, N., Inoue, S., & Machi, Y. (1992). Deposition mechanism of hydrogenated hard-carbon films in a CH<sub>4</sub> rf discharge plasma. *Journal of Applied Physics*, 72(1), 43-53.

- Mutsukura, N., & Miyatani, K. (1995). Deposition of diamond-like carbon film in CH<sub>4</sub>-He r.f. plasma. *Diamond and Related Materials*, 4(4), 342-345.
- Neyts, E., Bogaerts, A., & Van De Sanden, M. (2007). *Reaction mechanisms and thin aC: H film growth from low energy hydrocarbon radicals*.
- Othman, M., Ritikos, R., Khanis, N. H., Rashid, N. M. A., Gani, S. M. A., & Rahman, S. A. (2012). Effect of N<sub>2</sub> flow rate on the properties of CN<sub>x</sub> thin films prepared by radio frequency plasma enhanced chemical vapour deposition from ethane and nitrogen. *Thin Solid Films*.
- Othman, M., Ritikos, R., Khanis, N. H., Rashid, N. M. A., Rahman, S. A., Gani, S. M. A., & Muhamad, M. R. (2011). Effects of rf power on the structural properties of carbon nitride thin films prepared by plasma enhanced chemical vapour deposition. *Thin Solid Films*, 519(15), 4981-4986.
- Pandey, M., & Patil, D. S. (2007). Raman and photoluminescence spectroscopy of a-C:H films deposited by microwave-assisted plasma CVD under D.C. bias and pulse bias. *Diamond and Related Materials*, 16(11), 1912-1917.
- Papakonstantinou, P., Zhao, J., Richardot, A., McAdams, E., & McLaughlin, J. (2002). Evaluation of corrosion performance of ultra-thin Si-DLC overcoats with electrochemical impedance spectroscopy. *Diamond and Related Materials*, 11(3), 1124-1129.
- Park, Y. S., Hong, B., & Kim, H. J. (2004). Tribological properties of hydrogenated amorphous carbon thin films by Close Field Unbalanced Magnetron sputtering method. *Journal of the Korean Physical Society*, 45(SUPPL.), S824-S828.
- Pascual, E., Andújar, J., Fernández, J., & Bertran, E. (1995). Optical and structural characterization of hydrogenated amorphous silicon carbide thin films prepared by rf plasma chemical vapour deposition. *Diamond and Related Materials*, 4(10), 1205-1209.
- Racine, B., Ferrari, A. C., Morrison, N. A., Hutchings, I., Milne, W. I., & Robertson, J. (2001). Properties of amorphous carbon-silicon alloys deposited by a high plasma density source. *Journal of Applied Physics*, 90(10), 5002-5012.
- Rajagopalan, T., Wang, X., Lahlouh, B., Ramkumar, C., Dutta, P., & Gangopadhyay, S. (2003). Low temperature deposition of nanocrystalline silicon carbide films by plasma enhanced chemical vapor deposition and their structural and optical characterization. *Journal of Applied Physics*, 94(8), 5252-5260.
- Rashid, N. M. A., Ritikos, R., Othman, M., Khanis, N. H., Gani, S. M. A., Muhamad, M. R., & Rahman, S. A. Amorphous silicon carbon films prepared by hybrid plasma enhanced chemical vapor/sputtering deposition system: Effects of r.f. power. *Thin Solid Films*(0). doi: 10.1016/j.tsf.2012.09.032
- Rashid, N. M. A., Ritikos, R., Othman, M., Khanis, N. H., Gani, S. M. A., Muhamad, M. R., & Rahman, S. A. (2013). Amorphous silicon carbon films prepared by hybrid plasma enhanced chemical vapor/sputtering deposition system: Effects of r.f. power. *Thin Solid Films*, 529(0), 459-463.
- Raveh, A., Klemberg-Sapieha, J. E., Martinu, L., & Wertheimer, M. (1992). Deposition and properties of diamondlike carbon films produced in microwave and radio frequency plasma. *Journal of Vacuum Science & Technology A: Vacuum, Surfaces, and Films*, 10(4), 1723-1727.
- Rhallabi, A., & Catherine, Y. (1991). Computer simulation of a carbon-deposition plasma in CH<sub>4</sub>. *Plasma Science, IEEE Transactions on*, 19(2), 270-277. doi: 10.1109/27.106824
- Ritala, M., Niinisto, J., Jones, A. C., & Hitchman, M. L. (2008). *Chemical vapour deposition: precursors, processes and applications*: Royal Society of Chemistry.

- Ritikos, R., Goh, B. T., Sharif, K. A. M., Muhamad, M. R., & Rahman, S. A. (2009). Highly reflective nc-Si:H/a-CN<sub>x</sub>:H multilayer films prepared by r.f. PECVD technique. *Thin Solid Films*, 517(17), 5092-5095.
- Robertson, J. (1995). Structural models of a-C and a-C:H. *Diamond and Related Materials*, 4(4), 297-301.
- Robertson, J. (1996). Recombination and photoluminescence mechanism in hydrogenated amorphous carbon. *Physical Review B*, 53(24), 16302-16305.
- Rusakov, G., Ivashchenko, L., Ivashchenko, V., & Porada, O. (2001). Peculiarities of preparing a-SiC:H films from methyltrichlorosilane. *Applied Surface Science*, 184(1), 128-134.
- Rusli, Amaratunga, G. A. J., & Silva, S. R. P. (1995). Photoluminescence in amorphous carbon thin films and its relation to the microscopic properties. *Thin Solid Films*, 270(1-2), 160-164.
- Rusli, Amaratunga, G. A. J., & Silva, S. R. P. (1996). Highly luminescent hydrogenated amorphous carbon (a-C:H) thin films. *Optical Materials*, 6(1-2), 93-98.
- Ryu, H. J., Kim, S. H., & Hong, S. H. (2000). Effect of deposition pressure on bonding nature in hydrogenated amorphous carbon films processed by electron cyclotron resonance plasma enhanced chemical vapor deposition. *Materials Science and Engineering: A*, 277(1), 57-63.
- S. Lin, E. Q. X., Q. Wen. (2002). Growth of  $\beta$ -SiC by RF Sputtering on Silicon Substrates. *Acta Metallurgica Sinica(English letters)*, 15(2), 210-214.
- Schwan, J., Ulrich, S., Batori, V., Ehrhardt, H., & Silva, S. (1996). Raman spectroscopy on amorphous carbon films. *Journal of Applied Physics*, 80(1), 440-447.
- Sha, Z. D., Wu, X. M., & Zhuge, L. J. (2005). Structure and photoluminescence properties of SiC films synthesized by the RF-magnetron sputtering technique. *Vacuum*, 79(3-4), 250-254.
- Shi, J. R., Shi, X., Sun, Z., Liu, E., Yang, H. S., Cheah, L. K., & Jin, X. Z. (1999). Structural properties of amorphous silicon-carbon films deposited by the filtered cathodic vacuum arc technique. *Journal of Physics Condensed Matter*, 11(26), 5111-5118.
- Silinskas, M., Grigonis, A., Kulikauskas, V., & Manika, I. (2008). Hydrogen influence on the structure and properties of amorphous hydrogenated carbon films deposited by direct ion beam. *Thin Solid Films*, 516(8), 1683-1692.
- Son, Y. H., Jung, W. C., Jeong, J. I., Park, N. G., Kim, I. S., & Bae, I. H. (2001). FTIR characteristics of hydrogenated amorphous carbon films prepared by ECR-PECVD. *Journal of the Korean Physical Society*, 39(4 SUPPL. Part 1), 713-717.
- Sundaram, K. B., & Alizadeh, J. (2000). Deposition and optical studies of silicon carbide nitride thin films. *Thin Solid Films*, 370(1-2), 151-154.
- Swain, B. P. (2006). Influence of process pressure on HW-CVD deposited a-SiC:H films. *Surface and Coatings Technology*, 201(3-4), 1132-1137.
- Swain, B. P., & Dusane, R. O. (2006). Multiphase structure of hydrogen diluted a-SiC:H deposited by HWCVD. *Materials Chemistry and Physics*, 99(2-3), 240-246.
- Swain, B. P., & Dusane, R. O. (2007). Effect of substrate temperature on HWCVD deposited a-SiC:H film. *Materials Letters*, 61(25), 4731-4734.
- Tachibana, K., Nishida, M., Harima, H., & Urano, Y. (1984). Diagnostics and modelling of a methane plasma used in the chemical vapour deposition of amorphous carbon films. *Journal of Physics D: Applied Physics*, 17(8), 1727-1742.
- Tomasella, E., Meunier, C., & Mikhailov, S. (2001). aC: H thin films deposited by radio-frequency plasma: influence of gas composition on structure, optical properties and stress levels. *Surface and Coatings Technology*, 141(2), 286-296.

- Umezu, I., Kohno, K., Aoki, K., Kohama, Y., Sugimura, A., & Inada, M. (2002). Effects of argon and hydrogen plasmas on the surface of silicon. *Vacuum*, 66(3-4), 453-456.
- Vakerlis, G., Halverson, W. D., Garg, D., & Dyer, P. N. (1991). Radio frequency plasma enhanced chemical vapor deposition process and reactor: Google Patents.
- Valentini, L., Kenny, J. M., Mariotto, G., & Tosi, P. (2001). Deposition of hydrogenated amorphous carbon films from CH<sub>4</sub>/Ar plasmas: Ar dilution effects. *Journal of Materials Science*, 36(21), 5295-5300.
- Veres, M., Tóth, S., & Koós, M. (2008). New aspects of Raman scattering in carbon-based amorphous materials. *Diamond and Related Materials*, 17(7), 1692-1696.
- Viana, G. A., Motta, E. F., da Costa, M. E. H. M., Freire Jr, F. L., & Marques, F. C. (2010). Diamond-like carbon deposited by plasma technique as a function of methane flow rate. *Diamond and Related Materials*, 19(7-9), 756-759.
- von Keudell, A., Meier, M., & Hopf, C. (2002). Growth mechanism of amorphous hydrogenated carbon. *Diamond and Related Materials*, 11(3-6), 969-975.
- Vovk, O. M., Na, B. K., Cho, B. W., & Lee, J. K. (2009). Electrochemical characteristics of amorphous carbon coated silicon electrodes. *Korean journal of chemical engineering*, 26(4), 1034-1039.
- Wang, G.-H., Li, W.-C., Jia, K.-M., Spliethoff, B., Schüth, F., & Lu, A.-H. (2009). Shape and size controlled  $\alpha$ -Fe<sub>2</sub>O<sub>3</sub> nanoparticles as supports for gold-catalysts: Synthesis and influence of support shape and size on catalytic performance. *Applied Catalysis A: General*, 364(1-2), 42-47. doi: <http://dx.doi.org/10.1016/j.apcata.2009.05.030>
- Wang, H. Y., Wang, Y. Y., Song, Q., & Wang, T. M. (1998). Formation of 6H-SiC due to subsequent annealing of sputtering a-SiC:H films. *Materials Letters*, 35(3-4), 261-265.
- Wang, Y. H., Lin, J., & Huan, C. H. A. (2002). Multiphase structure of hydrogenated amorphous silicon carbide thin films. *Materials Science and Engineering: B*, 95(1), 43-50.
- Xie, D., Liu, H., Deng, X., Leng, Y. X., & Huang, N. (2010). Effects of process parameters on the structure of hydrogenated amorphous carbon films processed by electron cyclotron resonance plasma enhanced chemical vapor deposition. *Surface and Coatings Technology*, 204(18-19), 3029-3033. doi: [10.1016/j.surfcoat.2010.02.012](http://dx.doi.org/10.1016/j.surfcoat.2010.02.012)
- Xu, J., Mei, J., Chen, D., Chen, S., Li, W., & Chen, K. (2005). All amorphous SiC based luminescent microcavity. *Diamond and Related Materials*, 14(11), 1999-2002.
- Xu, J., Yang, L., Rui, Y., Mei, J., Zhang, X., Li, W., Ma, Z., Xu, L., Huang, X., Chen, K. (2005). Photoluminescence characteristics from amorphous SiC thin films with various structures deposited at low temperature. *Solid State Communications*, 133(9), 565-568.
- Xu, M., Ng, V., Huang, S., Long, J., & Xu, S. (2005). Growth of SiC nanoparticle films by means of RF magnetron sputtering. *Plasma Science, IEEE Transactions on*, 33(2), 242-243.
- Yang, S., Pan, F., Yang, Y., & Zhang, W. (2009). Effects of flow ratios on surface morphology and structure of hydrogenated amorphous carbon films prepared by microwave plasma chemical vapor deposition. *Applied Surface Science*, 255(22), 9058-9061.

- Yoon, S. F., Tan, K. H., Rusli, Ahn, J., & Huang, Q. F. (2000). Effect of microwave power on diamond-like carbon films deposited using electron cyclotron resonance chemical vapor deposition. *Diamond and Related Materials*, 9(12), 2024-2030.
- Yu, W., Lu, W., Han, L., & Fu, G. (2004). Structural and optical properties of hydrogenated amorphous silicon carbide films by helicon wave plasma-enhanced chemical vapour deposition. *Journal of Physics D: Applied Physics*, 37(23), 3304-3308.
- Zhi-hong, Z., Huai-xi, G., Xian-quan, M., Ming-sheng, Y., Wei, Z., & Xiang-jun, F. (2008). Plasma enhanced chemical vapor deposition synthesizing carbon nitride hard thin films. *Chinese Physics Letters*, 15(12), 913.